CHALMERS
UNIVERSITY OF TECHNOLOGY

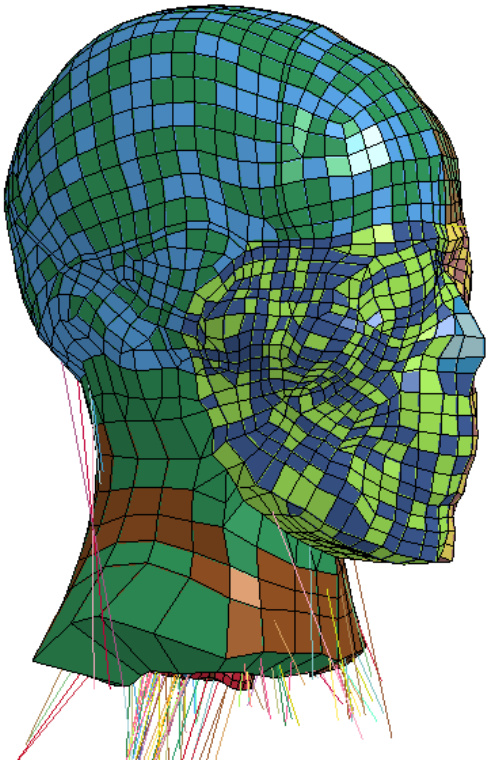

The influence of isometrically derived neck muscle spatial tuning patterns on head response in dynamic conditions

Master's Thesis in Biomedical Engineering

ANDREA IVANČIĆ
VIKRAM PRADHAN

Department of Applied Mechanics
CHALMERS UNIVERSITY OF TECHNOLOGY
Gothenburg, Sweden 2017

Master's thesis 2017:72

The influence of isometrically derived neck muscle spatial tuning patterns on head response in dynamic conditions

ANDREA IVANČIĆ
VIKRAM PRADHAN

CHALMERS
UNIVERSITY OF TECHNOLOGY

Department of Applied Mechanics
Division of Vehicle Safety
SAFER
Chalmers University of Technology
Gothenburg, Sweden 2017

The influence of isometrically derived neck muscle spatial tuning patterns on head response in dynamic conditions

ANDREA IVANČIĆ
VIKRAM PRADHAN

Supervisor: Jóna Marín Ólafsdóttir, Department of Applied Mechanics
Examiner: Karin Brolin, Department of Applied Mechanics

Master's Thesis 2017:72
Department of Applied Mechanics
Division of Vehicle Safety
SAFER
Chalmers University of Technology
SE-412 96 Gothenburg
Telephone +46 31 772 1000

Cover: THUMS model with implemented active muscles in LS-DYNA at Chalmers University of Technology, the Active Human Body Model, AHBM.

Gothenburg, Sweden 2017

The influence of isometrically derived neck muscle spatial tuning patterns on head response in dynamic conditions

ANDREA IVANČIĆ
VIKRAM PRADHAN
Department of Applied Mechanics
Division of Vehicle Safety
Chalmers University of Technology

Abstract

The Chalmers AHBM was setup in LS-DYNA to mimic maximum voluntary contraction (MVC) experiments, and to find the optimum cervical muscle activation parameters for a setup using an optimization model in LS-OPT. The setup in LS-DYNA incorporated a discrete beam element with a high stiffness, attached to the head of the AHBM, making it resistant to change in length. Pulling against this beam is similar to pushing against a rigid clamp used in the MVC experimental setups with human volunteers. The AHBM head is constrained in 3D space to have small translational and rotational displacements. Hence, it was considered an apt analogy in the numerical simulations of the AHBM, towards obtaining MVC. A linear response surface was used to obtain optimum values for muscle activation parameters in the design space, with sequential domain reduction and tolerance of convergence set to ±1%. The motion of the models was post-processed in LS-PrePost. Muscle activation patterns obtained from optimizations for the two models - one with 9 muscle groups and the other with 13 muscle groups in the neck, were compared with the MVC experiment conducted by Siegmund et al. (2007), and later used for simulation of the AHBM with applied dynamic load in 5 different directions, 0°, 45°, 90°, 135° and 180°, using a previously implemented 1 DOF PID controller for the AHBM by Östh (2014) as well as a newly developed 3 DOF PID controller, which was based on functions in LS-DYNA. The dynamic spatial tuning patterns for the optimization models were compared to those obtained from the human volunteer sled experiments conducted by Ólafsdóttir et al. (2015). The muscle activation patterns from the optimizations showed great variation compared to those obtained from the MVC experiments, due to difference in muscle modelling, constraints on the AHBM and the optimization setup. The dynamic spatial tuning patters for the optimization setups with 1 DOF PID controller were scaled in the same directions as the muscles were activated in the MVC optimizations, however, the 3 DOF PID controller behaved differently. Larger translational and rotational head displacements were observed in the optimization models as compared to the experimental model. Models with 3 DOF PID controller resulted in significantly different kinematics as compared to the models with 1 DOF PID controller.

Keywords: AHBM, LS-DYNA, LS-OPT, LS-PrePost, Optimization, Simulation, Muscle Activation, PID controller, DOF, MVC

Preface

This Master of Science Thesis was conducted at the Division of Vehicle Safety, at the department of Applied Mechanics at Chalmers University of Technology. Professor Karin Brolin was the examiner for the project and Jóna Marín Ólafsdóttir was the supervisor.

Acknowledgements

We would like to thank Professor Karin Brolin for giving us an opportunity to be a part of the ongoing research on the AHBM at SAFER, at Chalmers University of Technology. We acknowledge our supervisor Jóna Marín Ólafsdóttir for enlightening us in the area of impact biomechanics, and for her constant guidance and motivation towards a successful Master of Science thesis. We highly appreciate her propensity to bring out the best from us. We would like to extend our gratitude to Dr. Johan Iraeus for supporting us with the required resources during the course of the thesis, being available for consultation and motivating us to achieve the goals of the project. We would also like to thank SAFER, the Division of Vehicle Safety, for making us feel like an important part of the organization and providing us the best possible work environment in order to carry out research to the best of our potential.

Andrea Ivančić & Vikram Pradhan, Gothenburg, June 2017

Notations

Variables

α	Activation level in the muscle
$\sigma_{CE}(l)$	Parallel contractile element stress
$\sigma_{PE}(l)$	Parallel elastic element stress
$\sigma_{DE}(v)$	Parallel elastic element viscous stress
σ_{max}	Maximum isometric stress in the muscle
τ	Time differential notation
A_i	Physiological cross section area of the i_{th} muscle
$D(t)$	External force
D_x	Displacement of node at head center of gravity in x direction
D_y	Displacement of node at head center of gravity in y direction
$e(t)$	Error signal
$f_l(l)$	Muscle force-length relation
$f_v(v)$	Muscle force-velocity relation
F_{head}	Forces acting on the environment through head center of gravity
F_i	Force in the i_{th} muscle
$ie(t)$	Integrated error signal
J	Cost function for optimization
l	Instantaneous muscle length
l_{opt}	Optimal muscle length for maximum isometric muscle contraction
M_{head}	Moment acting on environment through head center of gravity
M_{des}	Matrix composed of the desired neck joint torques
M_{pas}	Matrix composed of passive moments exerted at joints
N	Neck moment arm matrix
$N_a(t)$	Activation state
$N_e(t)$	Neural excitation
$r(t)$	Reference angle
R	Muscle moment arm matrix
$u(t)$	Control signal
v	Instantaneous rate of muscle contraction

Variables

V	Muscle shortening velocity
V_{max}	Maximum muscle shortening velocity
V_1	Vector connecting the head center of gravity and T1
V_2	Vector connecting the head center of gravity at t=0 and T1 at t=0
$y(t)$	Absolute angle of deviation of head with respect to the vertical axis

Constants

σ_{max}	Maximum isometric contraction
C_{mvl}	Asymptotic value for increased eccentric muscle elongation
C_{lng}	Transition between eccentric and concentric muscle shortening
C_{PE}	Passive elastic muscle stiffness
C_{sh}	Shape of contraction rate curve for concentric muscle shortening
Δt	Time step
D	Passive viscous muscle stiffness
$(D_s)_{critical}$	Critical damping factor
k_p	Proportional gain
k_i	Integral gain
k_d	Derivative gain
m	Mass of the muscle segment
S	Permissible stress for the muscle
T_{de}	Neural delay
T_f	Time constant of the derivative filter
T_{na}	Time constant of the muscle activation dynamics
T_{ne}	Time constant of the neural muscle excitation
T_{naa}	Time constant of the neural muscle activation
T_{nad}	Time constant of the neural muscle deactivation
ω_{min}	Natural frequency

Acronyms

AHBM	Active Human Body Model
ATD	Anthropomorphic Test Device
CE	Contractile Element
CNS	Central Nervous System
DE	Parallel Viscous (Damping) Element
DOF	Degree Of Freedom
EMG	Electromyography
FEM	Finite Element Method
HBM	Human Body Model
MB	Multi Body
MVC	Maximum Voluntary Contractions
PCSA	Physiological Cross Sectional Area
PE	Parallel Elastic Element
PID	Proportional, Integrative and Derivative
PNS	Peripheral Nervous System
SRSM	Successive Response Surface Method
THUMS	Total Human Model for Safety

Contents

List of Figures

List of Tables

1
Introduction

Injuries due to road accidents have become a common phenomenon in recent years with increase in population and number of road vehicles. It is essential to give considerable attention to the study of injury mechanisms, so that it can pave the way for development of injury prevention strategies like development of passive safety systems (Vezin and Verriest, 2005), and integration of these systems with active safety systems (Östh et al., 2015b), in order to provide improved protection to the society (Schoeneburg and Breitling, 2005).

The process of development is possible through gaining an insight into the interaction between a human and the surrounding, which could either be the deployed restraint system or the interior of the vehicle upon impact (Schoeneburg and Breitling, 2005). One of the major causes of deaths and disabilities in the US is motor vehicle crashes. The fatality rate for occupants in motor vehicles was estimated at 12.7 per 100,000 population in 2004 (Administration et al., 2006). The fatality rate in Sweden owing to road traffic accidents was 14 per 100,000 in 1975, and 9 per 100,000 in 1992, being one of the largest single cause of deaths (Boström et al., 2001). In 2016, 270 people were killed and 2347 were critically injured in road accidents (Analysis, 2016). It has been predicted that the road traffic crashes would be the 7th main cause of deaths by 2030, if no action would be taken (WHO, 2016). These statistics suggest that road crashes have been one of the major contributing factors towards injuries as well as fatalities, and there is a serious need to bring down these large numbers in order for the society to lead a better life (Crandall et al., 2011; Vezin and Verriest, 2005; Östh et al., 2015b).

In the past few decades, there has been an attempt to understand the vehicle occupant responses in various pre-crash and crash scenarios. A number of anthropomorphic test devices (ATDs) or crash test dummies have been developed on a large scale for studying these vehicle occupant responses. Although they have been capable of providing valuable experimental data on occupant responses, they lack some essential physiological properties like human tissues that can significantly alter the responses. Human cadavers are also being used extensively for crash testing, however, there are some ethical and legislative issues involved (Jones, 1995). Human volunteers that can provide the most valuable information in crash tests, by most closely resemble the vehicle occupant, can not be put in dangerous impact situations. These challenges enforce the development of a concept that is repeatable, biofidelic and can be tested for various crash scenarios in a risk-free environment. The availability of higher computational power, paved the way for development of

numerical human body models (HBMs). These models are robust and can be easily modified to suit the requirements of a crash test. They offer a great advantage of understanding and predicting injury mechanisms and injury criteria with ease, thereby aiding the development of better safety systems and saving precious lives though a better biomechanical analysis (Wismans et al., 2005).

1.1 Ongoing research and development work

During pre-crash scenarios, occupant kinematics are affected by reflexive muscle contractions. Therefore, it is of great importance to study the active muscle recruitment patterns in different pre-crash scenarios, to be able to better predict the kinematics of the vehicle occupant. It has been made possible through the simulations of the HBMs (Östh et al., 2015a).

At the Division of Vehicle Safety at Chalmers University of Technology, there is an ongoing research project, where a method for modelling active muscle responses in Finite Element (FE) HBMs has been developed. The modeling of the HBM has been performed for motions in the sagittal plane. The research in this area is expanding the HBMs capabilities to simulate omnidirectional motions, which in turn requires knowledge and understanding of the spatial tuning of the included muscles in the HBM (Östh, 2014). The occupant in a vehicle can be subjected to an impact in any direction, causing complex kinematics of the occupants body and thereby leading to injuries. The cervical spine in particular is very sensitive in crashes and prone to whiplash injuries. Hence, it is of great importance to understand how the cervical muscles are activated in omnidirectional loading of the spine during crashes. The spatial tuning patterns of the muscles are useful when mimicing the vehicle occupant neck kinematics when incorporated in the HBM with the particular load case. A biomechanical analysis using the HBM would support the development of restraint systems that would reduce whiplash injuries.

1.2 Aim

The aim of the project is to establish model specific spatial tuning patterns for the neck muscles of the SAFER Active Human Body Model under isometric conditions, and study the influence of using these patterns compared to experimentally derived patterns in dynamic conditions.

1.3 Objectives

The main objective of this study is to setup the AHBM for maximum voluntary contractions (MVCs) in LS-DYNA using an explicit method. Neck muscles of the AHBM were grouped based on similar anatomical location and function and would be activated independent of each other. The muscles within the same muscle group

would receive the same activation level in the range of 0-100% during the optimization, and would produce a force based on hill-type muscle modelling described in Section 2.4. Different muscles have different force generating capacities and hence would produce a different force although the activation level received is the same. The optimization in this project is based on the optimal balance of force in a beam attached to a head, see Section 5.1.1, and the forces produced by the muscles, while preventing the model from violating the constraints that have been laid on the head center of gravity and the center of each vertebra of the cervical spine to mimic an isometric environment, in LS-OPT, see Section 5.1.3. The activation levels of muscle groups would be increased gradually, thereby generating more force in the beam, until an equilibrium position of the model is reached that lies within the specified constraints. These activation levels corresponding to the maximum force generated in the beam would be referred to as the optimized muscle recruitment patterns that need to be utilized in the AHBM, which would be subjected to a dynamic load case. The resulting kinematics need to be compared to the kinematics obtained through the simulation of muscle recruitment patterns obtained from sled experiments on human volunteers, in the AHBM. An additional objective is to develop and implement a 3 DOF PID controller, using both the experimental muscle recruitment patterns and the isometric muscle recruitment patterns obtained through the optimization, for the AHBM, and to compare the model's dynamic response to that resulting from the existing 1 DOF PID controller.

1.4 Scope

The project is limited to the optimization of isometric recruitment patterns for the neck muscles of the SAFER AHBM specifically. The muscle recruitment patterns would heavily rely on the method of optimization, and thus different optimization methods could generate different muscle activation patterns, and validating all the methods will be time consuming, hence the focus would be restricted to 1-2 optimization methods.

1.5 Tools

The simulations were executed in LS-DYNA® r8.0.0 (LSTC Inc., Livermore, CA, USA), the optimization simulations in LS-OPT® v4.3 (LSTC Inc., Livermore, CA, USA), and the pre- and post-processing of the model in LS-PREPOST® (LSTC Inc., Livermore, CA, USA) and MATLAB® (The Mathworks Inc., Natic, MA, USA).

2
Background

Section 2.1 in this chapter highlights some of the important restraint systems that are used in vehicle occupant protection. Tools that are useful in evaluating the safety performance of restraint systems are described in Section 2.2. Section 2.3 deals with relevant aspects that need to be considered while incorporating active musculature in HBMs, while Section 2.4 describes how those aspects are utilized towards modelling active muscle elements in the numerical HBMs. Section 2.6 presents the importance of studying head and neck muscles in the AHBM, and the motivation towards using isometrically derived model-specific spatial tuning patterns of muscles for simulations involving HBMs are described in Section 2.7. Finally, Section 2.8 describes techniques used in optimization studies on AHBMs.

2.1 Use of restraint systems for improving safety

A major step towards increased vehicle safety over the last 30 years, has been the development of restraint systems, such as the three point seat belt and the airbag. The effectiveness of a particular restraint system increases when it is used in conjunction with another restraint system. Development of smart restraint systems, which easily adapt to the vehicle occupant, have been of great interest (Cesari, 1997). Pretensioners, load limiters and energy absorbers are said to be systems that provide good protection in case of rollover accidents. The prediction that these existing restraint systems will be well supported by devices like inflatable head restraints, side window curtains, seatbelt pretensioners, seatbelt retractor locks, active roll bar, pop up headrest and enhanced support structures for convertibles, has been made (Berg et al., 2004).

2.2 Tools for assessment of restraint systems

Before the restraint systems are deployed in vehicles on a large scale, it is mandatory to assess their safety performance. This testing of restraint systems has traditionally been done through crash tests on dummies. However, human cadavers, human volunteers, finite element (FE) human body models (HBMs), and FE active human body models (AHBMs) have been used as well (Viano and Arepally, 1990; Crandall et al., 2011; Meijer et al., 2013). Several kinematic parameters, such as velocity of the assessment tool with respect to the interior of the vehicle, the rebound velocity as a fraction of maximum forward velocity, the kinetic energy of the assessment tool with respect to the interior of the vehicle, change in angle of the upper torso and

displacement of the pelvis, are measured through these tests and plugged into a suitable injury criteria to know if the restraint system succeeded in providing the desired constraining forces and control the excursions of the assessment tool, or if there is a need to enhance the performance by improving the design or deployment strategy of the restraint system (Viano and Arepally, 1990). The results from the studies involving the assessment tools, provide key information on understanding neck and whiplash injuries, which could further help improve the restraint systems (Lawrence et al., 2008). The different tools for evaluation of safety performance of restraints have been described in detail below.

2.2.1 Crash test dummies

Anthropomorphic test devices, ATDs, crash test dummies, are widely used for the development and evaluation of vehicle safety systems. ATDs provide the possibility to perform repeatable high and low impact crash tests, which are of great importance for evaluation of restraint systems in vehicles (Engineering, 2016). ATDs represent the human population only through three different population sizes as of now (Vezin and Verriest, 2005), which limits their biofidelity as well as their potential to provide valid data for the development of integrated safety systems (Crandall et al., 2011). Moreover, ATDs do not include human reflex responses in pre-crash scenarios and are stiffer compared to human beings, which results in a stiffer response during development and evaluation of vehicle safety systems (Seacrist et al., 2010).

2.2.2 Human cadavers

Post-mortem human surrogates, PMHS, or human cadavers, have been used in a wide range of scenarios for improvement of occupant safety, such as development of restraint systems as well as improvement of external vehicle structures, considering safety aspects of vulnerable road users such as cyclists and pedestrians, as they are a human specimen and have anatomical and physiological features in close resemblance of a living human. However, cadavers lack some representation of the living tissues that could have otherwise yielded a different response, which is one major drawback towards working with them (Crandall et al., 2011). Cadavers also produce a higher average maximum force in tensed muscles of lower extremities in low impact crashes compared to human volunteers, which indicates that they lack biofidelity (Iwamoto et al., 2012). High costs and complexity can be expected in test scenarios with cadavers, because the testing of tissues require extensive protocols as they can be biohazardous, and procedural guidelines need to be followed with respect to the handling of the tissues. Another important aspect that must be taken into consideration, is the ethical aspects as well as the public acceptance of the usage of cadavers for test scenarios (Crandall et al., 2011).

2.2.3 Human volunteers

Low impact crash tests with human volunteers can be used for development and evaluation of vehicle restraint systems in pre-crash scenarios (Engineering, 2016).

It has been shown that the response of a human volunteer in low impact crashes is different from that of the dummies and cadavers, which indicates the importance of biofidelic tools for assessment of restraint systems (Iwamoto et al., 2012). However, it is impossible to risk a human life in high impact crash testing and thus crash test dummies and human cadavers play a major role in overcoming this problem (Engineering, 2016). When using human volunteers in laboratory studies and epidemiologic studies, all ethical and legal standards need to be followed by development of extensive protocols regarding protection of the human volunteers welfare and rights (Crandall et al., 2011).

2.2.4 Finite element human body models

In order to overcome the drawbacks of crash tests with anthropomorphic test devices, human cadavers and human volunteers, numerical finite element (FE) human body models (HBMs) have been developed. In the recent years, the automotive industry distinctly increased the usage of FE HBMs for development of passive, active as well as integrated safety systems (Fressmann et al., 2007). Although they involve high computational cost (Crandall et al., 2011), they are excellent means of reconstructing the crash scenarios and studying the injury mechanisms in humans, thereby providing a positive impetus to the development of safety systems (Belwadi, 2011).

THUMS, or Total Human Model for Safety, is a numerical FE model that represents a 50th percentile American male and has been developed by Toyota Motor Corporation for initiating studies on crash scenarios, occupant kinematics and injury mechanisms (Fressmann et al., 2007). However, a shortcoming that could alter the response compared to a human volunteer and thereby affect the development of restraint systems, is the absence of neuromuscular activity in dummies, cadavers and FE HBMs (Engineering, 2016). In order to overcome the drawbacks of the crash tests, which are expensive and time consuming, as well as the dummies, cadavers and FE HBMs, numerical HBMs with active musculature are being developed and implemented (Crandall et al., 2011; Vezin and Verriest, 2005; Östh et al., 2015b).

2.2.5 Finite element active human body models

To mimc the response of a human being in crash scenarios, FE HBMs with active muscles have been developed. The active HBM resembles the human being in a way that ATDs, human cadavers and HBMs can not achieve as they lack muscle reflex activity and neuromuscular control (Crandall et al., 2011; Vezin and Verriest, 2005; Östh et al., 2015b). The active HBM can be used in high as well as low impact crash testing, and is repeatable, reproducible, biofidelic as well as robust. Active HBMs constitute the possibility to analyze the muscle activity in pre- and in-crash scenarios, which can improve the development of restraint systems and safety aspects of the vehicle interior design as well as implementation of active safety systems (Meijer et al., 2013).

2.3 Aspects to be considered for modelling active muscles in finite element human body models

The AHBM has been developed with the aim to resemble the human being in crash test scenarios. It is therefore of great importance to understand the muscle morphology and physiology as well as the neuromuscular control, for a robust and biofidelic implementation of muscles in the HBMs (Meijer et al., 2013).

2.3.1 Muscle morphology and physiology

The muscle is a soft tissue that consists of several fibers. The smallest contractile element of a muscle is called a sarcomere that is comprised of two proteins, namely actin and myosin (Marieb, 2001). The chain of interconnected sarcomeres forms the myofibril, which is surrounded by a layer of connective tissue called endomysium. Several myofibrils make up a muscle fibre and the tissue interwoven between these fibres is the perimysium. There are several bundles of these muscle fibres that unite to form a muscle, which in turn is surrounded by another layer of connective tissue called the epimysium (Nigg and Herzog, 2007). Actin is a globular protein with a double stranded helical structure. Actin filaments, or alternatively known as thin filaments, have a variable length. The other constituents that are bound to the actin filaments in their relaxed state are tropomyosin and troponin C. Tropomyosin is spread over several actin subunits and occludes the myosin binding sites. Myosin molecules consist of two identical chains with projecting globular heads, which are responsible for enzymatic activity as well as actin binding (Jones and Round, 1990; Tsianos and Loeb, 2013).

When the muscle is activated through motor neurons, there is a release of calcium into the sarcomeres. Tropomyosin undergoes a conformational change through the binding of a calcium-troponin C complex. This allows myosin to bind to actin, resulting in the formation of cross bridges and subsequent sliding of the actin filaments towards the center of the sarcomere, known as sliding filament theory, thus causing contraction of the muscle as shown in Figure 2.1 (Jones and Round, 1990; Tsianos and Loeb, 2013). The metabolic energy required to bend the myosin head to be able to link it to actin, is provided by ATP molecules, which are further replenished through oxidative catabolism of glucose and fatty acids in the mitochondria. In order to let the muscle reach its relaxed state, the calcium is pumped out of the sarcoplasm through ATP, thereby preventing cross bridge formation (Tsianos and Loeb, 2013).

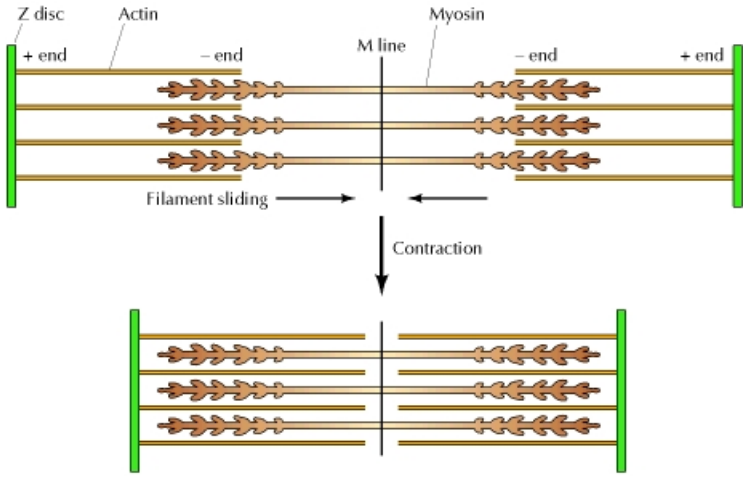

Figure 2.1: The process of contraction occurring in muscles through the sliding filament theory (Cooper, 2000).

2.3.2 Neuromuscular control

There are two parts to a peripheral nervous system (PNS) - namely motor division and the sensory division. The sensory division is responsible for sensing information and relaying it to the units of the central nervous system (CNS) - brain and spinal cord. The proprioceptors are an essential sensory system that react to changes in the muscle parameters and provide information about the position of limbs to the CNS (Marieb, 2001; Marieb and Hoehn, 2010). A neural signal is generated in the CNS in the form of an action potential. Henceforth, the signal is transferred between adjacent interneurons and subsequently to the neurons of the motor division through chemical substances known as neurotransmitters, which are released in the synapses between the neurons (Marieb, 2001; Marieb and Hoehn, 2010). Thus it takes a while for the signal to travel through the chemical synapse, a delay is associated with the neural signal (Marieb and Hoehn, 2010).

The propagation of action potential through a muscle fibre is controlled by the flux of sodium and potassium ions, which further aids in the release of calcium ions in the fibre that initiates the actin-filament binding for contraction (Marieb and Hoehn, 2010). The amount of activation of the muscles is representative of the neural signal provided by the CNS, and depends on the deviation of the limbs from their reference position, which the CNS tries to maintain through a closed loop feedback mechanism (De Vlugt et al., 2006). Muscle activation initiation through closed loop control, occurs when there exists a disturbance in the body (De Vlugt et al., 2006). CNS makes good use of prior knowledge to implement control. For instance, for the control of single-segment system, information about inertial load is utilized to modulate the amplitude and duration of muscle activation patterns. Whereas on multi-segment systems, information about intersegmental dynamics comes into play to generate coordinated movements (Abbas, 2015).

2.4 Modelling active muscles with Hill type elements in Finite Element HBM

Hill made an attempt, through thermodynamic measurements, to ascertain the muscle lengthening and shortening energy relations, and thereby the original Hill muscle model became established in 1939 (Hill, 1938). However, the original Hill muscle model was insufficient, particularly when individual forces were determined in distinct muscle elements of a single muscle as well as when transient replications of a muscle were performed. Nevertheless, the Hill muscle model continued to remain one of the most utilized muscle models (Winters, 1990).

The Hill model, see Figure 2.2, consists of two main parts, a representation of the active muscle force part together with a passive muscle force part. The active muscle force is modelled as a parallel contractile element (CE) and represents the function of the sarcomeres. The passive muscle force consist of two components, the parallel elastic element (PE) and the parallel viscous (damping) element (DE), which represents the passive function of the muscle and its encompassing tissue (Winters, 1990; Hill, 1938; Winter, 2009). An alternative option to the Hill model is to include the series elastic element (SE) modelled as a spring, which would represent the passive properties of the tendon (Zajac, 1989).

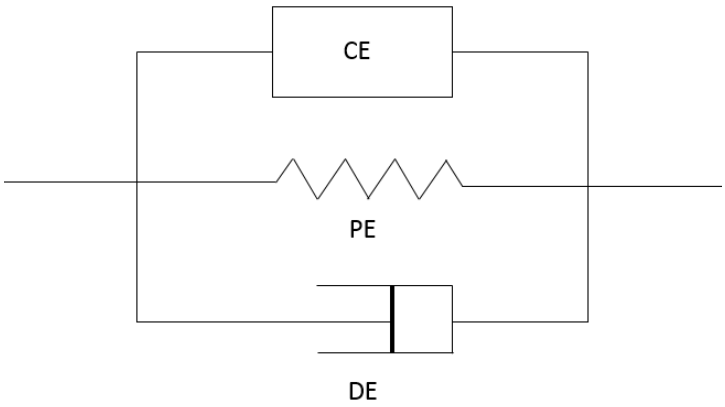

Figure 2.2: The Hill model, where CE represents the parallel contractile element, the active muscle force, PE represents the parallel elastic element and DE represents the parallel viscous (damping) element, which are the passive muscle components.

As mentioned above, the total muscle force (F_M) in the Hill model includes both the active muscle force (F_{CE}) and the passive muscle force (F_{PE}), as can be seen in Equation 2.1 (Wittek and Kajzer, 1997).

$$F_M = F_{CE} + F_{PE} = (\sigma_{CE} + \sigma_{PE} + \sigma_{DE})PCSA \tag{2.1}$$

Where σ_{CE} represents the stress generated in CE, σ_{PE} the stress generated in PE, σ_{DE} the viscous stress in DE, and PCSA the physiological cross sectional area of

the muscle (Hill, 1938; Zajac, 1989). The active muscle force depends upon several factors, such as the activation state ($N_a(t)$), the force-length relation ($f_l(l)$), the force-velocity relation ($f_v(v)$) as well as on the maximum stress (σ_{max}) of the muscle, see Equation 2.2. As can be seen in Equation 2.3 the force-length relation is based on the muscle length, at the instantaneous moment (l), and at the optimal muscle length (l_{opt}), as well as on the contraction rate shape curve (C_{sh}). The normalized rate of muscle contraction (v), which depends on the muscle shortening velocity (V), the maximum muscle shortening velocity (V_{max}), as well as the curve shape parameters (C_{sh}, C_{mvl}, C_{lng}) impacts the force-velocity relation, as seen in Equation 2.4 (Zajac, 1989; Wittek and Kajzer, 1997). The rate of lengthening and the rate of shortening of the muscle rely on the amount of connected actin-myosin bridges. The maximum amount of connected actin-myosin bridges is achieved at the optimal muscle length, and there is more muscle elongation at lower amount of connected actin-myosin bridges (Winter, 2009).

$$\sigma_{CE} = N_a(t) f_l(l) f_v(v) \sigma_{max} \tag{2.2}$$

$$f_l(l) = e^{-\left[\left(\frac{l}{l_{opt}}-1\right)/C_{sh}\right]^2} \tag{2.3}$$

$$f_v(v) = \begin{cases} 0 & \text{if } v \leq -1 \\ \frac{(1+v)}{\left(1-\frac{v}{C_{sh}}\right)} & \text{if } -1 < v \leq 0, \quad v = V/V_{max} \\ \frac{\left[1+v\left(\frac{C_{mvl}}{C_{lng}}\right)\right]}{\left(1+\frac{v}{C_{lng}}\right)} & \text{if } v > 0 \end{cases} \tag{2.4}$$

As mentioned above, the passive muscle force includes both the parallel elastic element (σ_{PE}), which is based on the current muscle length, and the parallel viscous element (σ_{DE}), as can be seen in Equations 2.5 and 2.6 (Wittek and Kajzer, 1997; Wittek et al., 2000).

$$\sigma_{PE} = \left(\frac{\sigma_{max}}{[e^{C_{PE}} - 1]}\right)\left(e^{\left[\left(\frac{C_{PE}}{PE_{max}}\right)\left(\frac{l}{l_{opt}}-1\right)\right]} - 1\right) \tag{2.5}$$

$$\sigma_{DE} = \left(\frac{D}{l_{opt}}\right) v \tag{2.6}$$

The force-length relation as well as the force-velocity relation of the muscle impacts the passive and the active muscle forces in the Hill model, which can be seen in Figure 2.3. The used Hill muscle model parameters in equation 2.1-2.6 are explained in Table 2.1 (Wittek and Kajzer, 1997; Wittek et al., 2000; Zajac, 1989; Hill, 1938).

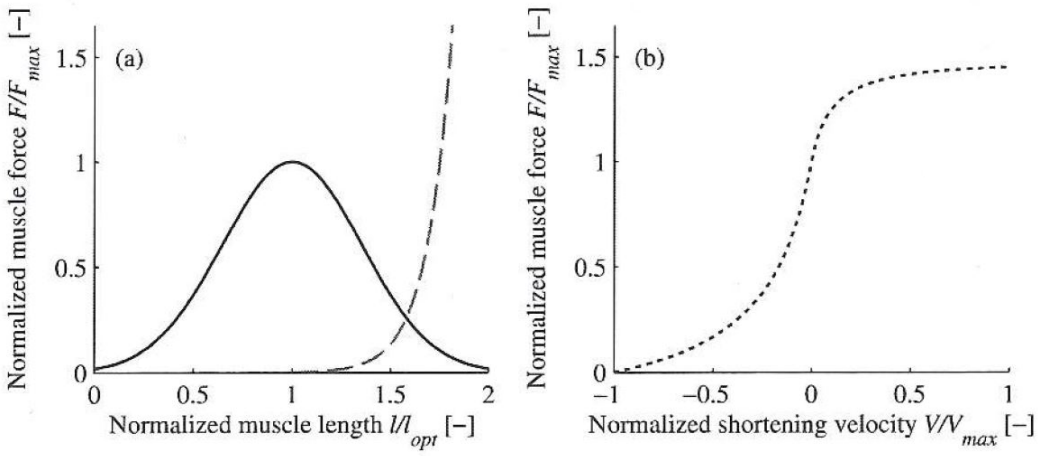

Figure 2.3: The solid line represents the active muscle force-length relation, the dotted line represents the active muscle force-velocity relation, and the dashed line represents the passive muscle force-length relation in the Hill muscle model adopted from Östh (2014).

Table 2.1: Hill muscle model parameters.

Hill muscle model parameters	
$PCSA$	Physiological cross sectional area
F_M	Total muscle force
F_{CE}	Force generated in the parallel contractile element
F_{PE}	Force generated in the parallel elastic element
σ_{max}	Maximum muscle stress
σ_{CE}	Stress generated in the parallel contractile element
σ_{PE}	Stress generated in the parallel elastic element
σ_{DE}	Viscous stress in the parallel elastic element
$N_a(t)$	Activation state
$f_l(l)$	Force-length relation
$f_v(v)$	Force-velocity relation
v	Instantaneous rate of muscle contraction
V	Muscle shortening velocity
V_{max}	Maximum muscle shortening velocity
l	Instantaneous muscle length
l_{opt}	Optimal muscle length for maximum isometric muscle contraction
C_{sh}	Shape of contraction rate curve for concentric muscle shortening
C_{mvl}	Asymptotic value for increased eccentric muscle elongation
C_{lng}	Transition between eccentric and concentric muscle shortening
C_{PE}	Passive elastic muscle stiffness
PE_{max}	Maximum passive elastic element force estimated at l_{opt}
D	Passive viscous muscle stiffness

2.5 Relevance of using a PID controller in human body models to represent neuromuscular control

Human body models (HBMs) can replicate the motion of human beings only when the right control strategy is setup for the model. PID controllers are feasible and can be implemented with ease. The input that is considered is the error signal, which is based on the difference between the reference and the current state of the model in time and space. The output is a control signal that helps the model achieve its reference state. Hence, a PID controller acts like a black box. The gain parameters of a PID controller can be easily tuned as per the requirements of the system. These parameters, namely proportional gain k_p, integral gain k_i and differential gain k_d help in reducing and eliminating the error and overshoot of the error signal, which is an excellent means of restoring the original position of the model (Cominos and Munro, 2002). Moreover, it can be easily executed in a feedback loop, which constantly updates the error signal with respect to the position of the model at that time instant, and also takes into account a delay for the control which is similar to the neural delay in human. This mimics the neuromuscular control that is present in human beings and hence is effective when considered for the control of human body models (Östh, 2014).

2.6 Importance of head and neck muscles in the active human body model

A particular study conducted on human cadavers by Macnab (1973) has revealed that whiplash injuries are more common in rear end collisions with low speeds as compared to high speeds. The pelvis of the driver moves forward on the seat and the forces generated in the neck due to the motion at that time instant is reduced. Since the motion is higher in case of high speed collisions, the whiplash effect is smaller. This study was well supported by another study conducted by Emori and Horiguchi (1990) on anthropomorphic test dummies in low speed collisions. Another study by Mertz and Patrick (1967) on human volunteers and cadavers through sled tests, checked the influence of headrests on the cervical spine when loaded, and it was observed that the injury level is higher when the head was at a smaller distance from the restraint. These studies indicate the importance of studying the activation patterns of the cervical muscles in low speed collisions when the whiplash effect is higher. It is essential to know how the muscles affect the kinematics of the cervical spine in pre-crash and crash scenarios. This biomechanical study can help in development of restraint systems and the interior of the vehicles in a better way to reduce the whiplash effect.

2.7 Role of model-specific isometric muscle recruitment in the active human body model

Isometric muscle contraction occurs when a force is produced in the muscle without any change in the length of the muscle as well as without any kind of movement around a joint (Schneck, 1992). There is a balance of internal and external torques acting on the muscle (Tsai et al., 2014). Maximum isometric force is produced in a muscle when there is complete overlap between actin and myosin filaments, at the optimum length of the sarcomeres, resulting in the formation of maximum number of cross bridges (Herzog, 2014). Isometric contractions result in lower and slower energy expenditure as compared to concentric and eccentric muscle contractions (Hawkins and Molé, 1997).

Human volunteers are required for maximum voluntary contraction (MVC) in isometric experimental setups, resulting in high costs regarding legal aspects, welfare of the human being as well as costs regarding the equipment, as described in Section 2.2.3 (Crandall et al., 2011; Siegmund et al., 2007). In order to avoid the major drawbacks with the experimental setups, model-specific isometric muscle recruitment patterns in the AHBM could be obtained, which provides the opportunity to avoid the dependency of the existing limited test data from human volunteers, and resulting in repeatable cost-efficient test setups (de Bruijn et al., 2016; Siegmund et al., 2007; Meijer et al., 2013; Östh et al., 2015b).

2.8 Techniques used for optimizing muscle recruitment in human body models

A particular study accounted for the optimization of the neck muscle activation scheme while maintaining a stable upright posture under the influence of gravity, for 6 and 10 year old pediatric models and adult models (Dibb et al., 2013). Linear surface optimization was performed by varying the activation level α from 0 to 1 for 22 muscle pairs through Latin hypercube point selection, for 35 experiments per iteration. Optimization problems were defined for both relaxed and tensed activation state (Dibb et al., 2013).

In case of the relaxed state that represented an unaware subject, optimization was about minimizing the muscle fatigue, which was defined as the sum of squares of the ratio of muscle force to maximum muscle force, as shown in equation 2.7 (Pedotti et al., 1978).

$$min\ f(\alpha) = \sum_{i=1}^{22} \left(\frac{F_i}{F_{max,i}} \right)^2 = \sum_{i=1}^{22} \alpha^2 \tag{2.7}$$

This particular optimization was restricted to positive muscle forces and allowed a maximum of 0.5 mm displacement of anteroposterior head center of gravity as well as 0.3° head rotation. Initial activation level was chosen to be 0.15, a lower bound of 0.0001 and an upper bound of 0.25 were used. There were no initial translational

and rotational velocities in all directions for the model (Dibb et al., 2013).

In case of the tensed state, which represented an aware subject, optimization was about maximizing the total muscle force, which has been shown below in Equation 2.8 (Dibb et al., 2013).

$$max\ f(\alpha) = \sum_{i=1}^{22} F_i \tag{2.8}$$

This particular optimization was restricted to positive muscle forces and allowed a maximum of 1 mm displacement of anteroposterior head center of gravity as well as 0.6° head rotation. Initial activation level was chosen to be 0.75, a lower bound of 0.0001 and an upper bound of 1 were used. There were no initial translational and rotational velocities in all directions for the model (Dibb et al., 2013).

It was observed that the optimized activation states under both relaxed and tensed conditions were able to maintain the upright position of the head and neck. The displacement and rotation of the head center of gravity fell within the specified range. The muscle activations caused compression of the cervical spine. Muscles in the tensed state produced a force that was roughly 32 times the force produced by muscles in the relaxed state (Dibb et al., 2013).

Another study, by Toosizadeh and Haghpanahi (2011), implemented an optimization algorithm that involved minimizing the summation of cubed stresses in the muscles of the cervix. The cost function associated with it has been shown below in Equation 2.9 (Toosizadeh and Haghpanahi, 2011).

$$Cost = \sum_{i=1}^{n} \left(\frac{F_i}{A_i}\right) \tag{2.9}$$

A_i is the physiological cross section area of the i^{th} muscle. Constraints laid on the optimization process have been shown below in Equation 2.10 (Toosizadeh and Haghpanahi, 2011).

$$\begin{cases} F_i > 0 \\ \frac{F_i}{A_i} < S \end{cases} \tag{2.10}$$

These constraints were in place to ensure that the muscles only generate positive forces, and that the muscle stress does not exceed the permissible stress S, which was fixed at 100 Ncm^{-1}. CATIA optimization toolbox was used for the optimization problem. Optimization resulted in asymmetric flexion and extension with respect to the magnitude of rotational stiffness, which was higher for extension as compared to flexion (Toosizadeh and Haghpanahi, 2011). Previous studies of the same setup had reported similar results (Panjabi et al., 1988). Posterior muscles like sternocleidomastoid and scalenes contributed majorly towards flexion whereas anterior muscle like longus colli, trapezius and splenius capitis had an enhanced force generated in extension. Muscles like semispinalis capitis and longus capitis assisted in reducing the lower joint reaction forces, and played a key role in stabilization of the head and neck posture (Toosizadeh and Haghpanahi, 2011).

3

Review of studies on cervical muscles

Human volunteers have been used in experimental setups, where their cervical muscle activity has been measured in dynamic and isometric conditions using EMG. The influence of muscle activity on the kinematics of the vehicle occupants have been studied in pre-crash and in-crash scenarios, and have been described in Sections 3.1 and 3.2. The obtained data from these studies have been used for validation of results obtained from this project. Section 3.3 describes an FE HBM optimization setup, where the isometric strength of neck muscles was measured, which was the baseline for setting up the optimization setup in this study. Further, Section 3.4 highlights the use of a 3 DOF PID controller in a human head and neck model, which provides a subtle motivation towards developing a 3 DOF PID controller for the Chalmers AHBM as part of this project.

3.1 Cervical muscle activation patterns derived from a dynamic sled test on human volunteers

Ólafsdóttir et al. (2015) conducted a study to obtain spatial tuning patterns of cervical muscles, representing their recruitment in specific directions in a dynamic load case for the development and validation of the active human body model (AHBM). This study included 8 participants (2 females and 6 males). The participants were seated without any restraints in a sled mounted car. They were initially asked to exert maximum possible force under isometric conditions in 8 directions, beginning with the direction in which the participants were faced and followed by 45° intervals in the transverse plane. The resultant MVC was recorded for the muscles using electromyography (EMG). The participants were then subjected to low speed perturbations in the same directions. The reflex muscle activity was measured using EMG after the perturbations, and reported as fractions of MVC.

Results showed that muscle contraction is both direction-specific as well as muscle-specific for volunteers in low-speed crashes. For instance, the sternocleidomastoid muscle had a strong directional preference towards the direction forward (0°), along with a low contribution to cervical extension and posterolateral extension to the contralateral side. Knowing the fact that the main function of the sternohyoid muscle is to depress the hyoid bone, see Table 4.2, it was activated in the directions

forward (0°) and forward oblique (±45°), suggesting a possible role in the stabilization of the head. These results were consistent with the isometric data in literature (Vasavada et al., 2001). Therefore, an oversimplification would be made if muscles were grouped into antagonist and agonist groups, for instance, for the AHBM (Ólafsdóttir et al., 2015).

3.2 Cervical muscle activation patterns derived from maximum voluntary contraction tests on human volunteers

3 male subjects participated in a test conducted by (Siegmund et al., 2007). Head was restrained from any kind of motion and a force plate was attached to the head clamp, with the head centered in the transverse plane. The torso was restrained using two taut belts. Subjects were then instructed to apply maximum possible force in 8 directions in the transverse plane, each separated by 45° interval. Visual feedback was provided to the subjects to let them know about the direction and magnitude of their applied force. EMG activity was recorded and normalized with respect to the maximum activity recorded.

Bilateral symmetry was observed for both sternohyoid and multifidus muscles whereas the sternocleidomastoid, trapezius, levator scapulae, splenius capitis, semispinalis capitis and semispinalis cervicis were activated more towards the ipsilateral side. It was noticed that the muscle activation patterns for the 3 subjects were in close resemblance, except for the splenius capitis muscle. The patterns for all muscles except splenius capitis were as well in fine tune with their anatomical position with respect to the spine. Splenius capitis was involved in lateral and anterolateral flexion inspite of its location on the posterior side of the spine.

In a similar study by Gabriel et al. (2004) wherein 18 subjects with clamped heads were asked to apply maximum force in 12 directions, starting with the direction in which the participants were faced and followed by 30° intervals in the clockwise direction, it was observed that there was no bilateral symmetry as was expected in the extension direction. Maximum extension force was oriented towards the right side of the body. The sternocleidomastoid muscle displayed maximum activity in the direction of right lateral bending, implying that it is an agonist for static contractions when flexion force was applied. It acted as a synergist in case of lateral bending, and antagonist function associated with extension force was negligible. The scalenus muscle deviated from bilateral symmetry with right side having a maximum activity in the direction of anterolateral flexion and left side having the same in the direction of posterolateral extension. It acted as an agonist for static contractions in both extension and lateral bending and presented certain antagonist activity for flexion. The trapezius muscle showed bilateral symmetry in contrast to the sternocleidomastoid and scalenus muscles, and was observed to be an agonist for static contractions in both extension and lateral bending along with an antagonist activity for flexion.

The semispinalis capitis muscle had the highest asymmetry in terms of activation and displayed agonist activity for static contractions in extension, synergist activity for lateral bending and antagonist activity for flexion.

3.3 Cervical muscle activation patterns derived from an optimization simulation of a human head and neck model in an isometric condition

A particular study was focused on measuring the isometric strength of a dynamic non linear neck model (de Bruijn et al., 2016). The model was linearized to get a static model, thereby reducing the number of optimizations for active muscle recruitment. Linearization was performed in the neutral position with 3D rotational joints located at the instantaneous centers of rotation, thereby nullifying the effect of active muscle recruitment on translation and limiting the degrees of freedom (DOF) to 21 for the 7 joints. The maximum isometric horizontal head forces and head twist moments were estimated using the system equilibrium Equation 3.1 and load sharing Equation 3.2, subjected to minimization of the cost function J as the optimization criteria given in Equation 3.3. An equilibrium around all 7 joints in 3 moment directions was considered for the study, and a tolerance of 1% was allowed on cost function J for obtaining a realistic numerical solution.

$$M_{des} = N \begin{pmatrix} F_{head} \\ M_{head} \end{pmatrix} \tag{3.1}$$

$$M_{des} = F_{CE} \cdot R + M_{pas} \tag{3.2}$$

$$min\ J = 0.5m^k \left(\frac{F_{CE}^k}{PCSA^k} \right) + 0.5m^k \left(\frac{F_{CE}^k}{PCSA^k \cdot \sigma_{max}} \right) \tag{3.3}$$

Here, M_{des} is the matrix composed of the desired neck joint torques. N is the neck moment arm matrix derived from the location of head joints with respect to the center of gravity of the head, F_{head} and M_{head} are the forces and moments acting on the environment through the head center of gravity respectively. F_{CE} is the active force generated by the contractile element of the muscle, R is the muscle moment arm matrix and M_{pas} is the matrix composed of passive moments exerted at the joints. $PCSA$ is the physiological cross section area of the muscle, m is the mass of the muscle segment under consideration and σ_{max} is the maximum isometric stress in the muscle (de Bruijn et al., 2016).

The results from the static model were validated by using the dynamic model. The deviation was observed to be less than 11% for all directions, which confirmed the appropriateness of using a linearized static model in concomitance with the dynamic model (de Bruijn et al., 2016). The obtained maximum transversal head forces and moments were in fine tune with those from the experiments, though the forces in case of extension were higher (Siegmund et al., 2007). The two main reasons for the

deviation given by de Bruijn et al. (2016), are that the model lacks susceptibility to fatigue as well as motivation unlike human volunteers, and vertebral dynamics below T1 was ignored by assuming all joints below T1 to be rigidly connected, which could overestimate the results (de Bruijn et al., 2016).

Full spinal equilibrium resulted in reduction in flexion by 47%, lateral bending by 20%, extension by 4% and axial rotation by 81% when compared to balanced moments around T1-C7 (Nelson et al., 2004). Data for axial rotation turned out to be weaker in relation to the experimental data (Vasavada et al., 2001). It was observed that the trapezius, levator scapulae and rhomboid minor muscles majorly contributed to excessive extension and lateral moment. The values for extension and lateral moment were reduced significantly to 338N and 194N respectively when they were disabled (Siegmund et al., 2007). On the whole, substantial similarity was found with the EMG data, with the exception of the model's splenius capitis muscle where all of the muscle's six segments were primarily active in extension, where the insertion points of the measuring electrodes in case of experiment could influence the results conducted by Siegmund et al. (2007).

3.4 Implementation of a PID controller in a human head and neck model to control the cervical muscle activity

Nemirovsky and Van Rooij (2010) tried to implement head and neck stability control through the use of three independent PID controllers for the 3 different degrees of freedom - roll, pitch and yaw, of the muscles. A combination of vectors received as outputs from the three PID controllers, representing the 3 different motions, would then act as activation levels to the muscles that would result in their complex rotation, which is theoretically possible when compared to a human being. A single reference position was considered in the study, however, it was shown that different reference positions would not affect the development of the controller. A co-contraction level that did not have a resultant torque on the neck, was used in combination with the 3 PID controllers. The setup was handled through a Variable Contraction Setpoint (VCS), which varied dynamically for sleepy and aware people. Validation was performed using a rear end impact sled test on human volunteers, for the pitch direction.

Through comparison, it was revealed that the controller did not have sufficient time to react quickly, thereby affecting the stabilization control of the head and neck model. When the controller was turned off, an increase in damping of the motion with an increase in co-contraction level was found, thus increasing the similarity with human tests. Although a biofidelic frequency response was observed, it was seen that the controller applied too much control in the lower frequencies when compared to human volunteers. Validation was performed for the pitch direction during the study conducted by Nemirovsky and Van Rooij (2010).

4

Active Human Body Model of Chalmers

In the recent years, development of finite element HBMs with active musculature (AHBM) has been performed, with the aim for the AHBM to be more representative of the human population on a larger scale and to mimic the physiological response of a human being (Meijer et al., 2013; Crandall et al., 2011; Vezin and Verriest, 2005; Östh et al., 2015b). This has been performed by SAFER, where active musculature has been incorporated in the original passive model of THUMS, which could now be referred to as the SAFER Active Human Body Model (AHBM) (Östh, 2014). The head and neck of the AHBM can be seen in Figure 4.1.

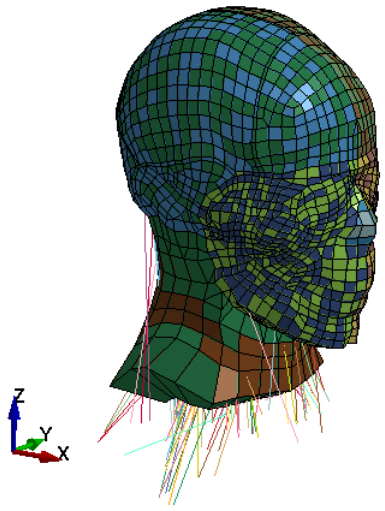

Figure 4.1: Head and neck of the SAFER AHBM used for the project.

Neck muscles, which are of particular interest for the project, have been modelled as beam and discrete elements with material properties derived from literature and experiments using Hill type elements, see Section 2.4. The contacts between the muscles were modelled as nodes tied to the surface. Joints, ligaments, tendons and intervertebral discs have also been appropriately modelled to resemble the human body closely (Fressmann et al., 2007).

4.1 PID control algorithm

A PID controller has been implemented in the AHBM to control the activity of the cervical muscles of the AHBM, and thereby maintain the reference position of the head, which would have deviated from its reference position upon application of load to the AHBM. The PID controller operates through a feedback loop in the AHBM, shown as a block diagram in Figure 4.2. The PID controller takes in the difference of two inputs - the reference position of the head in space, $r(t_n)$, and the time delayed position of the head in space at the particular time instant in the simulation, $y_d(t_n)$, to account for the neural delay observed in humans (Östh, 2014). This difference in between the two inputs is referred to as the error signal, $e(t_n)$, and can be seen in Equation 4.2. The time delayed position of the head, $y_d(t_n)$, has been shown in Equation 4.3. The final control signal produced by the PID controller is based on Equation 4.1 (Östh, 2014; Elliasson and Wass, 2015).

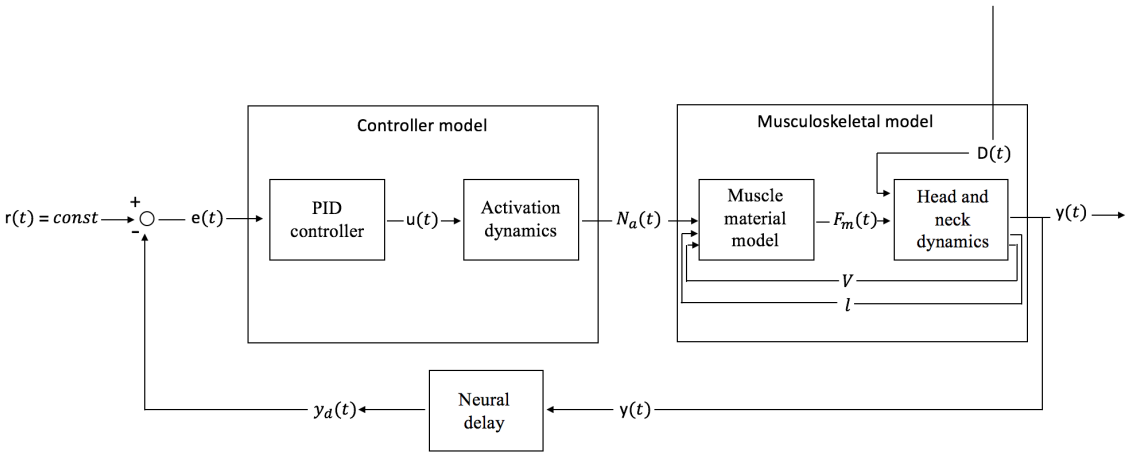

Figure 4.2: AHBM implementation in FE solver, schematic view of the interaction between the controller model and musculoskeletal model.

$$u(t_n) = k_p e(t_n) + k_i \int_{t_0}^{t_n} e(\tau) d\tau + k_d \left(\frac{de(t_n)}{dt} \right) \tag{4.1}$$

$$e(t_n) = r(t_n) - y_d(t_n) \tag{4.2}$$

$$y_d(t_n) = y(t_n) - T_{de} \tag{4.3}$$

The used PID control parameters in Equations 4.1-4.3 are explained in Table 2.1 and 4.1.

Table 4.1: PID control parameters of the AHBM.

PID control parameters	
T_{de}	Neural delay
k_p	Proportional gain
k_i	Integral gain
k_d	Derivative gain
$r(t)$	Reference angle
$e(t)$	Error signal
$u(t)$	Control signal
$y(t)$	Segment signal
$D(t)$	External force
$N_a(t)$	Activation state
$N_e(t)$	Neural excitation

4.2 Muscle activation dynamics

The activation dynamics of the AHBM muscles are described as seen in Equations 4.4-4.5, and modelled in series as two first order low pass filters, where Equation 4.4 represents the first filter and Equation 4.5 represents the second filter (Östh, 2014).

$$T_{ne}\left(\frac{dN_e}{dt}\right) = u_s(t) - N_e(t) \tag{4.4}$$

$$T_{na}\left(\frac{dN_a}{dt}\right) = N_e(t) - N_a(t) \tag{4.5}$$

Where T_{ne} is the time constant for the neural excitation of the muscle, T_{na} is the time constant for the muscle contraction dynamics, and $u_s(t)$ is the scaled control signal of each muscle group in the AHBM. As described in Section 2.3.2, the level of activation and deactivation of the muscles depends on the release and absorption of the calcium ions. The release of calcium ions is more rapid than the absorption of calcium ions, and therefore division of the muscle contraction constant into two is attained, T_{nad} for deactivation and T_{naa} for activation (Östh, 2014).

4.3 Calculation of angle of deviation of head and the projection in transverse plane

The control signal for maintaining the reference position of the head is calculated on the basis of the absolute angle, by which the head deviates when a load acts on the AHBM. In order to calculate the absolute angle of deviation of head, a vector V_1 connecting the node at head center of gravity to the node at thoracic vertebra T1 was defined in space. The absolute angle is then calculated with respect to the vector V_2 connecting the node at head center of gravity at time t=0 to the node at thoracic vertebra T1 at time t=0. This angle, represented by $y(t)$, has been shown

in Equation 4.6 below.

$$y(t) = \cos^{-1}\left(\frac{V_1 \cdot V_2}{|V_1||V_2|}\right) \tag{4.6}$$

The angle of projection of the absolute angle of deviation of head, $\theta(t)$, in the transverse plane, has been calculated as shown in Equation 4.7 below.

$$\theta(t) = \tan^{-1}\left(\frac{D_y}{D_x}\right) \cdot \pi/180 \tag{4.7}$$

Where D_y and D_x represent the displacements of the node at head center of gravity relative to T1 in Y and X directions respectively. The X, Y and Z axis for the AHBM can be seen in Figure 4.1.

4.4 Modelled head and neck muscles in the AHBM.

The included muscles in the AHBM have been listed in Table 4.2 along with their origin, insertion and function.

Table 4.2: Modelled head and neck muscles in the AHBM (Östh, 2014). Ant indicates Anterior Arch, CE Cervical Extension, CF Cervical Flexion, Cl. Clavicula, HB Hyoid Bone, HE Head Extension, HF Head Flexion, LB Lateral Bending, LL Left Muscle Left Axial Rotation, LR Left Muscle Right Axial Rotation, Ma Manubrium, OB Occipital Bone, Axial Rotation, St Sternum, SJ. Sternoclavicular Joint, TC Thyroid Cartilage, AT Anterior Tubercle, MP Mastoid Process, PT Posterior Tubercle, SAP Superior Articular Process, SP Superior Process, TP Transverse Process, and VB Vertebral Body (Marieb, 2001; Rusnak-Smith et al., 2001).

Muscle	Origin	Insertion	Function
Erector spinae longissimus cervicis	TP C2-C6	TP T2-T6	CE, LB, LL
Erector spinae iliocostalis cervicis	PT C4-C6	Rib 4th-6th	CE, LB, LL
Erector spinae longissimus capitis	MP	TP C4-T4	HE, LB, LL
Levator scapulae	TP C1-C4	Scapula	CE, LB, LR
Longus capitis	OB	TP C3-C6	HF, LB, LL
Longus colli superior oblique	Ant C1	TP C3-C5	CF, LB, LL
Longus colli vertical	VB C2-C4	VB C7-T3	CF, LB, LL
Longus colli inferior oblique	TP C5-C6	VB T1-T2	CF, LB, LL
Multifidus cervicis	SP C2-C7	TP C5-T4	CE
Obliquus capitis inferior	TP C1	SP C2	CE, LL
Obliquus capitis superior	OB	TP C1	HE, LB
Rectus capitis anterior	Skull	C1	HF, LB
Rectus capitis lateralis	Skull	C1	HE, LB
Rectus capitis posterior major	OB	Spine of C2	HE, LL
Rectus capitis posterior minor	OB	PT C1	HE
Scalenus anterior	AT C3-C6	1st Rib	CF, LB, LL
Scalenus medius	C2-C7	1st Rib	CF, LB, LL
Scalenus posterior	TP C4-C6	1st Rib	CF, LB, LL
Semispinalis capitis	OB	SAP C4-C7	HE, LR
Semispinalis cervicis	SP C2-C5	TP T1-T4	CE, LR
Semispinalis thoracis	SP C6-C7	TP T5-T6	CE, LR
Splenius capitis	MP	SP C5-T3	HE, LB, LL
Splenius cervicis	TP C1-C3	SP T3-T5	CE, LB, LL
Sternocleidomastoid	MP	Cl & St	HF, LB, LR
Sternohyoid	Ma & SJ	HB	HF
Sternothyroid	Ma & St	HB	HF
Trapezius	Skull	Cl	HE, LR

5
Method

Section 5.1 presents the AHBM implementation in LS-DYNA and in LS-OPT, whereas Section 5.2 describes the test setup for the dynamic AHBM simulation in LS-DYNA. Implementation of 3 DOF PID controller for the head and neck of the AHBM in LS-DYNA has been shown in Section 5.3.

5.1 Optimization for muscle activation

The MVC optimization setup in LS-OPT for the AHBM has been presented in the following sections, where Section 5.1.1 describes the AHBM setup with a discrete beam attached to the skull. The optimization parameters for 9 muscle groups and 13 muscle are shown in Section 5.1.2. Sections 5.1.3-5.1.5 describe the optimization constraints, the optimization criteria and the optimization convergence criteria implemented in LS-OPT, whereas Section 5.1.6 shows the optimization setup of the AHBM in LS-OPT.

5.1.1 AHBM setup in LS-DYNA

In order to simulate maximum voluntary contractions (MVCs) in the AHBM in LS-DYNA, a discrete beam element with a spring stiffness of 10 kN/mm was attached to the head at one of its end. The discrete beam was constrained in all degrees of freedom (DOF) at the other end, keeping the beam approximately parallel to the transverse plane of the AHBM. Considering symmetry of the AHBM around the sagittal plane, five different directions were chosen for orienting the beam element in one half of the transverse plane, 0°, -45°, -90°, -135° and ±180°. The selected point of attachment of discrete beam element on the head of the AHBM, for each of the directions, have been shown in Figures 5.1 and 5.2. Global damping has been used on the AHBM to dampen out the fluctuations during stabilization of the spine. The used damping factor, 0.2618, has been calculated through Equation 5.1 (LSTC, 2001).

$$(D_s)_{critical} = 2\omega_{min} \tag{5.1}$$

Here $(D_s)_{critical}$ is the critical damping factor for the lowest frequency mode of interest and applies to all translational and rotational DOF and ω_{min} is the natural frequency of the system in the unit rad/s, which is obtained from undamped transient analysis of the same system. A simulation time of 300 ms has been chosen for the simulations, as this is the minimum time it would take for the force in the discrete beam element to stabilize (obtained from preliminary tests).

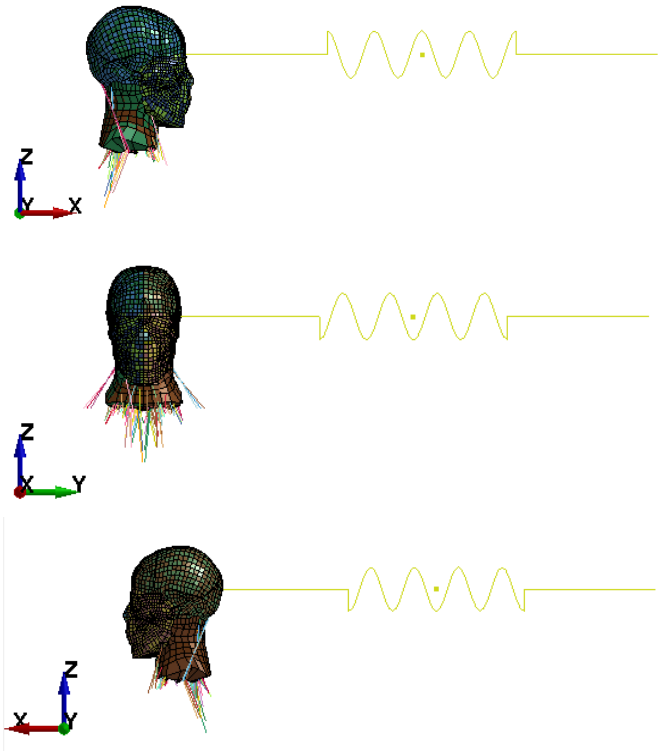

Figure 5.1: Angle of orientation of attached discrete beam to the AHBM for the MVC optimization setup. First figure from the top corresponds to attached discrete beam at -0°, middle figure at -90°, and the bottom figure at ±180°.

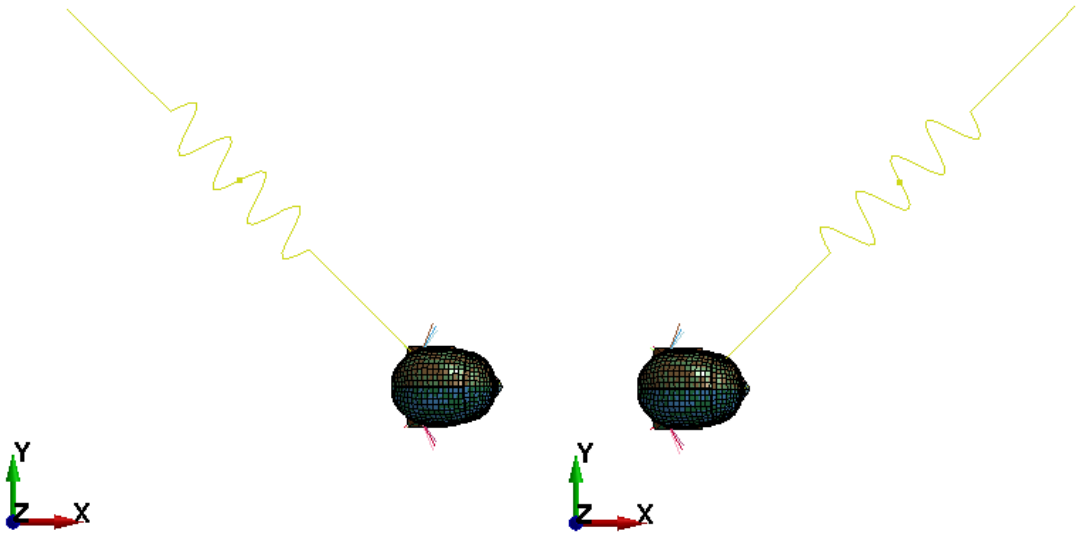

Figure 5.2: Angle of orientation of attached discrete beam to the AHBM for the MVC optimization setup. Left figure corresponds to attached discrete beam at -135°, and the right figure at -45°.

5.1.2 Optimization parameters

The muscles on either side of the sagittal plane (left and right) of the AHBM were initially grouped into 9 groups each, based on the study performed by Ólafsdóttir et al. (2015). Each muscle group on both left and right sides was individually provided with an activation level parameter, which was optimized as part of this study in LS-OPT, thereby accounting for a total of 18 parameters for 9 muscle groups. The parameters for this grouping scheme have been listed in Table 5.1.

Table 5.1: Grouping scheme with 9 muscle groups and 18 parameters for muscle activations (Ólafsdóttir et al., 2015).

Muscle Group	Muscles Involved	Optimization Parameters (Left)	Optimization Parameters (Right)
SCM	Rectus capitis anterior Scalenus posterior Scalenus medius Scalenus anterior Sternocleidomastoid	p1_L	p1_R
STH	Longus colli superior oblique Longus colli vertical Longus colli inferior oblique Longus capitis Sternohyoid Sternothyroid	p2_L	p2_R
LS	Levator scapulae	p3_L	p3_R
Trap	Trapezius	p4_L	p4_R
SCap	Semispinalis capitis Rectus capitis posterior minor Rectus capitis posterior major Obliquus capitis superior	p5_L	p5_R
SCerv	Erector spinae longissimus capitis Erector spinae longissimus cervicis Erector spinae iliocostalis cervicis Semispinalis cervicis Semispinalis thoracis Splenius cervicis	p6_L	p6_R
CM-C4	Multifidus cervicis	p7_L	p7_R
CM-C6	Multifidus cervicis Obliquus capitis inferior Rectus capitis lateralis	p8_L	p8_R
SPL	Splenius capitis	p9_L	p9_R

A new grouping scheme for the muscles was also considered for this study, based on similarity of positioning and functionality of the muscles. The new scheme generated

a total of 13 muscle groups on either side of the sagittal plane, thereby accounting for a total of 26 parameters for activation levels. The parameters for this grouping scheme have been listed in Table 5.2.

Table 5.2: Grouping scheme with 13 muscle groups and 26 parameters for muscle activations.

Muscle Group	Muscles involved	Optimization Parameters (Left)	Optimization Parameters (Right)
SCal	Rectus capitis anterior Scalenus posterior Scalenus medius Scalenus anterior	p1_L	p1_R
STM	Sternocleidomastoid	p2_L	p2_R
LOM	Longus colli superior oblique Longus colli vertical Longus colli inferior oblique Longus capitis	p3_L	p3_R
Ster	Sternohyoid Sternothyroid	p4_L	p4_R
LS	Levator scapulae	p5_L	p5_R
Trap	Trapezius	p6_L	p6_R
SOCap	Semispinalis capitis Obliquus capitis superior	p7_L	p7_R
RCap	Rectus capitis posterior minor Rectus capitis posterior major	p8_L	p8_R
ES	Erector spinae longissimus cervicis Erector spinae iliocostalis cervicis Semispinalis cervicis Semispinalis thoracis Splenius cervicis	p9_L	p9_R
ECap	Erector spinae longissimus capitis	p10_L	p10_R
MCerv	Multifidus cervicis	p11_L	p11_R
ORCap	Obliquus capitis inferior Rectus capitis lateralis	p12_L	p12_R
SPL	Splenius capitis	p13_L	p13_R

5.1.3 Optimization constraints

Maximum voluntary contraction (MVC) requires movement of the head and neck to be kept at minimum. In order to replicate the experimental scenario, constraints were enforced on the model in LS-OPT. The nodes selected from each of the vertebrae from C1-C7, T1 and node corresponding to head center of gravity C0 for applying these constraints, have been shown in Table 5.3. The thoracic vertebra T1

was fixed in all degrees of freedom. All other cervical vertebrae C1 to C7 and head were given a constraint of 10mm in each of X and Y translational DOF, 20mm in z translational DOF, and 10° in each of X, Y and Z rotational DOF.

Table 5.3: Nodes selected for the different parts of the AHBM for applying constraints in LS-OPT

Part of the AHBM	Node selected for applying constraint
Head	43700101
C1	8710001
C2	8710293
C3	8710654
C4	8710876
C5	8711143
C6	8711458
C7	8711776
T1	8910145

5.1.4 Optimization criteria

The optimization criteria was defined as: maximize the objective function, the force in the discrete beam for each direction. The optimized force in the discrete beam is further compared to the experimental average MVC results from the study performed on 3 male subjects by Siegmund et al. (2007), in which the subjects performed MVCs in the same eight directions as simulated in this study. When the discrete beam was attached at 0° on the AHBM, MVC was performed in the direction of extension for the model, ±180°, and thus compared to the MVC value at ± 180° from the study. When the discrete beam was attached at -45°, -90°, -135° and ±180°, comparison was made respectively to the MVC values at 135°, 90°, 45° and 0° from the experimental study.

5.1.5 Optimization convergence criteria

The optimization convergence criteria was defined as: objective function accuracy tolerance of ±1%, which allows the force in the discrete beam to deviate ±1%, as well as a tolerance of ±1% for the activation parameters, and a metamodel accuracy tolerance of ±1%.

5.1.6 Optimization setup in LS-OPT

The overview of the optimization setup for the two cases with 18 parameters and 26 parameters in LS-OPT, is shown in Figures 5.3 and 5.4 respectively. Stage 1 provides the LS-DYNA executable required for running the simulations in LS-OPT, and stores all the parameters to be optimized. The history and response variables, which are the nodal displacements and rotations for the head center of gravity, cervical vertebrae and first thoracic vertebra in the current study are located in stage 1.

The strategy used for optimization was Successive Response Surface Method (SRSM). In this method, a lower and upper bound are set for each of the parameters. Depending on the initial size for the range of the parameters, an optimum is calculated in the design space for parameters, which is centered at the initial values of the parameters, through a response surface. Based on the new optimum and the oscillatory nature of the solution, a new region of interest that is a subset of the design space for parameters is chosen. This updated design space is now centered at the new optimum. Therefore, a sequential domain reduction is carried out in successive iterations in order to reach a converged solution for the parameters being optimized (Stander and Craig, 2002).

Number of simulations per iteration are required to be at least one and a half times the number of parameters, and therefore were set to 40 for the two cases involving 18 and 26 parameters. The optimization metamodel was sampled using a linear polynomial and D-optimal point selection. The optimizations in 0° and ±180° were performed both with and without symmetry about the sagittal plane, wherein muscles on both the left and right sides were given the same activation parameters, thereby reducing the number of parameters for the two cases from 18 and 26 to 9 and 13 respectively. The optimization objective, constraints and convergence criteria have been described in Sections 5.1.4, 5.1.3 and 5.1.5.

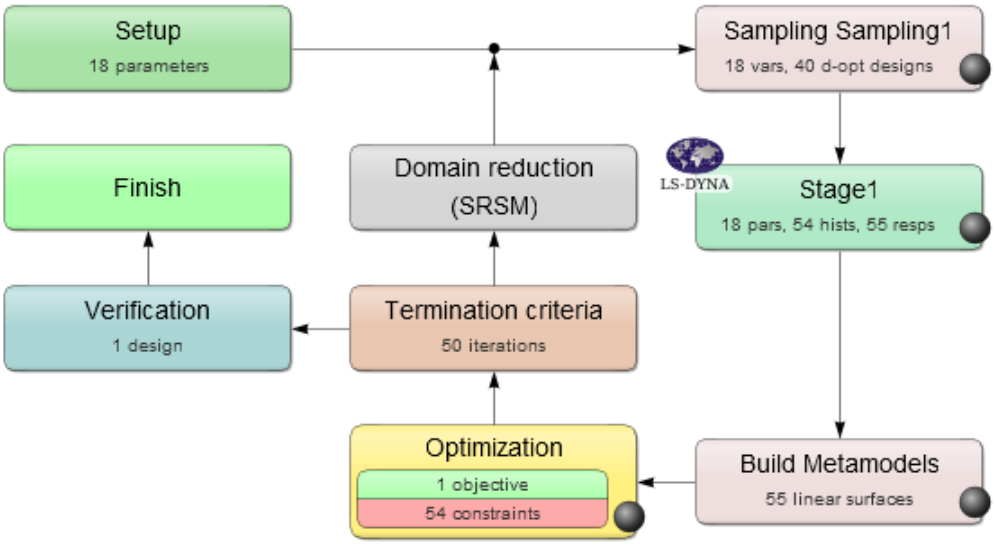

Figure 5.3: Optimization setup in LS-OPT for 18 parameters, 9 muscle groups.

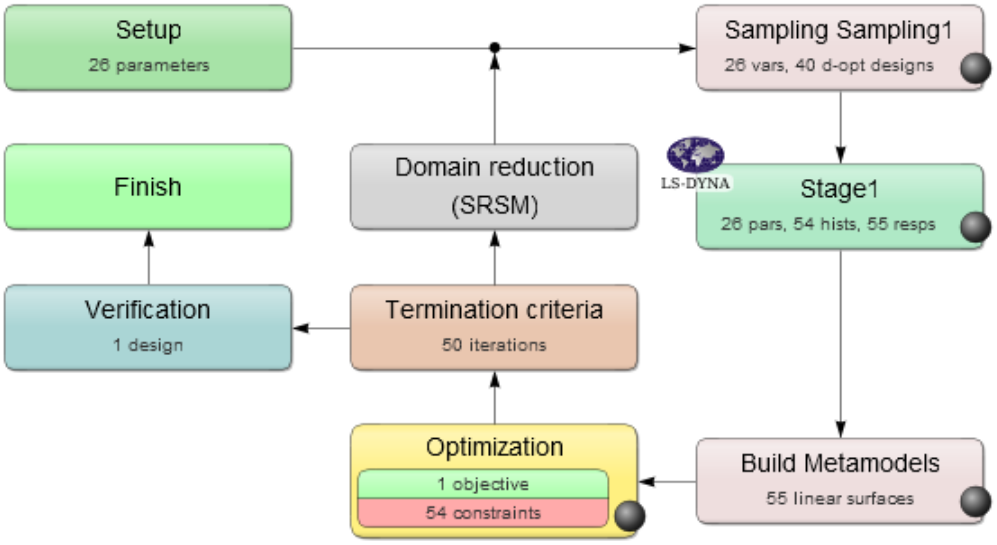

Figure 5.4: Optimization setup in LS-OPT for 26 parameters, 13 muscle groups.

5.2 Dynamic AHBM simulation

In order to evaluate the obtained model specific muscle activation patterns from this isometric study in a dynamic environment, the muscle activation patterns obtained from sled tests on human volunteers in dynamic conditions, were exchanged with the model specific optimized muscle activation patterns. The load considered for testing these patterns in a dynamic condition is gravity in 5 different directions of the transverse plane, which are 0°, 45°, 90°, 135° and 180°. The evaluation and comparison of the model specific muscle activation patterns to the patterns obtained from volunteer experiments was performed on the basis of the resulting kinematics of the AHBM, which included the head displacements as well as head and vertebral rotations around the three global axes, X, Y, and Z axis, for each of the loading directions. The different models considered for dynamic simulations are the passive model with no muscle activation, experimental model with 1 DOF PID controller for 9 muscle groups, experimental model with 3 DOF PID controller for 9 muscle groups, optimization model with 1 DOF PID controller for 9 muscle groups, optimization model with 3 DOF PID controller for 9 muscle groups, optimization model with 1 DOF PID controller for 13 muscle groups and optimization model with 3 DOF PID controller for 13 muscle groups. The results from the different experimental and optimization models have been compared to the passive model to check for muscle activation.

5.3 3 DOF PID controller of the AHBM head and neck

The 1 DOF PID controller implemented by Östh (2014) only utilizes the absolute angle of deviation of the head in space, irrespective of how much the head rotates

around the X, Y or Z axis. This implies that only one control signal is used to control the absolute deviation of the head. In reality, the head of the vehicle occupant undergoes complex kinematics and and in order to mimic this complex motion in an AHBM, it is necessary to control the motion around all 3 axes separately using independent control signals. Thus, a 3 DOF PID controller has been defined for the AHBM in LS-DYNA. The procedure to evaluate angles that are used to calculate the control signals for the 3 motions of the AHBM, which are flexion/extension, lateral bending and axial rotation, has been described in Sections 5.3.1-5.3.2.

5.3.1 Angle calculation in the sagittal and frontal planes

The keyword *DEFINE_CURVE_FUNCTION in LS-DYNA was used to define the angle of projection of the deviation of the head in the sagittal plane. In order to calculate the angle, a vector V_{1xz} between the head center of gravity and the center of the vertebral body of T1 was defined. The angle was then calculated with respect to vector V_{2xz} connecting the node at head center of gravity at time t=0 to the node at thoracic vertebra T1 at time t=0, and thereby projected onto the sagittal plane. The angle, represented by $y_{xz}(t)$, has been shown in equation 5.2 below.

$$y_{xz}(t) = \cos^{-1}\left(\frac{V_{1xz} \cdot V_{2xz}}{|V_{1xz}| \cdot |V_{2xz}|}\right) \tag{5.2}$$

The control signal for the sagittal plane was finally calculated using this angle, as described in Section 4.1.

The angle for frontal plane was calculated in a similar way. See Appendix A.1.1 for detailed implementation specifications in LS-DYNA.

5.3.2 Rotations about X, Y and Z axis

A local coordinate system was defined at the head center of gravity using the *DEFINE_COORDINATE_NODES keyword. The rotational velocities of the head center of gravity were calculated using the WX, WY and WZ functions of the *DEFINE_CURVE_FUNCTION keyword as shown in Equations 5.3, 5.4 and 5.5.

$$\text{Rotational velocity of head center of gravity around X axis} = \text{WX(head center of gravity)} \tag{5.3}$$

$$\text{Rotational velocity of head center of gravity around Y axis} = \text{WY(head center of gravity)} \tag{5.4}$$

$$\text{Rotational velocity of head center of gravity around Z axis} = \text{WZ(head center of gravity)} \tag{5.5}$$

Three dummy nodes were defined at the head center of gravity, and the rotational velocities of the head center of gravity in X, Y and Z directions calculated earlier were prescribed as translational displacements to the 3 nodes respectively using *BOUNDARY_PRESCRIBED_MOTION_NODE keyword. This implied that the

rotational displacement of the head center of gravity at each time instant would be equal to the translational displacements of the dummy nodes in the 3 axes respectively, as shown in Equations 5.6, 5.7 and 5.8.

$$\text{Rotational displacement of head center of gravity around X axis} = \text{Translational displacement of dummy node 1 in Y axis} \tag{5.6}$$

$$\text{Rotational displacement of head center of gravity around Y axis} = \text{Translational displacement of dummy node 2 in Y axis} \tag{5.7}$$

$$\text{Rotational displacement of head center of gravity around Z axis} = \text{Translational displacement of dummy node 3 in Z axis} \tag{5.8}$$

These translational displacements that equalled rotational displacements of the head center of gravity were measured using the DX, DY and DZ functions of the *DEFINE_CURVE_FUNCTION keyword, as shown in Equations 5.9, 5.10 and 5.11.

$$\text{Rotational displacement of head center of gravity around X axis} = \text{DX(dummy node 1)} \tag{5.9}$$

$$\text{Rotational displacement of head center of gravity around Y axis} = \text{DY(dummy node 2)} \tag{5.10}$$

$$\text{Rotational displacement of head center of gravity around Z axis} = \text{DZ(dummy node 3)} \tag{5.11}$$

See Appendix A.1.2 for detailed implementation specifications in LS-DYNA.

5.3.3 Scaling factors for activation levels for muscle groups in axial rotation

The definitions of scaling factors for muscle activations during axial head rotations, presented in Table 5.4 and 5.5, have been based on several criteria, due to lack of experimental data. The individual contribution of each muscle towards rotation of the head and cervical spine have been reviewed in literature, considering the mechanical and anatomical function of each individual muscle. The muscle modelling in the AHBM has been decided by using the muscles cross sectional area as well as the origin and insertion of the muscle beams, as presented in Table 4.2. The scaling factor for muscle activation in axial rotation for the muscle group SCerv has been assigned the value 0.2 for all directions, thus the muscle group contains both left muscles that contribute to left axial rotation and left muscles that contribute to right axial rotation, which balances the muscle activation level for the left side of the muscle group. The same method has been applied for the chosen value of 0.2 for the right SCerv muscle group. The scaling factor for muscle activation in axial rotation for the muscle groups CM-C4 and MCerv have been assigned the value 0.1 for all directions, hence the muscle is involved in stabilization of the cervical spine. The scaling factor for muscle activation in axial rotation for the muscle group Ster has been assigned the value 0 for all directions, because the muscle group is not involved in axial rotation.

Table 5.4: Rotational scaling factors for 9 muscle groups, 18 parameters. LM represents Left muscle, LAR Left axial rotation, RM Right muscle, and RAR Right axial rotation.

Muscle Group	Muscles Involved	LM LAR	LM RAR	RM LAR	RM RAR
SCM	Rectus capitis anterior Scalenus posterior Scalenus medius Scalenus anterior Sternocleidomastoid	0.2	0.7	0.7	0.2
STH	Longus colli superior oblique Longus colli vertical Longus colli inferior oblique Longus capitis Sternohyoid Sternothyroid	0.2	0.1	0.1	0.2
LS	Levator scapulae	0.2	0.4	0.4	0.2
Trap	Trapezius	0.3	0.5	0.5	0.3
SCap	Semispinalis capitis Rectus capitis posterior minor Rectus capitis posterior major Obliquus capitis superior	0.2	0.5	0.5	0.2
SCerv	Erector spinae longissimus capitis Erector spinae longissimus cervicis Erector spinae iliocostalis cervicis Semispinalis cervicis Semispinalis thoracis Splenius cervicis	0.2	0.2	0.2	0.2
CM-C4	Multifidus cervicis	0.1	0.1	0.1	0.1
CM-C6	Multifidus cervicis Obliquus capitis inferior Rectus capitis lateralis	0.2	0.1	0.1	0.2
SPL	Splenius capitis	0.5	0.2	0.2	0.5

Table 5.5: Rotational scaling factors for 13 muscle groups, 26 parameters. LM represents Left muscle, LAR Left axial rotation, RM Right muscle, and RAR Right axial rotation.

Muscle Group	Muscles involved	LM LAR	LM RAR	RM LAR	RM RAR
SCal	Rectus capitis anterior Scalenus posterior Scalenus medius Scalenus anterior	0.3	0.1	0.1	0.3
STM	Sternocleidomastoid	0.2	0.7	0.7	0.2
LOM	Longus colli superior oblique Longus colli vertical Longus colli inferior oblique Longus capitis	0.3	0.1	0.1	0.3
Ster	Sternohyoid Sternothyroid	0.0	0.0	0.0	0.0
LS	Levator scapulae	0.2	0.4	0.4	0.2
Trap	Trapezius	0.3	0.5	0.5	0.3
SOCap	Semispinalis capitis Obliquus capitis superior	0.2	0.5	0.5	0.2
RCap	Rectus capitis posterior minor Rectus capitis posterior major	0.4	0.2	0.2	0.4
ES	Erector spinae longissimus cervicis Erector spinae iliocostalis cervicis Semispinalis cervicis Semispinalis thoracis Splenius cervicis	0.3	0.1	0.1	0.3
ECap	Erector spinae longissimus capitis	0.3	0.1	0.1	0.3
MCerv	Multifidus cervicis	0.1	0.1	0.1	0.1
ORCap	Obliquus capitis inferior Rectus capitis lateralis	0.2	0.1	0.1	0.2
SPL	Splenius capitis	0.5	0.2	0.2	0.5

5.3.4 Algorithm for implementation of 3 DOF PID controller

A 3 DOF PID controller algorithm was implemented in LS-DYNA. The angle calculations in the sagittal plane, frontal plane and the axial rotation have been described in Sections 5.3.1-5.3.2.

The AHBM location in 3D space was identified using the SIGN function of the keyword *DEFINE_CURVE_FUNCTION. The sign of the rotations around the three axes were transferred to a constant curve of ones. If the value of the curve was 1, it showed that the AHBM was on the positive side of the X, Y or Z axis and if the value was -1, it showed that the AHBM was on the negative side of the X, Y or Z axis.

The scaling factors for the sagittal plane, corresponding to 0° and ±180°, and for the frontal plane, corresponding to 90° and -90°, were picked from the muscle group activation patterns in the transverse plane, using the keyword *DEFINE_CURVE_FUNCTION scaling_factor_muscle_of_interest(angle_of_interest). The muscle group activation patterns were defined with the keyword *DEFINE_FUNCTION_TABULATED for each muscle group listed in Table 5.1 and 5.2. The scaling factors for axial rotation, corresponding to left and right axial rotation were used through their definition in the keyword *DEFINE_CURVE, for each muscle group listed in Table 5.4 and 5.5.

Scaling factors for the sagittal plane, frontal plane and axial rotation were picked on the basis of the position of the AHBM in space. An IF function was implemented, using the keyword *DEFINE_CURVE_FUNCTION IF(lcid 1, lcid 2, lcid 3, lcid 4) for the sagittal plane, frontal plane and axial rotation, which assigned the picked scaling factors to curves defined for each muscle group. See Equation 5.12, (LSTC, 2001).

$$IF = \begin{cases} \text{ordinate of lcid 2} & \text{if} \quad \text{ordinate of lcid 1} < 0 \\ \text{ordinate of lcid 3} & \text{if} \quad \text{ordinate of lcid 1} = 0 \\ \text{ordinate of lcid 4} & \text{if} \quad \text{ordinate of lcid 1} > 0 \end{cases} \tag{5.12}$$

For the sagittal plane, the lcid 1 represents the sign obtained from rotation around Y axis, lcid 2 represents the scaling factor for muscle activation at ±180°, and lcid 4 represents scaling factor for muscle activation at 0°. For the frontal plane, the lcid 1 represents the sign obtained from the rotation around X axis, lcid 2 represents the scaling factor for muscle activation at -90°, and lcid 4 represents the scaling factor for muscle activation at 90°. For the rotation about Z axis, the lcid 1 represents the sign obtained from the rotation around Z axis, lcid 2 represents the right axial rotation and lcid 4 represents the left axial rotation.

The scaled control signal for the muscle group is then calculated using the keyword *DEFINE_CURVE_FUNCTION, see Equation 5.13. Muscle activation dynamics is further implemented as described in Section 4.2. See Appendix A.1.4 for detailed

implementation specifications in LS-DYNA.

$$\begin{aligned}\text{Scaled control signal(muscle group)} = MAX(&\text{muscle scaling factor in sagittal plane}* \\ &ABS(\text{control signal in sagittal plane}) + \text{muscle scaling factor in frontal plane}* \\ &ABS(\text{control signal in frontal plane}) + \text{muscle scaling factor for axial rotation}* \\ &ABS(\text{control signal for axial rotation}), \text{co-contraction})\end{aligned} \tag{5.13}$$

6
Results

The optimized MVC muscle activation patterns for the models with 9 muscle groups and 13 muscle groups are presented in Section 6.1. Section 6.2 presents the dynamic spatial tuning patterns for the 5 models; Experimental model with 1 DOF PID controller for 9 muscle groups, Experimental model with 3 DOF PID controller for 9 muscle groups, Optimization model with 1 DOF PID controller for 9 muscle groups, Optimization model with 3 DOF PID controller for 9 muscle groups, and Optimization model with 1 DOF PID controller for 13 muscle groups, whereas Sections 6.2.2 and 6.2.3 present the translational and rotational X, Y and Z displacements for the dynamic simulations.

6.1 Optimization simulation

The obtained muscle activation patterns from the optimization setup for 9 muscle groups and 13 muscle groups are presented in Section 6.1.1 and 6.1.2 respectively.

6.1.1 Muscle activation patterns: 9 muscle groups

Optimized muscle activation patterns for 9 muscle groups, 18 parameters, are presented through polar-plots in Figure 6.2. The corresponding optimized force in the discrete beam is presented in Figure 6.1.

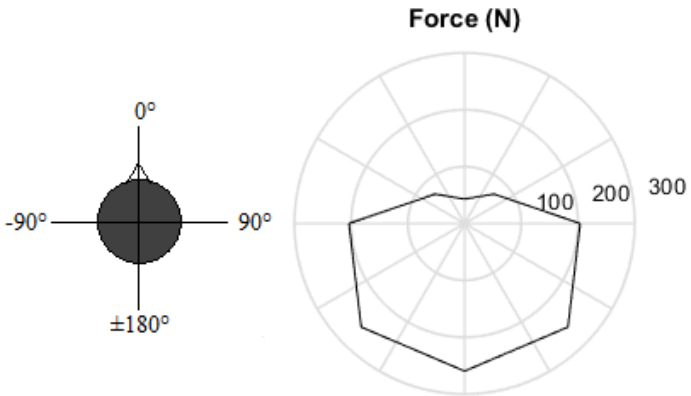

Figure 6.1: Optimized force in the discrete beam for the AHBM with 9 muscle groups.

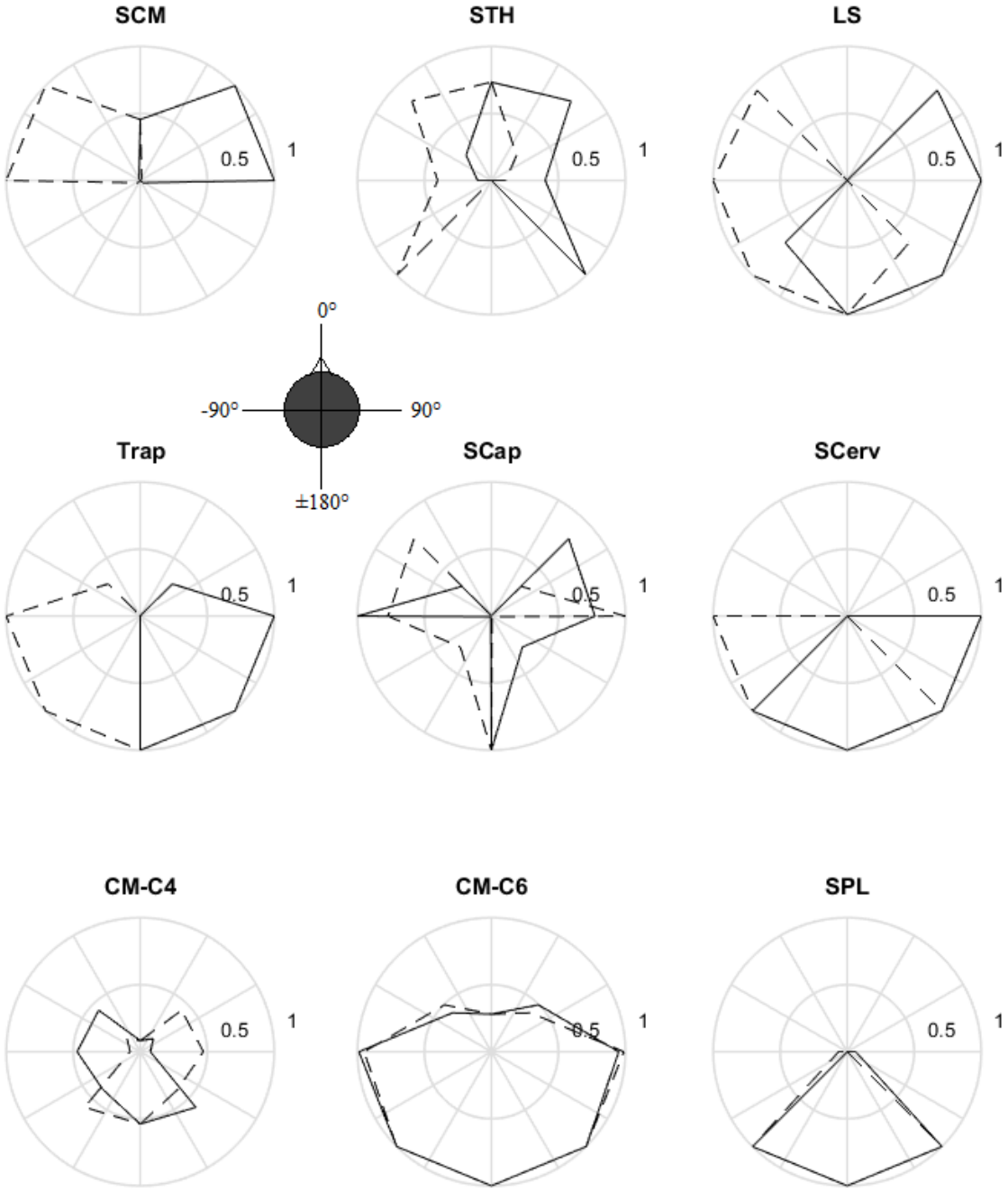

Figure 6.2: Optimized AHBM specific muscle activation patterns for 9 muscle groups. Right muscles represented by solid lines and left muscles by dashed lines, where the angles represent the direction in which the model applies the force.

Results with respect to the left muscle have been presented here. Results for the right muscle were symmetric about the sagittal plane. The groups SCM, STH and CM-C6 were activated to about 50%, 75% and 25% respectively when the model was in flexion, corresponding to the direction of flexion (0°) in Figure 6.2, thereby accounting for a significant contribution to the force in flexion, which was found to be around 50N, as seen in Figure 6.1. The other groups LS, Trap, SCap, Scerv,

CM-C4 and SPL received negligible activations for this particular case. Considering the case of the model being in extension, which corresponds to the direction of extension (±180°) in Figure 6.2, the groups LS, Trap, Scap, Scerv, CM-C6 and SPL were activated maximally to 100% and the group CM-C4 was activated to about 50%, being the major contributers for the force in extension, which was around 250N, as seen in Figure 6.1. No activation was observed in groups SCM and STH. Groups SCM, LS, Trap, Scap and Scerv received full activation in lateral bending whereas group STH was activated to half its maximum capacity for the same case, corresponding to the direction of left lateral bending (-90°) in Figure 6.2, together generating a force of 100N in this direction as seen in Figure 6.1. SPL did not play any role in this direction as it stayed deactivated. For planes other than the sagittal and frontal planes, SCM and LS were fully activated in case of the direction of left anterolateral flexion (-45°) in Figure 6.2, providing a maximum force little over 100N as seen in Figure 6.1, with contributions from STH and Scap that were activated to about 80% and CM-C6 to 50%. Trap also received an activation of roughly 25% in this case. Groups STH, LS, Trap, Scerv, CM-C6 and SPL obtained an activation level of 100% in the direction of left posterolateral extension (-135°) in Figure 6.2, whereas activations of around 50% and 25% were observed in groups CM-C4 and Scap respectively. These groups mutually generated a total force of 250N in the specified direction as seen in Figure 6.1. Muscles that received activation on the other side of the sagittal plane were STH and CM-C4 with about 20% and 40% activations in the direction of right anterolateral flexion (45°) respectively, SCap and CM-C6 receiving full activation in right lateral bending (90°) direction and LS, Scerv and SPL with about 60%, 100% and 100% activations respectively in the direction of right posterolateral extension (135°), as seen in Figure 6.2 .

6.1.2 Muscle activation patterns: 13 muscle groups

Optimized muscle activation patterns for 13 muscle groups, 26 parameters are presented through polar-plots in Figures 6.4-6.5. The corresponding optimized force in the discrete beam is presented in Figure 6.5.

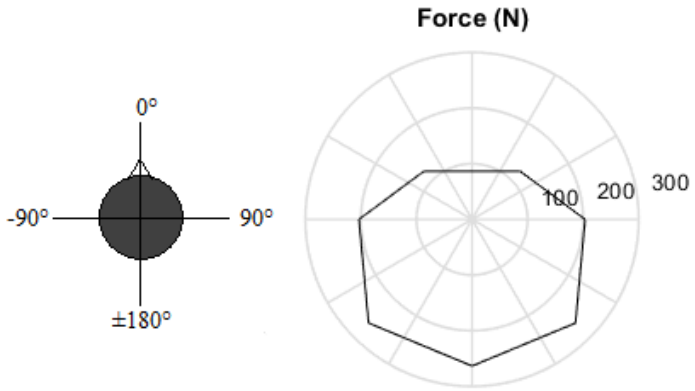

Figure 6.3: Optimized force in the discrete beam for the AHBM with 13 muscle groups.

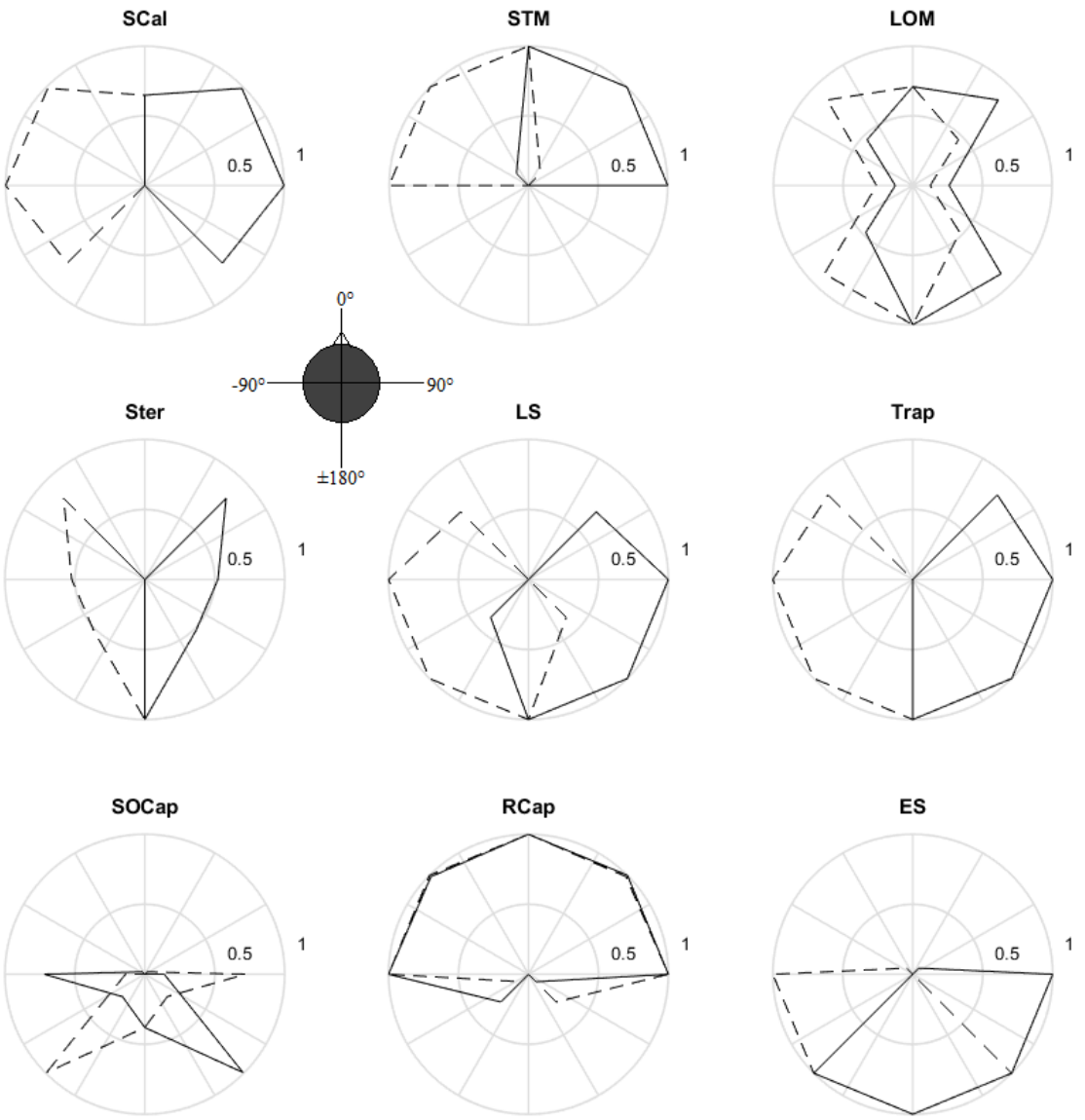

Figure 6.4: Optimized muscle activation patterns for 13 muscle groups. Right muscles represented by solid lines and left muscles by dashed lines, where the angles represent the direction in which the model applies the force.

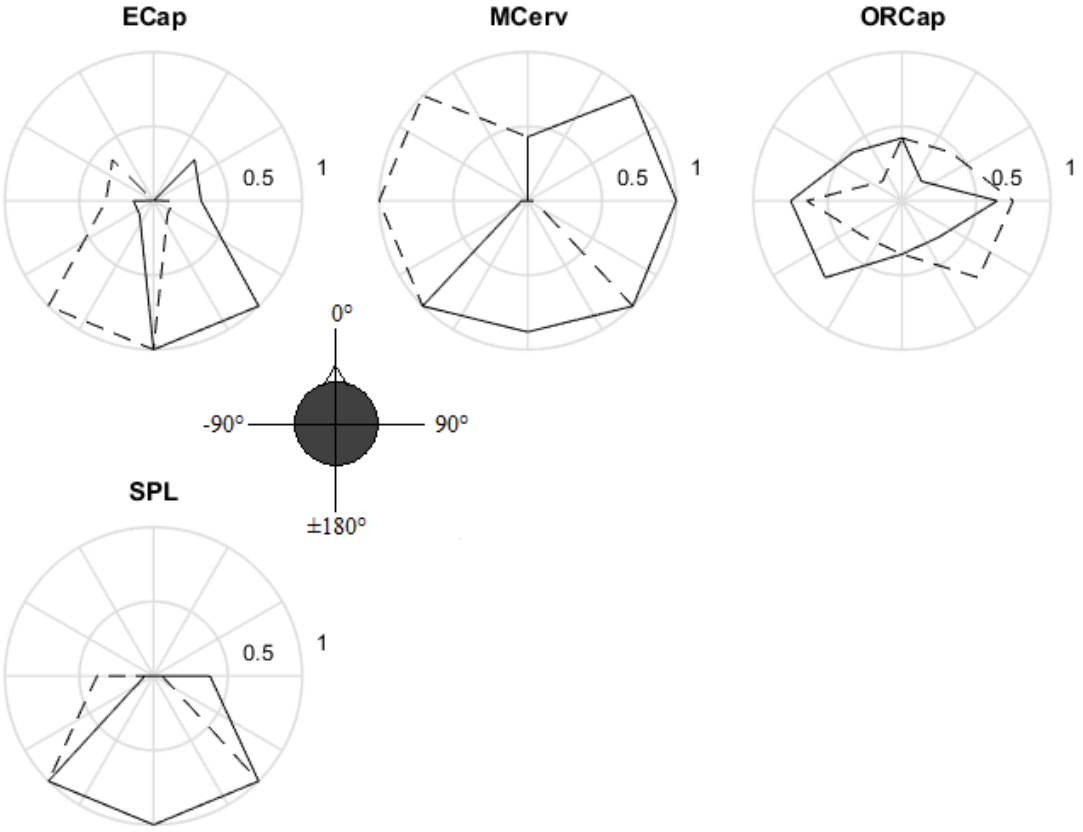

Figure 6.5: Optimized muscle activation patterns for 13 muscle groups. Right muscles represented by solid lines and left muscles by dashed lines, where the angles represent the direction in which the model applies the force.

The stated results are corresponding to the left muscles and symmetrical results were obtained for the right muscles. The groups STM and RCap were fully activated when the model was in flexion (0°), as seen in Figure 6.4, thereby accounting for a significant contribution to the force of 100N, as seen in Figure 6.3. The other contributers to flexion were Scal, LOM, Mcerv and ORCap with roughly 70%, 70%, 50% and 50% respectively, as is seen in Figures 6.4 and 6.5. When the model was in extension (±180°), as seen in Figures 6.4 and 6.5, the groups LOM, Ster, LS, Trap, ES, ECap and SPL were activated maximally to 100%, and the groups SOCap, MCerv and ORCap were activated to about 40%, 90% and 40% respectively. The muscle activation level for Trap in the direction of extension (±180°) has been taken from the optimization simulation with no symmetry around the sagittal plane, due to non-representative results from the optimization simulation considering symmetry. The force in extension was around 250N, as seen in Figure 6.3. No activation towards extension (±180°) was observed in groups SCal, STM and RCap. The muscle activation level for STM in the direction of extension (±180°) has been taken from the optimization simulation with no symmetry around the sagittal plane, due to non-representative results from the optimization simulation considering symmetry. Considering the direction of left lateral bending (-90°), groups SCal, STM, LS, Trap, RCap, ES and MCerv received full activation whereas groups LOM, Ster, SOCap,

Ecap, ORCap and SPL had smaller activations ranging from 20%-60%, as seen in Figures 6.4 and 6.5, together generating a force of 100N for this direction as seen in Figure 6.3. For planes other than the sagittal and frontal planes, SCal, STM, RCap and MCerv were fully activated in case of the direction of left anterolateral flexion (-45°), as seen in Figures 6.4 and 6.5, along with activations in the range of 20%-80% for the groups LOM, Ster, LS, Trap and ORCap, providing a maximum force little over 100N as seen in Figure 6.3. There was negligible activation for the groups SOCap, ES and SPL in this case. Groups LS, Trap, SOCap, ES, ECap, MCerv and SPL obtained an activation level of 100% in the direction of left posterolateral extension (-135°), as seen in Figures 6.4 and 6.5, whereas activations ranged from of 30%-80% in groups Scal, LOM, Ster and ORCap. These groups together produced a total force of 250N in this direction, as is seen in Figure 6.3. The muscles which showed signs of activations on the other side of the sagittal plane were LOM with about 50% activity in both the directions of right anterolateral flexion (45°) and right posterolateral extension (135°), LS with roughly 35% activity in 135°, SOCap and RCap with 70% and 100% activities in the direction of right lateral bending (90°) respectively, ES, MCerv and SPL with full activations in the direction of right posterolateral extension (135°) and ORCap with about 75% activity in the same direction.

6.2 Dynamic AHBM simulation

The dynamic spatial tuning patterns for the different models are presented in Section 6.2.1. The translational displacement of the head center of gravity and the rotational displacements of the head center of gravity, the 4th cervical vertebra (C4) and the 7th cervical vertebra (C7) during the dynamic simulations, for the directions 0°, 45°, 90°, 135° and ±180°, are presented in Section 6.2.2 and 6.2.3 respectively.

6.2.1 Dynamic spatial tuning patterns for the different models

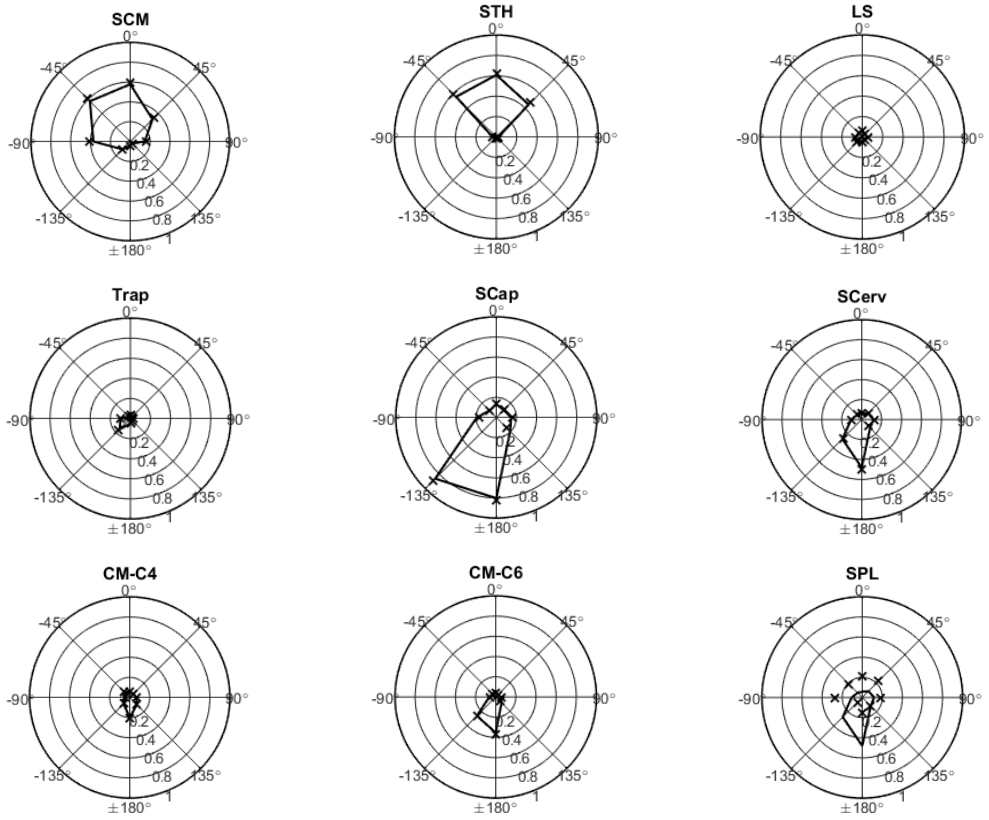

Figure 6.6: Spatial tuning patterns for the experimental model with 1 DOF PID controller for 9 muscle groups, represented through the solid line. The 'x' represents the muscle activation patterns from the experiment, conducted by Ólafsdóttir et al. (2015). Muscle activation level at 110ms after loading onset is presented for the left muscle groups, where the angles represent the direction in which the muscles pull the head to counter the motion due to the load in opposite direction.

The spatial tuning patterns for 9 different groups of muscles using the muscle activation data from the experiment conducted by Ólafsdóttir et al. (2015), and the 1 DOF PID controller, have been shown in Figure 6.6. The SCM group was activated to about 60% in the direction of flexion (0°) and left anterolateral flexion (-45°),

which was the same for STH group in the corresponding directions. Activation level of about 40% was observed in the right anterolateral flexion (45°) direction for both SCM and STH, and the same activation level was observed in the left lateral bending direction for the STH group. These muscles remained highly inactive in the other directions. Negligible activation was observed in both LS and Trap muscle groups. Scap and SCerv groups received activation levels of about 80% and 20% respectively in the left posterolateral extension (-135°) direction, and about 80% and 40% respectively in the direction of extension (±180°). Regarding the other directions for these muscle groups and for all directions of CM-C4 group, activation levels fell below 20%. CM-C6 and SPL had activation patterns similar to SCerv group.

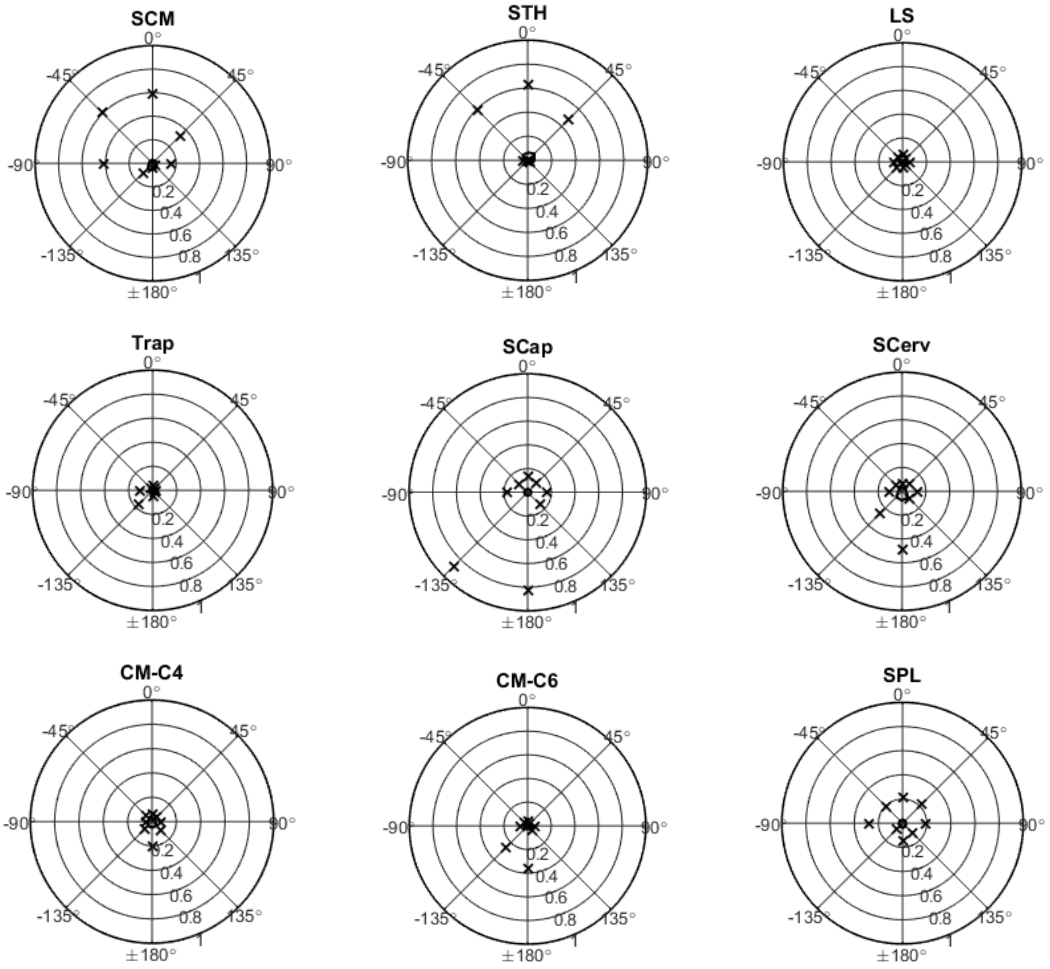

Figure 6.7: Spatial tuning patterns for the experimental model with 3 DOF PID controller for 9 muscle groups, represented through the solid line. The 'x' represents the muscle activation patterns from the experiment conducted by Ólafsdóttir et al. (2015). Muscle activation level at 110ms after loading onset is presented for the left muscle groups, where the angles represent the direction in which the muscles pull the head to counter the motion due to the load in opposite direction.

The spatial tuning patterns for 9 different groups of muscles using the muscle activation data from the experiment conducted by Ólafsdóttir et al. (2015), and the

3 DOF PID controller, have been shown in Figure 6.7. All muscle groups had an activation under 20%.

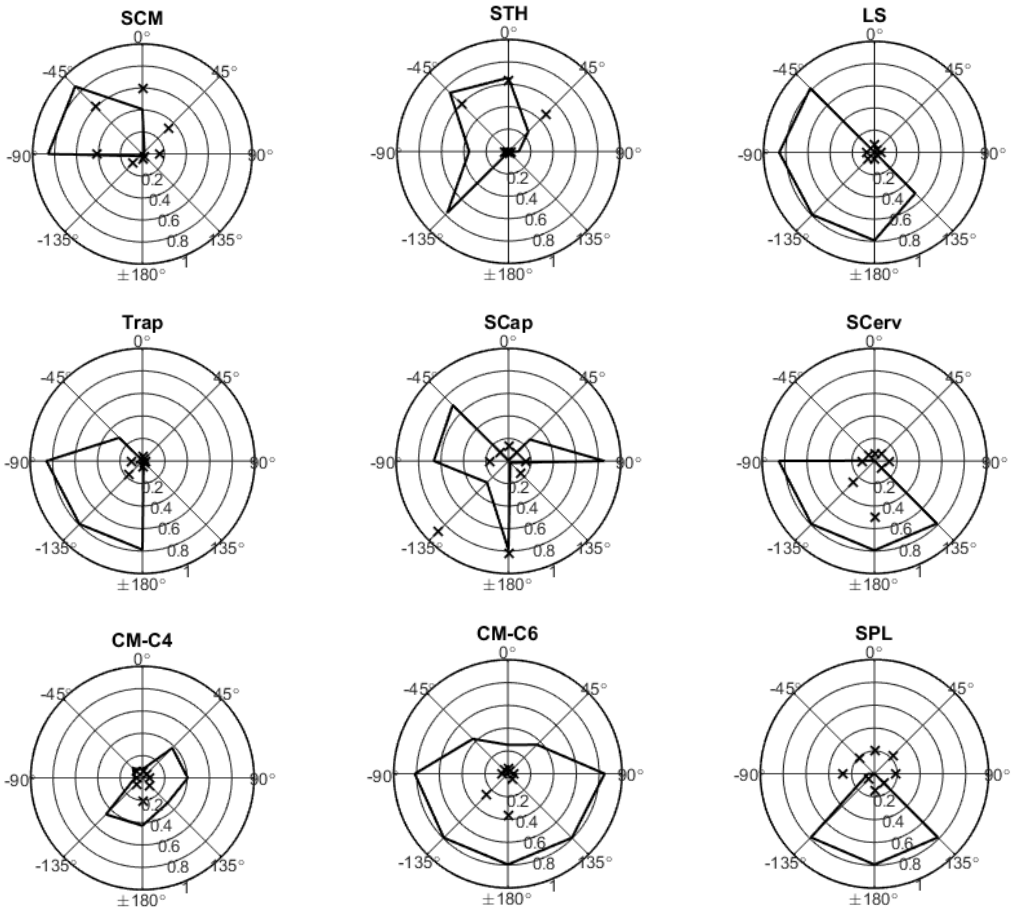

Figure 6.8: Spatial tuning patterns for the optimization model with 1 DOF PID controller for 9 muscle groups, represented through the solid line. The 'x' represents the muscle activation patterns from the experiment conducted by Ólafsdóttir et al. (2015). Muscle activation level at 110ms after loading onset is presented for the left muscle groups, where the angles represent the direction in which the muscles pull the head to counter the motion due to the load in opposite direction.

The spatial tuning patterns for 9 different groups of muscles using the muscle activation data from the optimization study in this project, and the 1 DOF PID controller, have been shown in Figure 6.8. The SCM group was active on the left side of the sagittal plane in the direction of flexion (0°), anterolateral flexion (-45°) and lateral bending (-90°), with levels of around 40%, 80% and 80% respectively. STH group was activated to around 60% in flexion (0°) and left anterolateral flexion (-45°), 20% in right anterolateral flexion (45°), 40% in left lateral bending (-90°), and 80% in left posterolateral extension (-135°) directions. The LS, Trap, SCerv and CM-C6 groups had similar activations to about 80% in left lateral bending (-90°), left posterolateral extension (-135 °) direction as well as in the direction of extension (±180°). LS and SCerv groups were activated to roughly 80% in the right posterolateral extension (135°) direction. CM-C6 group had almost equal activation on both sides of

the sagittal plane in the extension half that was about 80%, and some activation in the flexion half in the range of 20-40%. CM-C4 group on the other hand had activation levels falling below 40% on the right side of the sagittal plane and the left posterolateral extension (-135°) direction. SPL group was activated to 80% in the right (135°) and left posterolateral extension (-135°) directions as well as in the direction of extension (±180°). SCap was highly active in left (-90°) and right (90°) lateral bending, as well as in extension (±180°) and left anterolateral flexion (-45°) directions, in the range of 60-80%.

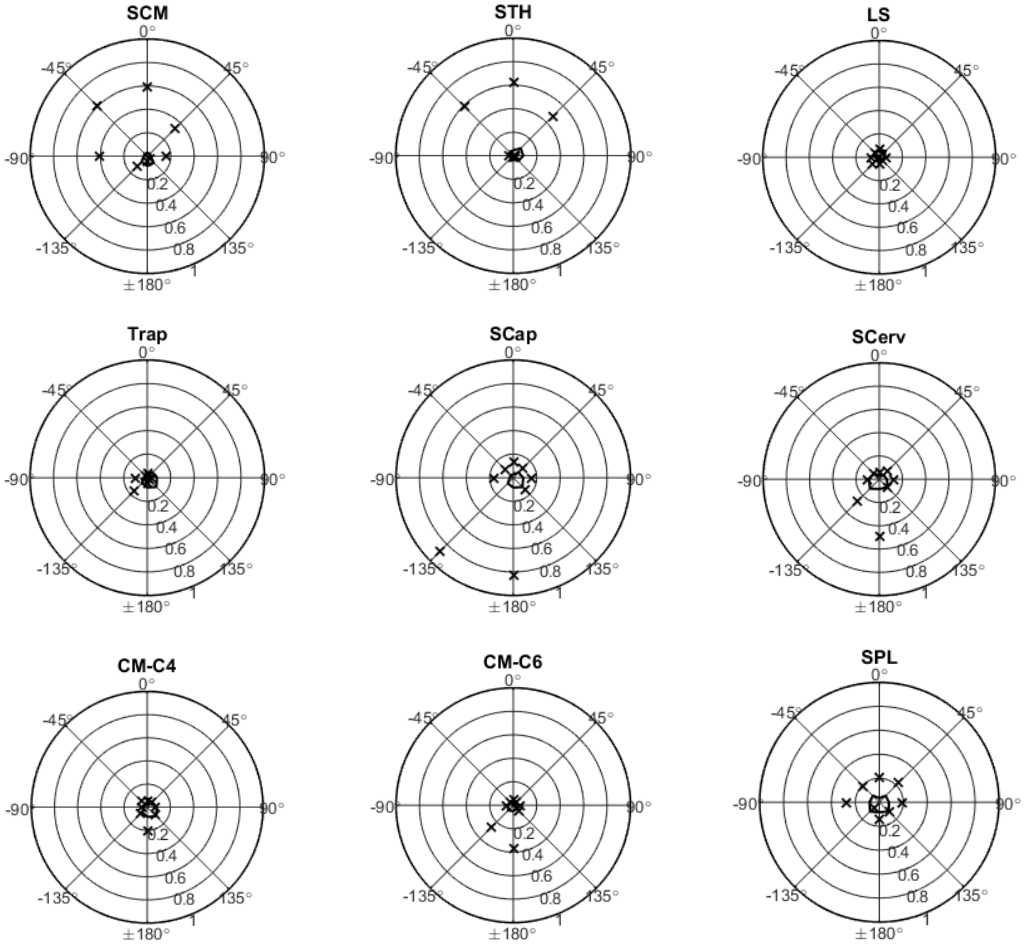

Figure 6.9: Spatial tuning patterns for the optimization model with 3 DOF PID controller for 9 muscle groups, represented through the solid line. The 'x' represents the muscle activation patterns from the experiment conducted by Ólafsdóttir et al. (2015). Muscle activation level at 110ms after loading onset is presented for the left muscle groups, where the angles represent the direction in which the muscles pull the head to counter the motion due to the load in opposite direction.

The spatial tuning patterns for the 9 different groups of muscles using the muscle activation data from optimization study in this project, and the 3 DOF PID controller, have been shown in Figure 6.9. All muscle groups had an activation under 20%.

The spatial tuning patterns for 13 different groups of muscles using the muscle activation data from the optimization study in this project, and the 1 DOF PID controller, have been shown in Figure 6.10 below. SCal and STM groups were both activated to about 80% in the left anterolateral flexion (-45°) and left lateral bending (-90°) directions. An activation level of 60% and 80% was also observed in SCal and STM groups respectively in the direction of flexion (0°). SCal activated to about 60% in the left posterolateral extension direction (-135°). The muscle group LOM was activated roughly to the same amount on both left and right side of the sagittal plane in all directions, ranging from 20% to 80%. The Ster muscle group was mainly active on the left side of the sagittal plane, however, it had an activation of about 50% in the right anterolateral flexion (45°) direction as well. LS and Trap had similar activation patterns on the left side of the sagittal plane that went upto 80%, however, the LS group had an activation level of about 30% on the right side in the posterolateral extension (135°) direction. SOCap group was activated to around 60% in the right lateral bending direction (90°) and 70% in the left posterolateral extension (-135°) direction. It had around 10-30% activation in the right posterolateral extension (135°), extension (±180°) and left lateral bending (-90°) directions. RCap muscle group was highly active in the flexion half of the transverse plane to about 80%, whereas ES group was active in the extension half of the transverse plane to about 80%, except in the right lateral bending (90°) direction where it remained inactive. ECap group had activations ranging from 30-80% on the left side of the sagittal plane, including the extension (±180°) direction. It had a small activation in the direction of right lateral bending (90°). MCerv group was highly active throughout the spectrum except for the right anterolateral flexion (45°) and right lateral bending directions (90°). ORCap was active throughout the spectrum with activation levels ranging from 20-60%, and the SPL group was activated to about 80% in the right (135°) and left (-135°) posterolateral extension direction as well as in the direction of extension (±180°), along with an activation of about 30% in left lateral bending (-90°).

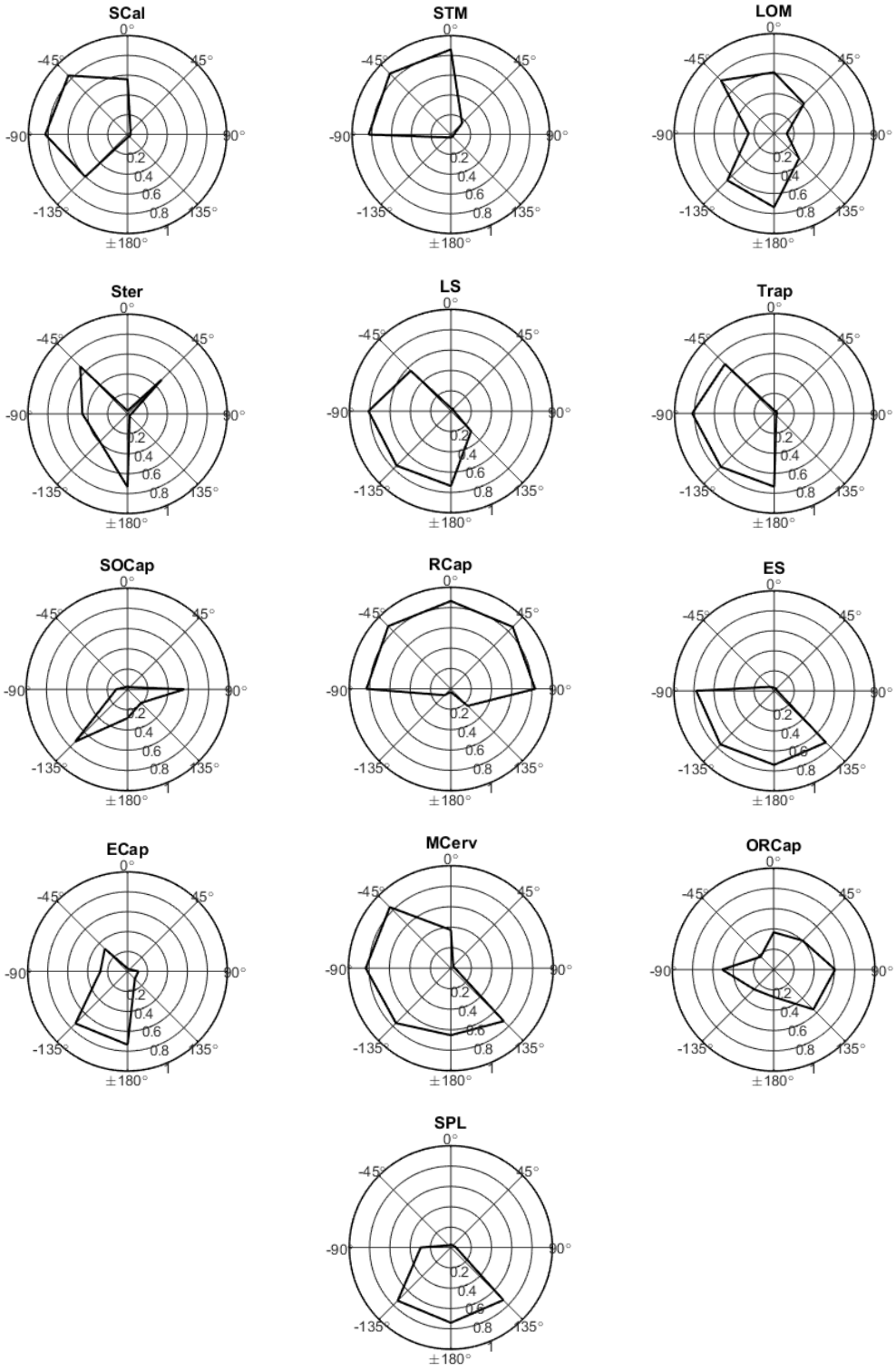

Figure 6.10: Spatial tuning patterns for the optimization model with 1 DOF PID controller for 13 muscle groups, represented through the solid line. The 'x' represents the muscle activation patterns from the experiment conducted by Ólafsdóttir et al. (2015). Muscle activation level at 110ms after loading onset is presented for the left muscle groups, where the angles represent the direction in which the muscles pull the head to counter the motion due to the load in opposite direction.

6.2.2 Head center of gravity translational displacements for the different models

X, Y and Z translational displacement of the head center of gravity for the 7 models in a local coordinate system defined at the head center of gravity, in the directions 0°, 45°, 90°, 135° and ±180°, have been presented in Figure 6.11. The direction of load always corresponds to the local X axis at the head center of gravity.

The passive model received the largest X translational displacement of head center of gravity for the directions 0° (about 160mm), 45° (about 150mm), 135° (about 150mm) and ±180° (about 170mm), whereas the optimization model with 1 DOF PID controller for 9 muscle groups and the optimization model with 1 DOF PID controller for 13 muscle groups received the largest X translational displacement for the direction 45°, which was about 130mm for both models. The optimization model with 1 DOF PID controller for 9 muscle groups obtained X translational displacement for head center of gravity of about -50mm for the direction 0° and about -40mm for the direction 45°. The remaining models were in the range of about -10mm to 130mm for X translational displacement of head center of gravity for the direction 0°, about 40mm to 120mm for the direction 45°, about 50mm to 120mm for the direction 90°, about 70mm to 130mm for the direction 135°, and about 80mm to 140mm for the direction ±180°. However, the optimization model with 3 DOF PID controller for 13 muscle groups, was stable during the simulations for all directions except the direction of 45°, as seen in Figure 6.11.

The Y translational displacement of head center of gravity for the directions 0° and ±180°, was close to 0mm for all 7 models. The passive model obtained about 50mm Y translational displacement of head center of gravity for the direction 45°, whereas the optimization model with 1 DOF PID controller for 9 muscle groups obtained about -100mm Y translational displacement. The remaining models were in the range of -100mm to 50mm. The experimental model with 1 DOF PID controller for 9 muscle groups obtained about 20mm Y translational displacement of head center of gravity for the direction of 90°, whereas the optimization model with 1 DOF PID controller for 9 muscle groups got the largest Y translational displacement that where about -50mm. The remaining models were in the range of -50mm to 20mm. Regarding the direction 135°, the optimization model with 1 DOF PID controller for 13 muscle groups obtained about 40 mm Y translational displacement of head center of gravity, whereas the passive model and the optimization model with 3 DOF PID controller for 9 muscle groups got the largest Y translational displacement (about -50mm). The remaining models were in the range of -50mm to 40mm.

The experimental model with 1 DOF PID controller for 9 muscle groups received the smallest Z translational displacement of head center of gravity for the directions 0°, 45°, 90° and 135°, which were about -5mm, -5mm, -10mm and -20mm respectively. The passive model obtained the largest Z translational displacement of head center of gravity for the directions 0°, 45° and ±180° (about -130mm, -80mm and -100mm respectively), whereas the optimization model with 1 DOF PID controller

for 9 muscle groups obtained the largest Z translational displacement of head center of gravity for the directions 90° and 135° (about -70mm for both models). Same model obtained the smallest Z translational displacement of head center of gravity for the direction ±180°, which was about -30mm. The remaining models were in the range of about -10mm to -50mm for the Z translational displacement of head center of gravity for the direction 0°, about -10mm to -40mm for the direction 45°, about -10mm to -40mm for the direction 90°, about -40mm to -60mm for the direction 135°, and about -40mm to -70mm for the direction ±180°.

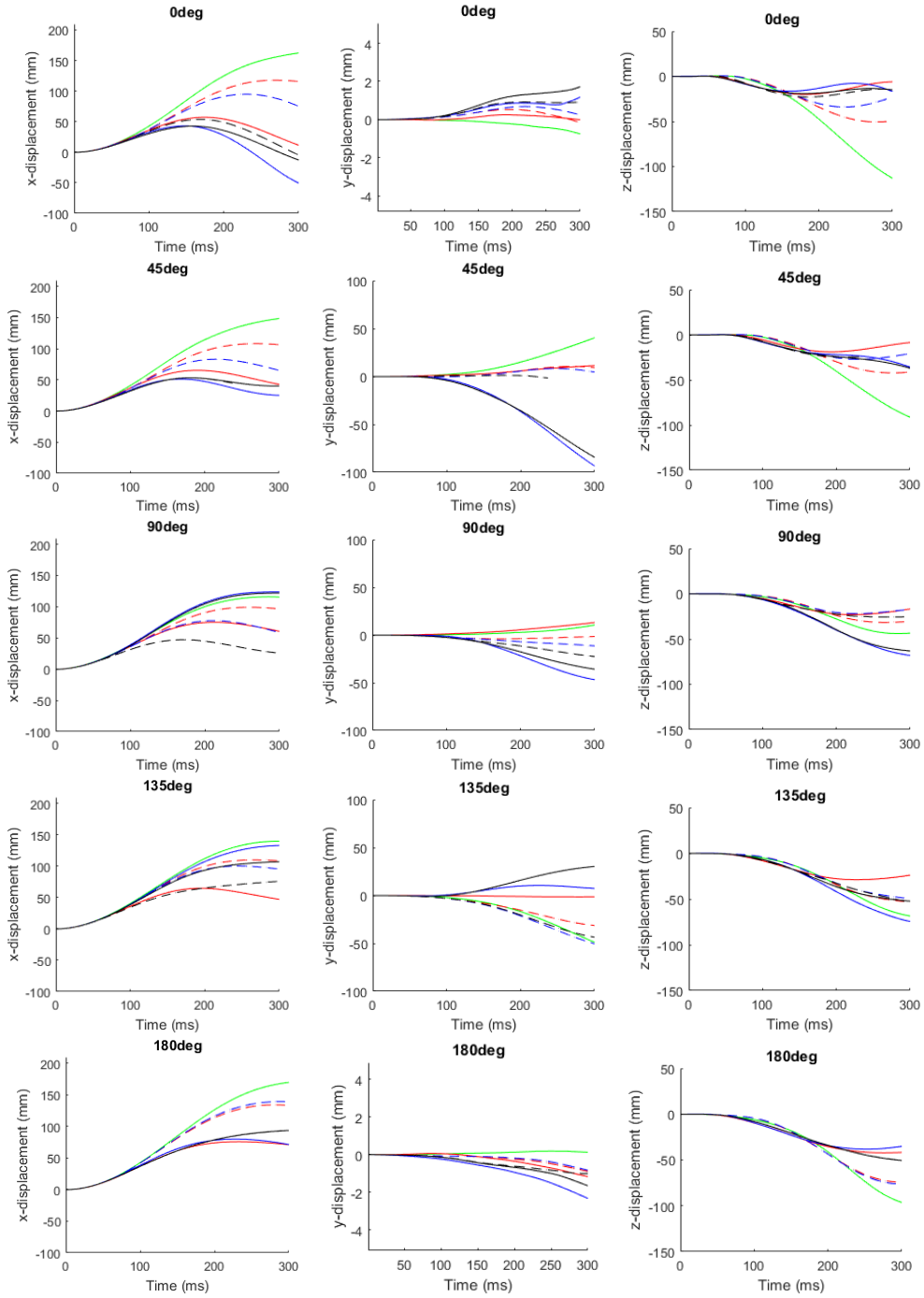

Figure 6.11: X, Y and Z translational displacements in the local coordinate system defined at the head center of gravity, in the directions 0°, 45°, 90°, 135° and ±180°, corresponding to the directions of applied load of the head center of gravity (H) for the 7 models; Passive model (green line), Experimental model with 1 DOF PID controller for 9 muscle groups (red line), Experimental model with 3 DOF PID controller for 9 muscle groups (red dashed line), Optimization model with 1 DOF PID controller for 9 muscle groups (blue line), Optimization model with 3 DOF PID controller for 9 muscle groups (blue dashed line), Optimization model with 1 DOF PID controller for 13 muscle groups (black line), and Optimization model with 3 DOF PID controller for 13 muscle groups (black dashed line).

6.2.3 X, Y and Z rotational displacements for the different models

The X , Y and Z rotational displacements for the 7 different models; the passive model, the experimental model with 1 DOF PID controller for 9 muscle groups, the experimental model with 3 DOF PID controller for 9 muscle groups, the optimization model with 1 DOF PID controller for 9 muscle groups, the optimization model with 3 DOF PID controller for 9 muscle groups, the optimization model with 1 DOF PID controller for 13 muscle groups, and the optimization model with 3 DOF PID controller for 13 muscle groups, have been shown in Figures 6.1 and 6.2. Data has been presented for the head center of gravity, the 4th cervical vertebra (C4) and the 7th cervical vertebra (C7) in the directions 0°, 45°, 90°, 135° and ±180°, at the time point where maximum head rotational displacement was found for a given model in a given direction.

Table 6.1: X, Y and Z rotational displacements of the head center of gravity (H), the 4th cervical vertebra (C4) and the 7th cervical vertebra (C7), for the passive model (9.1.Passive model), the experimental model with 1 DOF PID controller for 9 muscle groups (9.1.Experimental model), the experimental model with 3 DOF PID controller for 9 muscle groups (9.3.Experimental model), the optimization model with 1 DOF PID controller for 9 muscle groups (9.1.Optimization model), the optimization model with 3 DOF PID controller for 9 muscle groups (9.3.Optimization model), the optimization model with 1 DOF PID controller for 13 muscle groups (13.1.Optimization model), and the optimization model with 3 DOF PID controller for 13 muscle groups (13.3.Optimization model), for the directions 0°, 45° and 90°. The rotational displacements are presented in degrees and the time instant in ms.

		0°				45°				90°			
		t	H	C4	C7	t	H	C4	C7	t	H	C4	C7
9.1.Passive model	x	297	0.2	-0.1	-0.1	268	31.2	21.4	5.6	277	47.7	33.0	9.2
	y	300	72.4	61.93	18.6	300	57.0	51.52	15.3	300	12.1	7.4	0.1
	z	300	-1.3	0.2	0.7	207	-8.5	-8.8	-2.2	300	-15.1	-13.6	-2.1
9.1.Experimental model	x	300	0.3	-0.5	-0.4	177	7.1	14.4	5.0	214	19.8	24.5	8.3
	y	300	-12.7	12.0	3.4	176	6.3	20.5	8.3	300	-4.5	15.0	8.0
	z	105	0.0	-0.2	-0.2	179	-8.3	-7.1	-1.8	207	-17.2	-9.3	-1.7
9.3.Experimental model	x	158	0.2	-0.1	-0.1	286	22.6	22.1	7.3	271	34.1	30.8	9.7
	y	270	30.3	45.9	13.1	250	19.1	33.4	10.3	300	-7.0	5.5	3.0
	z	300	-0.3	-0.3	-0.1	174	-8.4	-6.3	-1.0	203	-13.6	-9.4	0.0
9.1.Optimization model	x	0	0.0	0.0	0.0	300	33.5	26.6	8.6	300	50.0	41.6	13.6
	y	300	-33.4	-7.6	-4.2	300	25.9	-15.8	-7.4	300	-25.4	-11.0	-10.8
	z	300	-0.4	-0.4	-0.7	131	-3.1	-3.7	-1.5	285	-10.7	-9.6	0.3
9.3.Optimization model	x	154	0.1	-0.2	-0.2	213	14.8	16.2	5.5	216	23.5	23.9	7.27
	y	220	21.6	34.5	11.7	208	13.0	24.1	7.8	300	-10.5	1.9	0.4
	z	0	0.0	0.1	0.1	192	-9.4	-6.1	-1.2	211	-17.1	-9.6	-1.0
13.1.Optimization model	x	71	0.0	-0.1	-0.1	300	34.9	28.0	10.0	300	47.6	42.5	15.8
	y	164	9.9	12.6	6.8	300	-19.0	-9.0	-3.3	300	-20.0	-3.0	-3.8
	z	300	-0.5	-0.1	-0.5	121	-3.6	-5.3	-2.3	297	-11.9	-7.8	0.5

Table 6.2: X, Y and Z rotational displacements of the head center of gravity (H), the 4th cervical vertebra (C4) and the 7th cervical vertebra (C7), for the passive model (9.1.Passive model), the experimental model with 1 DOF PID controller for 9 muscle groups (9.1.Experimental model), the experimental model with 3 DOF PID controller for 9 muscle groups (9.3.Experimental model), the optimization model with 1 DOF PID controller for 9 muscle groups (9.1.Optimization model), the optimization model with 3 DOF PID controller for 9 muscle groups (9.3.Optimization model), the optimization model with 1 DOF PID controller for 13 muscle groups (13.1.Optimization model), and the optimization model with 3 DOF PID controller for 13 muscle groups (13.3.Optimization model), for the directions 135° and ±180°. The rotational displacements are presented in degrees and the time instant in ms.

		135°				180°			
		t	H	C4	C7	t	H	C4	C7
9.1.Passive model	x	255	31.5	18.9	4.9	177	0.1	0.1	0.2
	y	300	-41.1	-49.7	-20.0	300	-68.0	-62.6	-29.1
	z	300	-11.5	-3.5	4.3	164	0.0	-0.2	-0.2
9.1.Experimental model	x	202	15.3	15.0	5.2	71	0.1	0.0	-0.1
	y	216	-13.6	-15.3	4.7	260	-29.7	-21.9	6.0
	z	193	-11.4	-7.4	-0.9	300	-0.4	-0.6	-0.7
9.3.Experimental model	x	232	22.9	19.8	6.1	300	0.1	-0.2	-0.6
	y	300	-40.2	-33.0	-4.2	300	-54.6	-44.1	-12.6
	z	206	-8.9	-4.6	2.5	300	-0.3	-0.5	-0.3
9.1.Optimization model	x	300	45.1	33.6	9.9	0	0.0	0.0	0.0
	y	300	-36.8	-32.2	-14.0	241	-26.3	-23.9	-3.5
	z	263	-4.5	-5.4	2.5	164	-0.4	-0.4	0.4
9.3.Optimization model	x	207	18.6	17.3	5.1	300	0.3	0.0	-0.5
	y	300	-40.8	-36.1	-8.4	299	-53.9	-49.0	-17.5
	z	209	-11.8	-5.8	1.5	300	-0.4	-0.7	-0.4
13.1.Optimization model	x	300	37.0	34.2	11.4	34	0.0	0.0	0.0
	y	300	-20.4	-15.7	-5.6	300	-45.4	-23.7	-1.4
	z	121	-3.1	-2.7	0.2	154	-0.2	-0.3	-0,4

7 Discussion

This chapter discusses the AHBM optimization simulations in LS-OPT, the dynamic spatial tuning patterns obtained for the different models considered in the study and finally the future work that could be relevant for research in this area.

7.1 AHBM optimization simulations in LS-OPT

The human is not fully symmetrical around the sagittal plane, and therefore it is not possible to achieve symmetrical forces on either side of the sagittal plane in an experimental MVC setup. This has been confirmed through the study by Siegmund et al. (2007). However in the AHBM, symmetry around the sagittal plane was assumed, and therefore the forces obtained from the MVC simulation setup are symmetrical around the sagittal plane.

The force obtained in the MVC simulation setup in the direction of extension ($\pm 180°$) was significantly higher than the force obtained in direction of flexion ($0°$) mainly due to the presence of greater number of extensors in the neck as compared to flexors, thereby contributing more to the force in extension as compared to the force in flexion. This was also verified from the study by Siegmund et al. (2007). The forces obtained in the directions of flexion ($0°$), right anterolateral flexion ($45°$) and left anterolateral flexion ($-45°$) from the MVC simulation setup were found to be lower than the average forces in the corresponding directions obtained from the experimental MVC setup by Siegmund et al. (2007). One reason for this could be the grouping of flexor muscles. All flexor muscles get activated independent of the other flexor muscles in the experimental MVC setup, whereas in the MVC simulation setup with 9 muscle groups, presented in Table 5.1, the flexor muscles were grouped into 2 and thus received only 2 activation levels, thereby increasing their dependence on each other and also increasing the possibility of achieving lower activations as compared to the scenario in the experimental MVC setup. Moreover, when the number of muscle groups were increased to 13, presented in Table 5.2, higher forces were observed in the directions of flexion ($0°$), right anterolateral flexion ($45°$) and left anterolateral flexion ($-45°$) in the MVC simulation setup. This could justify the fact that increasing the number of groups could reduce the dependence of flexor muscles on each other, thereby helping them achieve higher activations as compared to the case with 9 muscle groups and contribute more to the forces in the corresponding directions of flexion. The forces in the MVC simulation setup with 13 muscle groups have a higher resemblance with the average forces in these directions

for the experimental MVC setup by Siegmund et al. (2007), as compared to the forces in the MVC simulation setup with 9 muscle groups.

Another reason for a mismatch between the forces produced in flexion for the MVC simulation setup and the experimental setup could be the kind of constraints that were given to the AHBM setup in MVC simulation. The two important motions associated with flexion are rotation of the head and neck about the Y axis given that the model was faced in the X direction, and displacement of the head and neck in the positive X direction, which were constrained to 10° and 10mm respectively in the AHBM. A trial was performed during this study by limiting these constraints to reduced values of 5° and 5mm respectively, which resulted in reduced forces in flexion, confirming the fact that the constraints do have an important role to play in production of forces in optimization setups. Although the experimental setup involved constraining the head and torso, there was lack of information on the exact displacement and rotations of the head and neck. Hence, constraints for the AHBM were decided in an intuitive way, which could be responsible for producing different forces in the experiment and simulation for MVC.

Activation levels of muscle groups in the MVC simulation setup were compared to the individual muscle activations in the experimental MVC setup by Siegmund et al. (2007). Moreover, the activation patterns obtained from the MVC experiment varied among three subjects and hence it was considered necessary to compare the patterns obtained from the MVC simulation to the average activation patterns obtained from the experiment by Siegmund et al. (2007).

For the SCM group from the MVC setup with 9 muscle groups, as seen in Table 5.1, high activation levels were observed in the directions of left anterolateral flexion (−45°) and left lateral bending (−90°), which were also noticably found for the sternocleidomastoid muscle in the same directions in the MVC experiment by Siegmund et al. (2007). These activations were in accordance with the flexing and lateral bending capacity of the Sternocleidomastoid muscle and the scalene muscles respectively, as seen in Table 4.2. The activations remained high in these directions when the sternocleidomastoid muscle and scalene muscles were treated as separate groups, STM and SCal, in case of the MVC setup with 13 muscle groups. The activation of the SCM group in the direction of flexion (0°) was lower than the activation for the sternocleidomastoid muscle from the MVC experiment, probably due to the same reasons as mentioned above where flexors were grouped into two and constraints on the AHBM limited the force in flexion. When SCM group from the MVC setup with 9 muscle groups was segregated into SCal and STM groups in the MVC setup with 13 muscle groups, both these groups achieved higher activation in the direction of flexion (0°), and thereby mimicked the activation levels for sternocleidomastoid muscle in the MVC experiment more closely. In the MVC experiment, activations were observed for the sternocleidomastoid muscle in both the direction of right anterolateral flexion (45°) and right lateral bending (90°), but the SCM, SCal and STM groups from the two different MVC simulation setups received negligible activations. In reality the sternocleidomastoid muscle is able to generate

contralateral rotation, as mentioned in Table 4.2, which was not observed in the simulation and could be due to the constraint of 10° rotation around the Z axis. The way in which the muscle has been modelled in the AHBM could also influence this result, by not generating sufficient moment towards the opposite side as is seen in the MVC experiment by Siegmund et al. (2007).

The STH group from the MVC setup with 9 muscle groups, shown in Table 5.1, achieved activation levels that were within the same range as for the sternohyoid muscle in the MVC experiment by Siegmund et al. (2007), in the directions of flexion (0°), right lateral bending (90°), left lateral bending (−90°) and left anterolateral flexion (−45°). Significantly higher differences in activation levels were observed between the STH group from MVC simulation and the sternohyoid muscle from the MVC experiment for the directions of right anterolateral flexion (45°) and left posterolateral extension (−135°). As the muscles in the STH group are primarily involved in flexion, a high activation level in the −135° direction could suggest that when the model rotates, the STH group gets activated in order to counteract this rotation and thus prevent itself from violating the rotational constraints in the optimization setup, which was also observed when the STH group was subdivided into the muscle groups Ster and LOM. Moreover, the division into these groups also lead to an increased activation level in the right anterolateral flexion (45°) direction, which was within range for the sternohyoid muscle for the same direction. The sternohyoid and sternothyroid muscles in the STH group were modelled with two beams having one origin and two insertion points whereas the longus capitis, longus colli superior oblique, longus colli vertical and longus colli inferior oblique muscles were modelled as one beam with one origin and one insertion point, and thus might behave differently in tension and rotation. This could be the possible reason for a reduced activation level in the right anterolateral flexion (45°) direction in STH group, which got increased upon division into Ster and LOM groups, where they could independently tense and rotate.

The LS group in the grouping scheme with 9 muscle groups was not divided for the grouping scheme with 13 muscle groups, and close resemblance was observed in the muscle activation patterns when compared to the activation pattern of the levator scapulae muscle in the study by Siegmund et al. (2007), which suggests that the muscle might have been modelled in a way that represents the muscle in a human being.

The Trap groups from both the 9 as well as 13 muscle group setups had similar activations in the left posterolateral extension (−135°) and extension (±180°) directions as compared to the trapezius muscle in the study by Siegmund et al. (2007), which suggests that they might have a role to play in extending the head and neck. This experimental study showed that there was activation on the right side of the sagittal plane for the left muscle, which was not observed in the optimization setups with both grouping schemes. In reality, the trapezius muscle has a non uniform cross sectional area and it covers a large area across the head, shoulder and middle of the spine, thereby having a triangular shape, which is not the case in the AHBM

due to its representation as a beam with uniform cross sectional area as well as its origin and insertion point, see Table 4.2. For the left lateral bending ($-90°$) direction, a significantly higher activation was obtained through the optimization study with both 9 and 13 muscle groups as compared to the experimental study by Siegmund et al. (2007). This could be due to the use of a linear regression model for the optimization study, which tends to find the optimum value at the extremes of the specified range of optimization parameters. As trapezius is involved in lateral bending to the same side, the activation level could have been set to 1, which was the upper limit for activation, for this direction as a result of optimization.

As compared to the activation pattern of the semispinalis capitis muscle in the experimental study by Siegmund et al. (2007), it was not possible to deduce any similarities for the muscle groups SCap, SOCap and RCap from the optimization setup with 9 and 13 muscle groups. This was probably due to the difference in modelling of the muscles belonging to these groups in comparison to reality. In the optimization study, it was sensed that the activation patterns looked as they were probably due to helping the head and neck stabilize and not violate the translational and rotational optimization constraints on the model.

Scerv group was activated in the same directions as the semispinalis cervicis muscle from the experimental study by Siegmund et al. (2007). However, some of the directions received an activation of 100% in the model, which was not the case in the experiment. This may again be due to the linear regression model used for the optimization setup that tries to locate the optimum at one extreme depending on the most important functions of the muscles, which are extension, lateral bending and lateral extension for the SCerv group, see Table 4.2. Moreover, when the SCerv group was subdivided into the ES and ECap muscle groups in the optimization setup with 13 muscle groups, the ES group was activated in an identical way as the Scerv group. However, the ECap group behaved differently through its activation pattern. This may be due to the fact that the left erector spinae longissimus capitis from the ECap group was probably not involved in contralateral flexion and rotation unlike the semispinalis cervicis muscle, see Table 4.2, thereby lacking activation levels on the other side of the sagittal plane.

The resulting activation patterns for the CM-C4 and CM-C6 groups did not resemble the activation patterns for the the same muscles in the study conducted by Siegmund et al. (2007). Considering the direct attachment points of the CM-C6 muscles in the head of the AHBM, see Table 4.2, it could seem like these muscles were completely activated while trying to maximize the force in extension and lateral extension as per how the model has been setup for optimization. On the other hand, the CM-C6 group in the AHBM being closer to the spine, might be more involved in stabilization of the neck while trying to prevent the model from violating the optimization constraints. When these groups were separated into MCerv and ORCap muscle groups for the optimization study with 13 muscle groups, the MCerv group behaved similar to the multifidus muscles in the experimental study by Siegmund et al. (2007), but received higher activations in the corresponding di-

rections probably because of the linear regression model chosen for the optimization. Moreover, the MCerv groups showed signs of activation in both the flexion (0°) and left anterolateral flexion (−45°) directions, which may suggest that these activations had arisen due to neck stabilization effects while trying to prevent violation of optimization constraints. The ORCap muscle group behaved differently from the other groups, which could be due to difference in the origin and insertion points of the muscles in the ORCap group and the multifidus muscles. The difference in behaviour might have also been caused due to the optimization setup.

A large overlapping region was observed for the activation of the SPL groups from the optimization setup with both 9 and 13 muscle groups. However, a lot of difference was observed in the activation patterns of the 3 male subjects in the MVC experimental study by Siegmund et al. (2007) for the splenius capitis muscle. Thus, it was difficult to relate the patterns from optimization to those from the experiment. Considering the function of the splenius capitis muscle, see Table 4.2, it could be expected that large activations are obtained in extension, lateral bending and rotation of the head and neck, which could also be seen in the optimization patterns.

7.2 Dynamic AHBM simulations in LS-DYNA

Section 7.2.1 discusses the dynamic spatial tuning patterns for the different models, whereas Section 7.2.2 compares the AHBM kinematics between the experimental models and the optimization models with 1 DOF PID controller, for 9 and 13 muscle groups. The comparison of 1 DOF PID controller and the 3 DOF PID controller is shown in Section 7.2.3.

7.2.1 Dynamic spatial tuning patterns

The dynamic spatial tuning patterns obtained in the AHBM using the muscle activation patterns from the experiment conducted by Ólafsdóttir et al. (2015) and 1 DOF PID controller, see Figure 6.6, revealed that the muscles got activated in the same directions using the dynamic loading on AHBM as in the experimental sled test, suggesting that the muscles do have spatial preference in a particular loading condition. The SPL group in particular, which had shown multidirectional preference in the experiment against its anatomical position in the human body, was also consistent with the dynamic simulation on the AHBM.

As compared to Figure 6.6, Figure 6.7 representing the dynamic spatial tuning patterns obtained in the AHBM using the muscle activation patterns from the experiment conducted by Ólafsdóttir et al. (2015) and 3 DOF PID controller, showed that the muscles got activated in a different manner. The muscle activation levels were much lower when the 3 DOF PID controller was used at the same time instant after the application of load, suggesting a possible reduction in the control signal that scaled the activation levels to lower values. These results suggest that a change in controller possibly alters the activation preferences of the muscle groups during

dynamic loading due to different control signals generated for each of the directions. The rotational scaling factors have been assumed in this study as per the modelling of muscles, due to lack of data. These scaling factors could also be one reason as to why the muscles were activating differently in case of 1 DOF and 3 DOF PID controllers using the same set of isometrically derived patterns for the AHBM.

The activation levels for the 9 muscle groups in the dynamic spatial tuning patterns obtained from the optimization model with 1 DOF PID controller, see Figure 6.8, were scaled from the MVC optimization patterns shown in Figure 6.2. This indicates that the muscles were probably activated in the same way for the dynamic case as in the isometric case, using this controller. However, the dynamic spatial tuning patterns for the optimization model with 9 muscle groups and 3 DOF PID controller, see Figure 6.9, got significantly lower muscle activations as compared to the optimization model with 1 DOF PID controller for 9 muscle groups, which indicates that the control signals were considerable lower. The same reasoning as stated in the previous paragraph with the comparison of the experimental models with 1 DOF and 3 DOF PID controllers could be applied here.

The dynamic spatial tuning patterns for the optimization model with 13 muscle groups and 1 DOF PID controller, see Figure 6.10, were scaled from the the MVC optimization patterns shown in Figures 6.4 and 6.5, again suggesting that the muscles activated in the same way as from the MVC optimization, using this controller. The dynamic spatial tuning patterns for the optimization model with 13 muscle groups and 3 DOF PID controller could not be obtained due to a simulation crash in the 45° load case, which was because of negative volume found in some solid elements of the model. This would require some changes in the model. It was not possible to resolve this issue with instabilities within the timeframe of the current work and further investigation is needed on this front in order to compare the dynamic patterns of this case with the MVC optimization patterns.

7.2.2 Comparison of the experimental model with 9 muscle groups and optimization model with 9 and 13 muscle groups using 1 DOF PID controller based on the AHBM kinematics

The passive model was used as a reference to check if the other models produced muscle activations that resulted in different kinematics. In case of load in 0°, significant deviation was observed for X and Z displacements of the head from the passive model, see Figure 6.11. Moreover, the rotations of the head, C4 and C7 vertebrae were also significantly reduced, see Table 6.1. The rotation of the head around the Y axis was higher in the optimization model with 9 muscle groups as compared to the experimental model with 9 muscle groups. However, the difference was reduced when the 9 muscle groups were divided into 13 muscle groups, see Table 6.1. The models behaved similarly when it came to X and Z displacements of the head in case of the loading direction 45°. However, the Y displacement of the two optimization models deviated from the experimental model, see Figure 6.11. The rotation

of the head, C4 and C7 vertebrae differed largely from the experimental models, see Table 6.1. However, the optimization models did not have major differences in kinematics. In the case of load in 90°, there was a large deviation between the head displacements in X, Y and Z directions, see Figure 6.11, and the head and vertebral rotations around X, Y and Z axis, see Table 6.1, for the models. Dividing the muscle groups did not have a significant impact on the kinematics. When the models were loaded in the direction of 135°, although there was a large variation in the displacements and rotations, see Figure 6.11 and Table 6.2, the optimization model with 13 muscle groups had a lesser difference with the experimental model with 9 muscle groups as compared to the optimization model with 9 muscle groups. The optimization model with 13 muscle groups behaved in close resemblance to the experimental model with 9 muscle groups in case of a load in the direction of ±180°, when kinematics were compared. Due to lack of data on volunteer kinematics using this particular load case involving application of gravity, it is difficult to say if the model specific patterns obtained from the MVC optimizations could be used for dynamic simulations of the AHBM. On the whole, these results indicate that there is a high possibility of having AHBM kinematics in resemblance of the kinematics of volunteers from experiments, if there are a greater number of muscles that are individually optimized, rather than dividing them into groups based on some similarity in anatomical positions or functions, which leads to oversimplified solutions.

7.2.3 Comparison of 1 DOF PID controller and 3 DOF PID controller based on the AHBM kinematics

The experimental model with 9 muscle groups was used to compare the 1 DOF PID controller with the 3 DOF PID controller. The muscle activation patterns from the optimizations might not be a reliable source for comparison, because the muscle groups got activated in directions where they were not supposed to function as per their anatomy, as well as due to instabilities in the current optimization setup. This would further make it difficult to understand the differences that arise due to a change in controller. It was observed that there was significant difference between the head displacement in X direction in all load cases, with displacement in the case of 3 DOF PID controller being higher than that of the 1 DOF PID controller, see Figure 6.11. The rotations about the X, Y and Z axes were larger as well in case of the 3 DOF PID controller, see Tables 6.1 and 6.2. Although these kinematic parameters were higher in the model with 3 DOF PID controller, it was observed that the stability of the spine was maintained through muscle activation in the appropriate muscles for the specific load cases. As the control signal is now a sum of scaled control signals for the three directions to be controlled, the control signal could be smaller than that calculated from the absolute deviation of the head in case of the 1 DOF PID controller, resulting in lower muscle activations. Due to lack of available data on true volunteer kinematics for that particular load case, it is difficult to conclude if the kinematics of the AHBM using the patterns from the study conducted by Ólafsdóttir et al. (2015) represent the real scenario better with the 1 DOF PID controller or with the 3 DOF PID controller. There could also be a possible difference in the results of the 3 DOF PID controller if each control signal

was calculated using different PID parameters, fine tuned for the particular angle.

7.3 Future work

The way of defining the optimization setup can influence the muscle activations as well as the kinematics of the AHBM, and therefore, it is of great importance to analyze and evaluate the influence of different optimization setups on the AHBM. Section 7.3.1, presents an optimization setup where all individual head and neck muscles are separately optimized. Another possible optimization setup with the aim to mimic the experimental MVC setup on volunteers conducted by Siegmund et al. (2007), would be to constrain the AHBM head center of gravity in 3D space and calculate the obtained force in x and y directions, which is described in Section 7.3.2. Both model setups could subsequently be simulated in a dynamic setup to obtain the dynamic spatial tuning patterns, which is explained in Section 7.3.3.

A first order polynomial response surface has been used for this study in LS-OPT, however, implementation of higher order polynomial response surfaces in LS-OPT could be tested, to analyze the influence of chosen polynomial surface on the obtained muscle activation patterns for the AHBM, which has been described in Section 7.3.4.

7.3.1 AHBM muscle specific setup

Each muscle in the head and neck model on either side of the sagittal plane could be assigned a different parameter for optimization, resulting in 54 parameters in total. The setup that involves attaching a beam to different points on the head to measure MVC, as described in Section 5.1.1, could be applied. The optimization strategy, constraints, objective and convergence criteria could be the same as described in Sections 5.1.6, 5.1.3, 5.1.4 and 5.1.5 respectively. The minimum number of simulations per iteration could be set to 80, which would be approximately one and a half times the number of parameters. The simulation run time for this optimization setup would need to be reduced to be able to run the simulation due to time limitations on the used cluster. In order to achieve this, changes could be made to the brain of the AHBM, which could include a change from deformable shell and solid elements to rigid elements and removal of some contact definitions in the AHBM brain.

7.3.2 AHBM setup with constrained head center of gravity

To mimic the the volunteer experiments on MVC, another setup could involve fixation of AHBM head in space, by constraining the head center of gravity. This could be achieved by using the keyword *BOUNDARY_PRESCRIBED_MOTION_NODE in LS-DYNA, where all degrees of freedom of the head center of gravity would be constrained. Considering symmetry of the AHBM around the sagittal plane, five different directions could be chosen for measuring the maximum force as in the MVC in one half of the transverse plane, 0°, -45°, -90°, -135° and ±180°. The same set of parameters as were used for the previous setup with 9 muscle groups and the discrete beam element attached to the AHBM head, could be used for this setup, as shown in Table 5.1. The difference between the angle made by the vector corresponding to

the resultant force obtained from forces in the X and Y degrees of freedom of the constraint at the head center of gravity, through *DATABASE_BNDOUT keyword, α, and the particular orientation in which the force needs to be maximized, α_0, could be set to be less than ϵ and thereby used as a constraint for this optimization setup of the AHBM. ϵ could be chosen to be the movement in the transverse plane of the volunteers from the MVC experiments. Equation 7.1 shows how the constraint could be implemented.

$$|\alpha - \alpha_0| < \epsilon \tag{7.1}$$

Where α would be defined as shown in the Equation 7.2, where x_{force} and y_{force} would represent the forces in the X and Y degrees of freedom respectively.

$$\alpha = \tan^{-1}\left(\frac{x_{force}}{y_{force}}\right) \tag{7.2}$$

The optimization criteria could be defined as maximizing the resultant force obtained from x_{force} and y_{force} in the constraint in the transverse plane for each of the chosen angles for measuring the force, as shown in Equation 7.3 below. The same optimization convergence criteria as described in Section 5.1.5 could be applied for this AHBM setup.

$$Maximize : \sqrt{x_{force}^2 + y_{force}^2} \tag{7.3}$$

7.3.3 Dynamic AHBM simulation

The AHBM with the obtained muscle activation patterns, as described in Section 7.3.1 could be subjected to a dynamic load, mainly application of gravity, in different directions in the transverse plane. The kinematics from the obtained muscle activations of the AHBM head and neck could be compared to the kinematics from the muscle activations obtained from sled tests on volunteers conducted by Ólafsdóttir et al. (2015). The same procedure could be carried out by replacing the experimental patterns for muscle activations with the patterns obtained from the optimization using the AHBM setup with constrained head center of gravity as described in Section 7.3.2. A comparison of the kinematics of the AHBM from these two sets of muscle activation patterns would be done upon the application of a dynamic gravity load to different directions in the transverse plane, to analyze which model setup resembles more closely the kinematics obtained from volunteer experiments.

Another test could be to analyze the different load cases on the AHBM with the obtained muscle activations from the two setups described in Sections 7.3.1 and 7.3.2 respectively, using the newly developed 3 DOF PID controller, which is described in Section 5.3. A comparison of the AHBM kinematics for the 1 DOF PID controller and the 3 DOF PID controller could be made for both the optimization setups, to analyze which PID controller results in closeness of kinematics to those in experiments.

7.3.4 Implementation of higher order polynomial response surface in LS-OPT

The results from completed optimizations have revealed that the muscle activations tend to take the two extreme values 0 and 1, when a linear response surface is used in LS-OPT. Another approach could be to use a higher order polynomial response surface, which could find other optimum values within the response surface range. A limitation would be the time required for the completion of one iteration, thus it would be longer as compared to the use of a linear response surface. However, there is a possibility of locating the optimum within a fewer iterations with a higher order polynomial response surface as compared to the iterations required for linear response surface. Hence, there is a trade-off between the expensive nature and the ability to find a optimum for the curved response surface, and it could be tested to observe any kind of improvements in the kinematics of the head and neck using the obtained muscle activation patterns with the usage of the higher order polynomial response surface.

8
Conclusion

Muscle activation levels were optimized for 9 and 13 muscle groups of the AHBM for a MVC setup in LS-DYNA. The muscle groups showed spatial preference. Some results were in fine tune with the anatomical locations and functions of the muscles present in each muscle group. The muscle groups that showed an anomaly to this trend suggested that there is a need to improve the current optimization setup.The dynamic AHBM simulations, with the muscle activation patterns obtained from the optimizations for 9 and 13 muscle groups, with 1 DOF and 3 DOF PID controllers, showed great variation in the kinematics of the AHBM, and no conclusive evidence could be found on which model better mimics the real life scenario, due to lack of data from human volunteer experiments. To conclude if the isometrically derived model specific spatial tuning patterns for the head and neck of the AHBM could be biofidelic and thereby in the future, reduce the experimental tests with human volunteers, more experimental data is necessary. The parameters of the 3 DOF PID controller could be further fine tuned for motion around all three axes, as the obtained control signals were smaller in general as compared to the obtained control signals from the 1 DOF PID controller. Since the muscle scaling factors for the axial rotation in the 3 DOF PID controller were assumed based on anatomical data as well as the insertion and origin of the modelled muscle beams in LS-DYNA, they might induce significant variations in the obtained results, which indicates that experimental muscle data for axial rotations around the X, Y and Z axis is of great importance for the development of a 3 DOF PID controller.

Bibliography

Abbas, J. J. (2015). Neuromuscular control systems, models of. *Encyclopedia of Computational Neuroscience*, pages 2005–2011.

Administration, N. H. T. S. et al. (2006). Traffic safety facts 2004: A compilation of motor vehicle crash data from the fatality analysis reporting system and the general estimates system (dot hs 809 919). *Washington, DC: US Department of Transportation*.

Analysis, T. (2016). Road traffic injuries. http://www.trafa.se/en/road-traffic/road-traffic-injuries/.

Belwadi, A. N. (2011). Finite element reconstruction of real world aortic injury in near-side lateral automotive crashes with conceptual countermeasures. *Wayne State University Dissertations*.

Berg, A., Krehl, M., Behling, R., and Helbig, M. (2004). Rollover crashes-real world studies, tests and safety systems. *PROGRESS IN TECHNOLOGY*, 101:288–298.

Boström, L., Wladis, A., and Nilsson, B. (2001). A review of serious injuries and deaths among car occupants after motor vehicle crashes in sweden from 1987 to 1994. *Archives of orthopaedic and trauma surgery*, 121(1-2):1–6.

Cesari, D. (1997). Advanced restraint systems for occupant protection. In *Crashworthiness of Transportation Systems: Structural Impact and Occupant Protection*, pages 173–187. Springer.

Cominos, P. and Munro, N. (2002). Pid controllers: recent tuning methods and design to specification. *IEE Proceedings-Control Theory and Applications*, 149(1):46–53.

Cooper, G. M. (2000). *The cell: a molecular approach*. ASM Press, Sunderland, Mass;Washington, D.C;, 2nd edition.

Crandall, J. R., Bose, D., Forman, J., Untaroiu, C., Arregui-Dalmases, C., Shaw, C. G., and Kerrigan, J. (2011). Human surrogates for injury biomechanics research. *Clinical Anatomy*, 24(3):362–371.

de Bruijn, E., Van der Helm, F., and Happee, R. (2016). Analysis of isometric cervical strength with a nonlinear musculoskeletal model with 48 degrees of freedom. *Multibody System Dynamics*, 36(4):339–362.

De Vlugt, E., Schouten, A. C., and Van Der Helm, F. C. (2006). Quantification

of intrinsic and reflexive properties during multijoint arm posture. *Journal of neuroscience methods*, 155(2):328–349.

Dibb, A. T., Cox, C. A., Nightingale, R. W., Luck, J. F., Cutcliffe, H. C., Myers, B. S., Arbogast, K. B., Seacrist, T., and Bass, C. R. (2013). Importance of muscle activations for biofidelic pediatric neck response in computational models. *Traffic injury prevention*, 14(sup1):S116–S127.

Elliasson, E. and Wass, J. (2015). Industrialisation of a finite element active human body model for vehicle crash simulations. Master's thesis.

Emori, R. I. and Horiguchi, J. (1990). Whiplash in low speed vehicle collisions. Technical report, SAE Technical Paper.

Engineering, K. F. (2016). The pros and cons of using crash test dummies and human subjects. http://kodsiengineering.com/the-pros-and-cons-of-using-crash-test-dummies-and-human-subjects/. Accessed: 2017-06-01.

Fressmann, D., Münz, T., Graf, O., and Schweizerhof, K. (2007). Fe human modelling in crash–aspects of the numerical modelling and current applications in the automotive industry. *Frankenthal (Germany)*.

Gabriel, D., Matsumoto, J., Davis, D., Currier, B., and An, K.-N. (2004). Multidirectional neck strength and electromyographic activity for normal controls. *Clinical Biomechanics*, 19(7):653–658.

Hawkins, D. and Molé, P. (1997). Modeling energy expenditure associated with isometric, concentric, and eccentric muscle action at the knee. *Annals of biomedical engineering*, 25(5):822–830.

Herzog, W. (2014). Mechanisms of enhanced force production in lengthening (eccentric) muscle contractions. *Journal of Applied Physiology*, 116(11):1407–1417.

Hill, A. V. (1938). The heat of shortening and the dynamic constants of muscle. *Proceedings of the Royal Society of London B: Biological Sciences*, 126(843):136–195.

Iwamoto, M., Nakahira, Y., Kimpara, H., Sugiyama, T., and Min, K. (2012). Development of a human body finite element model with multiple muscles and their controller for estimating occupant motions and impact responses in frontal crash situations. *Stapp car crash journal*, 56:231.

Jones, D. A. and Round, J. M. (1990). *Skeletal muscle in health and disease: a textbook of muscle physiology*. Manchester University Press.

Jones, D. G. (1995). The human cadaver: An assessment of the value we place on the dead body. *Perspectives on Science and Christian Faith*, 47(1):43–51.

Lawrence, C., Fasanella, E. L., Tabiei, A., Brinkley, J. W., and Shemwell, D. M. (2008). The use of a vehicle acceleration exposure limit model and a finite element crash test dummy model to evaluate the risk of injuries during orion crew module landings.

LSTC (2001). Ls-dyna® keyword user's manual.

Macnab, I. (1973). . the whiplash syndrome. *Clinical neurosurgery*, 20:232–241.

Marieb, E. N. (2001). *Human anatomy & Physiology*. Pearson Education.

Marieb, E. N. and Hoehn, K. (2010). The integumentary system. *Human Anatomy and Physiology. 8th ed. San Francisco, CA: Benjamin Cummings*, 155.

Meijer, R., Elrofai, H., Broos, J., and van Hassel, E. (2013). *Evaluation of an active multi-body human model for braking and frontal crash events*. NHTSA.

Mertz, H. J. and Patrick, L. (1967). Investigation of the kinematics and kinetics of whiplash. Technical report, SAE Technical Paper.

Nelson, O., Pandy, M. G., Myers, B. S., Nightingale, R. W., and Chancey, V. C. (2004). Variation of neck muscle strength along the human cervical spine. *STAPP car crash journal*, 48:397.

Nemirovsky, N. and Van Rooij, L. (2010). A new methodology for biofidelic head-neck postural control. In *Proceedings of the International Research Council on the Biomechanics of Injury conference*, volume 38, pages 71–84. International Research Council on Biomechanics of Injury.

Nigg, B. M. and Herzog, W. (2007). *Biomechanics of the musculo-skeletal system*. John Wiley & Sons.

Panjabi, M., Dvorak, J., Duranceau, J., Yamamoto, I., Gerber, M., Rauschning, W., and Bueff, H. U. (1988). Three-dimensional movements of the upper cervical spine. *Spine*, 13(7):726–730.

Pedotti, A., Krishnan, V., and Stark, L. (1978). Optimization of muscle-force sequencing in human locomotion. *Mathematical Biosciences*, 38(1-2):57–76.

Rusnak-Smith, S., Moffat, M., and Rosen, E. (2001). Anatomical variations of the scalene triangle: dissection of 10 cadavers. *Journal of Orthopaedic & Sports Physical Therapy*, 31(2):70–80.

Schneck, D. (1992). Mechanics and energetics of muscular contraction. *Mechanics of Muscle (2nd ed.). New York, NY: New York University Press*, pages 165–196.

Schoeneburg, R. and Breitling, T. (2005). Enhancement of active and passive safety by future pre-safe systems. In *Proceedings of the 19th ESV Conference, Washington, DC, USA*.

Seacrist, T., Balasubramanian, S., García-España, J. F., Maltese, M. R., Arbogast, K. B., Lopez-Valdes, F. J., Kent, R. W., Tanji, H., and Higuchi, K. (2010). Kinematic comparison of pediatric human volunteers and the hybrid iii 6-year-old anthropomorphic test device. *Ann Adv Automot Med*, 54:97–108.

Siegmund, G. P., Blouin, J.-S., Brault, J. R., Hedenstierna, S., and Inglis, J. T. (2007). Electromyography of superficial and deep neck muscles during isometric, voluntary, and reflex contractions. *Journal of biomechanical engineering*, 129(1):66–77.

Stander, N. and Craig, K. (2002). On the robustness of a simple domain reduction scheme for simulation-based optimization. *Engineering Computations*, 19(4):431–450.

Toosizadeh, N. and Haghpanahi, M. (2011). Generating a finite element model of the cervical spine: Estimating muscle forces and internal loads. *Scientia Iranica*, 18(6):1237–1245.

Tsai, A.-C., Hsieh, T.-H., Luh, J.-J., and Lin, T.-T. (2014). A comparison of upper-limb motion pattern recognition using emg signals during dynamic and isometric muscle contractions. *Biomedical Signal Processing and Control*, 11:17–26.

Tsianos, G. A. and Loeb, G. E. (2013). Muscle physiology and modeling. *Scholarpedia*, 8(10):12388.

Vasavada, A. N., Li, S., and Delp, S. L. (2001). Three-dimensional isometric strength of neck muscles in humans. *Spine*, 26(17):1904–1909.

Vezin, P. and Verriest, J. P. (2005). Development of a set of numerical human models for safety. In *The 19th International ESV Conference*, pages 05–0163.

Viano, D. C. and Arepally, S. (1990). Assessing the safety performance of occupant restraint systems. Technical report, SAE Technical Paper.

WHO (Reviewed November 2016). Road traffic injuries. http://www.who.int/mediacentre/factsheets/fs358/en/. Accessed: 2017-02-21.

Winter, D. A. (2009). *Biomechanics and motor control of human movement*. John Wiley & Sons.

Winters, J. M. (1990). Hill-based muscle models: a systems engineering perspective. In *Multiple muscle systems*, pages 69–93. Springer.

Wismans, J., Happee, R., and Van Dommelen, J. (2005). Computational human body models. In *IUTAM Symposium on impact biomechanics: from fundamental insights to applications*, pages 417–429. Springer.

Wittek, A. and Kajzer, J. (1997). Modelling of muscle influence on the kinematics of the head-neck complex in impacts. *Memoirs - School of Engineering Nagoya University*, 49:155–205.

Wittek, A., Kajzer, J., and Eberhard, H. (2000). Hill-type muscle model for analysis of mechanical effect of muscle tension on the human body response in a car collision using an explicit finite element code. *JSME International Journal Series A Solid Mechanics and Material Engineering*, 43(1):8–18.

Zajac, F. E. (1989). Muscle and tendon properties models scaling and application to biomechanics and motor control. *Critical reviews in biomedical engineering*, 17(4):359–411.

Ólafsdóttir, J. M., Brolin, K., Blouin, J.-S., and Siegmund, G. P. (2015). Dynamic

spatial tuning of cervical muscle reflexes to multidirectional seated perturbations. *Spine*, 40(4):E211–E219.

Östh, J. (2014). Muscle responses of car occupants: numerical modeling and volunteer experiments under pre-crash braking conditions.

Östh, J., Brolin, K., and Bråse, D. (2015a). A human body model with active muscles for simulation of pretensioned restraints in autonomous braking interventions. *Traffic injury prevention*, 16(3):304–313.

Östh, J., Brolin, K., Ólafsdóttir, J. M., Davidsson, J., Pipkorn, B., Jakobsson, L., Törnvall, F., and Lindkvist, M. (2015b). Muscle activation strategies in human body models for the development of integrated safety. In *24th International Technical Conference on the Enhanced Safety of Vehicles (ESV)*, number 15-0345.

A
Appendix

The following sections presents the implementation of the 3 DOF PID controller in LS-DYNA for the AHBM at SAFER, at Chalmers University of Technology.

A.1 Implementation of 3 DOF PID controller in LS-DYNA

Implementation of angle calculations in LS-DYNA, for the sagittal and frontal planes, have been presented in section A.1.1, whereas section A.1.2 presents the implementation of X, Y and Z rotations in LS-DYNA. The calculation of the control signals has been presented in section A.1.3 and the algorithm for implementation of the 3 DOF PID controller has been presented in section A.1.4.

A.1.1 Implementation of angle calculations in LS-DYNA in the sagittal and frontal planes

```
$−−−−−−−−−−−−−−−−−−−−−−−−−−−−−− Angle of Projections −−−−−−−−−−−−−−−−−−
$−−−−−−−−−−−−−−−−−−−−−−−−−−−−−− zx plane −−−−−−−−−−−−−−−−−−−−−−−−−
*DEFINE_CURVE_FUNCTION
$#     lcid      sidr       sfa       sfo      offa      offo    dattyp
    110395         0  1.000000  1.000000     0.000     0.000         0
$# function y_zx(t)
ACOS(((LC43701101−LC43901131)*(CX(43700101)−CX(43900131))+
(LC43703101−LC43903131)*(CZ(43700101)−CZ(43900131)))/
(SQRT((LC43701101−LC43901131)**2+(LC43703101−LC43903131)**2)*
SQRT((CX(43700101)−CX(43900131))**2+(CZ(43700101)−
CZ(43900131))**2)))
*DEFINE_CURVE_FUNCTION
$#     lcid      sidr       sfa       sfo      offa      offo    dattyp
    110396         0  1.000000  1.000000     0.000     0.000         0
$# function
DELAY(110395,20.0,0.0)
$−−−−−−−−−−−−−−−−−−−−−−−−−−−−−− zy plane −−−−−−−−−−−−−−−−−−−−−−−−−
*DEFINE_CURVE_FUNCTION
$#     lcid      sidr       sfa       sfo      offa      offo    dattyp
    110397         0  1.000000  1.000000     0.000     0.000         0
$# function y_zy(t)
ACOS(((LC43702101−LC33302131)*(CY(43700101)−CY(33300131))+
(LC43703101−LC33303131)*(CZ(43700101)−CZ(33300131)))/
(SQRT((LC43702101−LC33302131)**2+(LC43703101−LC33303131)**2)*
SQRT((CY(43700101)−CY(33300131))**2+(CZ(43700101)−
CZ(33300131))**2)))
*DEFINE_CURVE_FUNCTION
$#     lcid      sidr       sfa       sfo      offa      offo    dattyp
    110398         0  1.000000  1.000000     0.000     0.000         0
$# function
```

DELAY(110397,20.0,0.0)

A.1.2 Implementation of rotations around X, Y and Z axis in LS-DYNA

```
$−−−−−−−−−−−−−−−−−−−−−−−−−−−−−−local coordinate system−−−−−−−−−−−−−−−−−−
*DEFINE_COORDINATE_NODES
$#     cid         N1         N2         N3      FLAG       DIR
  43700111  43700101  43700102  43700103         1         X
$−−−−−−−−−−−−−−−−−−−−−−−−rotations around the three axes−−−−−−−−−−−−−−−−−−−−
*DEFINE_CURVE_FUNCTION
$#    lcid      sidr       sfa       sfo      offa      offo    dattyp
       101         0  1.000000  1.000000     0.000     0.000         0
$# function x angular velocity
WX(43700101)
*DEFINE_CURVE_FUNCTION
$#    lcid      sidr       sfa       sfo      offa      offo    dattyp
       102         0  1.000000  1.000000     0.000     0.000         0
$# function y angular velocity
WY(43700101)
*DEFINE_CURVE_FUNCTION
$#    lcid      sidr       sfa       sfo      offa      offo    dattyp
       103         0  1.000000  1.000000     0.000     0.000         0
$# function z angular velocity
WZ(43700101)
*BOUNDARY_PRESCRIBED_MOTION_NODE_ID
$#      id                                                        heading
       43700106x_rotation
$#     nid       dof       vad      lcid        sf       vid     death     birth
  43700106         1         0       101      1.00          01.00000E28       0.0
*BOUNDARY_PRESCRIBED_MOTION_NODE_ID
$#      id                                                        heading
       43700107y_rotation
$#     nid       dof       vad      lcid        sf       vid     death     birth
  43700107         2         0       102      1.00          01.00000E28       0.0
*BOUNDARY_PRESCRIBED_MOTION_NODE_ID
$#      id                                                        heading
       43700108z_rotation
$#     nid       dof       vad      lcid        sf       vid     death     birth
  43700108         3         0       103      1.00          01.00000E28       0.0
*DEFINE_CURVE_FUNCTION_TITLE
Rotation around x axis
$#    lcid      sidr       sfa       sfo      offa      offo    dattyp
  11111297         0       1.0       1.0       0.0       0.0         0
$#                                                              function
DX(43700106)
*DEFINE_CURVE_FUNCTION_TITLE
Rotation around y axis
$#    lcid      sidr       sfa       sfo      offa      offo    dattyp
  11111295         0       1.0       1.0       0.0       0.0         0
$#                                                              function
DY(43700107)
*DEFINE_CURVE_FUNCTION_TITLE
Rotation around z axis
$#    lcid      sidr       sfa       sfo      offa      offo    dattyp
  11111299         0       1.0       1.0       0.0       0.0         0
$#                                                              function
DZ(43700108)
*DEFINE_CURVE_FUNCTION_TITLE
Absolute rotation around z axis
$#    lcid      sidr       sfa       sfo      offa      offo    dattyp
  11111301         0  1.000000  1.000000     0.000     0.000         0
$# function z rotation
ABS(LC11111299)
*ELEMENT_INERTIA
$#   eid       nid      csid
```

```
     11143700106       0
$#     ixx         ixy         ixz         iyy         iyz         izz         mass
  1.000000  0.000000  0.000000       1.000       0.000       1.000   1.000000
*ELEMENT_INERTIA
$#   eid        nid      csid
     22243700107       0
$#     ixx         ixy         ixz         iyy         iyz         izz         mass
  1.000000  0.000000  0.000000       1.000       0.000       1.000   1.000000
*ELEMENT_INERTIA
$#   eid        nid      csid
     33343700108       0
$#     ixx         ixy         ixz         iyy         iyz         izz         mass
  1.000000  0.000000  0.000000       1.000       0.000       1.000   1.000000
```

A.1.3 Calculation of control signals for all three directions in LS-DYNA

```
$---------------------------Reference angle ---------------------------
*DEFINE_CURVE
$#    lcid      sidr       sfa       sfo      offa      offo    dattyp
  43710002         0  1.000000  1.000000     0.000     0.000         0
$#                  a1                  o1
        0.00000e+000 0.0000000000000000
        4.00000e+003 0.0000000000000000
$---------------------------- Control Signals ----------------------------
$------------------------------ zx plane --------------------------------
$ e_xz(t)=r(t)-y_xz(t)
*DEFINE_CURVE_FUNCTION
$#    lcid      sidr       sfa       sfo      offa      offo    dattyp
  43712223         0  1.000000  1.000000     0.000     0.000         0
$# function
LC43710002-LC110396
$ ie_xz(t) = integral of e_xz(t) + initial integral error
*BOUNDARY_PRESCRIBED_MOTION_NODE
$#     nid       dof       vad      lcid        sf       vid     death     birth
  43712224         1         0  43712223  1.000000         0 1.0000E+20     0.000
*DEFINE_CURVE_FUNCTION
$#    lcid      sidr       sfa       sfo      offa      offo    dattyp
  43712224         0  1.000000  1.000000     0.000     0.000         0
$# function
DX(43712224)+LC43720002
$ de_xz/dt, unfiltered
*DEFINE_CURVE_FUNCTION
$#    lcid      sidr       sfa       sfo      offa      offo    dattyp
  43712215         0  1.000000  1.000000     0.000     0.000         0
$# function
ACCX(43712224)
*BOUNDARY_PRESCRIBED_MOTION_NODE
$#     nid       dof       vad      lcid        sf       vid     death     birth
  43712215         1         0  43712215  1.000000         0 1.0000E+20     0.000
*PART
$# title
cervical_dedt_filter
$#     pid     secid       mid     eosid      hgid      grav    adpopt      tmid
  43712215  43712215  43712215         0         0         0         0         0
$ The derivative time constant Tf is determined by the constant d for the damper:
$ E.g. Tf = m/d -> d = m/Tf = 1e-6/5e-3 = 2e-4
*MAT_DAMPER_NONLINEAR_VISCOUS
$#     mid       lcdr
  43712215  43720006
*SECTION_SPRING_DAMPER
$#   secid        dro         kd         v0         cl         fd
  43712215         0      0.000      0.000      0.000      0.000
$#     cdl        tdl
         0          0
*ELEMENT_DISCRETE
```

```
$#   eid       pid        n1        n2       vid                 s        pf            offset
437122154371221543712215437122 25     0          1.000000         0          0.000
*ELEMENT_MASS
$#   eid       nid              mass      pid
4371222543712225          1.0E-343712215
4371221543712215          1.0E-343712215
$ de_xz/dt, filtered
*DEFINE_CURVE_FUNCTION
$#     lcid      sidr       sfa       sfo      offa      offo     dattyp
  43712225         0  1.000000  1.000000     0.000     0.000          0
$# function
VX(43712225)
$ u_xz(t)= xdir*(u(t)=kp*e_xz(t)+ki*ie_xz(t)+kd*de_xz/dt)
*DEFINE_CURVE_FUNCTION
$#     lcid      sidr       sfa       sfo      offa      offo     dattyp
  43712226         0  1.000000  1.000000     0.000     0.000          0
$# function
LC43720003*LC43712223+LC43720004*LC43712224+LC43720005*LC43712225
$-----------------------------yz plane -----------------------------
$ e_yz(t)=r(t)-y_yz(t)
*DEFINE_CURVE_FUNCTION
$#     lcid      sidr       sfa       sfo      offa      offo     dattyp
  43713333         0  1.000000  1.000000     0.000     0.000          0
$# function
LC43710002-LC110398
$ ie_yz(t) = integral of e_yz(t) + initial integral error
*BOUNDARY_PRESCRIBED_MOTION_NODE
$#     nid       dof       vad      lcid        sf       vid     death     birth
  43713334         1         0  43713333  1.000000          01.0000E+20     0.000
*DEFINE_CURVE_FUNCTION
$#     lcid      sidr       sfa       sfo      offa      offo     dattyp
  43713334         0  1.000000  1.000000     0.000     0.000          0
$# function
DX(43713334)+LC43720002
$ de_yz/dt, unfiltered
*DEFINE_CURVE_FUNCTION
$#     lcid      sidr       sfa       sfo      offa      offo     dattyp
  43713315         0  1.000000  1.000000     0.000     0.000          0
$# function
ACCX(43713334)
*BOUNDARY_PRESCRIBED_MOTION_NODE
$#     nid       dof       vad      lcid        sf       vid     death     birth
  43713315         1         0  43713315  1.000000          01.0000E+20     0.000
*PART
$# title
cervical_dedt_filter
$#     pid     secid       mid     eosid      hgid      grav    adpopt      tmid
  43713315  43713315  43713315         0         0         0         0         0
$ The derivative time constant Tf is determined by the constant d for the damper:
$ E.g. Tf = m/d -–> d = m/Tf = 1e-6/5e-3 = 2e-4
*MAT_DAMPER_NONLINEAR_VISCOUS
$#     mid      lcdr
  43713315  43720006
*SECTION_SPRING_DAMPER
$#   secid       dro        kd        v0        cl        fd
  43713315         0     0.000     0.000     0.000     0.000
$#     cdl       tdl
         0         0
*ELEMENT_DISCRETE
$#   eid       pid        n1        n2       vid                 s        pf            offset
437133154371331543713315437133 35     0          1.000000         0          0.000
*ELEMENT_MASS
$#   eid       nid              mass      pid
4371333543713335          1.0E-343713315
4371331543713315          1.0E-343713315
$ de_yz/dt, filtered
*DEFINE_CURVE_FUNCTION
$#     lcid      sidr       sfa       sfo      offa      offo     dattyp
  43713335         0  1.000000  1.000000     0.000     0.000          0
$# function
```

```
VX(43713335)
$ u_yz(t)= ydir*(u(t)=kp*e_yz(t)+ki*ie_yz(t)+kd*de_yz/dt)
*DEFINE_CURVE_FUNCTION
$#     lcid      sidr       sfa       sfo      offa      offo    dattyp
  43713336         0  1.000000  1.000000     0.000     0.000         0
$# function
LC43720003*LC43713333+LC43720004*LC43713334+LC43720005*LC43713335
$---------- axial rotation around z----------
$ e_yz(t)=r(t)-y_yz(t)
*DEFINE_CURVE_FUNCTION
$#     lcid      sidr       sfa       sfo      offa      offo    dattyp
  43714443         0  1.000000  1.000000     0.000     0.000         0
$# function
LC43710002-LC11111301
$ ie_yz(t) = integral of e_yz(t) + initial integral error
*BOUNDARY_PRESCRIBED_MOTION_NODE
$#     nid       dof       vad      lcid        sf       vid     death     birth
  43714444         1         0  43714443  1.000000          01.0000E+20     0.000
*DEFINE_CURVE_FUNCTION
$#     lcid      sidr       sfa       sfo      offa      offo    dattyp
  43714444         0  1.000000  1.000000     0.000     0.000         0
$# function
DX(43714444)+LC43720002
$ de_yz/dt, unfiltered
*DEFINE_CURVE_FUNCTION
$#     lcid      sidr       sfa       sfo      offa      offo    dattyp
  43714415         0  1.000000  1.000000     0.000     0.000         0
$# function
ACCX(43714444)
*BOUNDARY_PRESCRIBED_MOTION_NODE
$#     nid       dof       vad      lcid        sf       vid     death     birth
  43714415         1         0  43714415  1.000000          01.0000E+20     0.000
*PART
$# title
cervical_dedt_filter
$#     pid      secid       mid     eosid      hgid      grav    adpopt      tmid
  43714415  43714415  43714415         0         0         0         0         0
$ The derivative time constant Tf is determined by the constant d for the damper:
$ E.g. Tf = m/d --> d = m/Tf = 1e-6/5e-3 = 2e-4
*MAT_DAMPER_NONLINEAR_VISCOUS
$#     mid       lcdr
  43714415  43720006
*SECTION_SPRING_DAMPER
$#   secid       dro        kd        v0        cl        fd
  43714415         0     0.000     0.000     0.000     0.000
$#      cdl       tdl
         0         0
*ELEMENT_DISCRETE
$#   eid       pid        n1        n2       vid                 s        pf            offset
43714415437144154371441543714445     0          1.000000         0             0.000
*ELEMENT_MASS
$#   eid       nid              mass      pid
4371444543714445          1.0E-343714415
4371441543714415          1.0E-343714415
$ de_yz/dt, filtered
*DEFINE_CURVE_FUNCTION
$#     lcid      sidr       sfa       sfo      offa      offo    dattyp
  43714445         0  1.000000  1.000000     0.000     0.000         0
$# function
VX(43714445)
$ u_yz(t)= ydir*(u(t)=kp*e_yz(t)+ki*ie_yz(t)+kd*de_yz/dt)
*DEFINE_CURVE_FUNCTION
$#     lcid      sidr       sfa       sfo      offa      offo    dattyp
  43714446         0  1.000000  1.000000     0.000     0.000         0
$# function
LC43720003*LC43714443+LC43720004*LC43714444+LC43720005*LC43714445
```

A.1.4 Implementation of algorithm for 3 DOF PID controller

```
$−−−−−−−−−−−−−−−−−−−−−−−−−−−−−−−−sign−−−−−−−−−−−−−−−−−−−−−−−−−−−−−−−−
$$ DEFINE_CURVE for a1 for DEFINE_CURVE_FUNCTION SIGN(a1,a2)
*DEFINE_CURVE
$#     lcid      sidr       sfa       sfo      offa      offo     dattyp
  11111111         0  1.000000  1.000000     0.000     0.000          0
$#                a1                  o1
        0.00000e+000       1.0000000000
        4.00000e+003       1.0000000000
$$ DEFINE_CURVE_FUNCTION SIGN for rotation in zx plane
*DEFINE_CURVE_FUNCTION
$#     lcid      sidr       sfa       sfo      offa      offo     dattyp
  11111195         0  1.000000  1.000000     0.000     0.000          0
$# function
SIGN(LC11111111,LC11111295)
$$ DEFINE_CURVE_FUNCTION SIGN for rotation in zy plane
*DEFINE_CURVE_FUNCTION
$#     lcid      sidr       sfa       sfo      offa      offo     dattyp
  11111197         0  1.000000  1.000000     0.000     0.000          0
$# function
SIGN(LC11111111,LC11111297)
$$ DEFINE_CURVE_FUNCTION SIGN for rotation around z axis
*DEFINE_CURVE_FUNCTION
$#     lcid      sidr       sfa       sfo      offa      offo     dattyp
  11111199         0  1.000000  1.000000     0.000     0.000          0
$# function
SIGN(LC11111111,LC11111299)
$−−−−−−−−−−−−−−−−−−−−−−−−−−−−−−−−u_tot(t)−−−−−−−−−−−−−−−−−−−−−−−−−−−−−−−
      u_tot(t)=scaling_factor_muscle_x∗u_x(t)+scaling_factor_muscle_y∗u_y(t)
$$ For stationary position
*DEFINE_CURVE
$#     lcid      sidr       sfa       sfo      offa      offo     dattyp
  22222111         0  1.000000  1.000000     0.000     0.000          0
$#                a1                  o1
        0.00000e+000       0.0000000000
        4.00000e+003       0.0000000000
$−−−−−−−−−−−−−−−−−−−−−−−−−−−−−−−−LEFT−−−−−−−−−−−−−−−−−−−−−−−−−−−−−−−−
$ SCM_L
*DEFINE_CURVE_FUNCTION
$#     lcid      sidr       sfa       sfo      offa      offo     dattyp
  22210180         0  1.000000  1.000000     0.000     0.000          0
$# function
scaling_factor_SCM_L(180.000e+000)
*DEFINE_CURVE_FUNCTION
$#     lcid      sidr       sfa       sfo      offa      offo     dattyp
  22210000         0  1.000000  1.000000     0.000     0.000          0
$# function
scaling_factor_SCM_L(0.00000e+000)
*DEFINE_CURVE_FUNCTION
$#     lcid      sidr       sfa       sfo      offa      offo     dattyp
  22210090         0  1.000000  1.000000     0.000     0.000          0
$# function
scaling_factor_SCM_L(90.0000e+000)
*DEFINE_CURVE_FUNCTION
$#     lcid      sidr       sfa       sfo      offa      offo     dattyp
  22210270         0  1.000000  1.000000     0.000     0.000          0
$# function
scaling_factor_SCM_L(−90.0000e+000)
$−−−−−−−−−−−−−−−−−−−−−−−−−−−−−−−−−−−−−−−−−−−−−−−−−−−−−−−−−−−−−−−−−−−−
$ STH_L
*DEFINE_CURVE_FUNCTION
$#     lcid      sidr       sfa       sfo      offa      offo     dattyp
  22220180         0  1.000000  1.000000     0.000     0.000          0
$# function
scaling_factor_STH_L(180.000e+000)
*DEFINE_CURVE_FUNCTION
```

```
$#     lcid      sidr       sfa       sfo      offa      offo    dattyp
  22220000         0  1.000000  1.000000     0.000     0.000         0
$# function
scaling_factor_STH_L(0.00000e+000)
*DEFINE_CURVE_FUNCTION
$#     lcid      sidr       sfa       sfo      offa      offo    dattyp
  22220090         0  1.000000  1.000000     0.000     0.000         0
$# function
scaling_factor_STH_L(90.0000e+000)
*DEFINE_CURVE_FUNCTION
$#     lcid      sidr       sfa       sfo      offa      offo    dattyp
  22220270         0  1.000000  1.000000     0.000     0.000         0
$# function
scaling_factor_STH_L(-90.0000e+000)
$---------------------------------------------------------------------
$ LS_L
*DEFINE_CURVE_FUNCTION
$#     lcid      sidr       sfa       sfo      offa      offo    dattyp
  22230180         0  1.000000  1.000000     0.000     0.000         0
$# function
scaling_factor_LS_L(180.000e+000)
*DEFINE_CURVE_FUNCTION
$#     lcid      sidr       sfa       sfo      offa      offo    dattyp
  22230000         0  1.000000  1.000000     0.000     0.000         0
$# function
scaling_factor_LS_L(0.00000e+000)
*DEFINE_CURVE_FUNCTION
$#     lcid      sidr       sfa       sfo      offa      offo    dattyp
  22230090         0  1.000000  1.000000     0.000     0.000         0
$# function
scaling_factor_LS_L(90.0000e+000)
*DEFINE_CURVE_FUNCTION
$#     lcid      sidr       sfa       sfo      offa      offo    dattyp
  22230270         0  1.000000  1.000000     0.000     0.000         0
$# function
scaling_factor_LS_L(-90.0000e+000)
$---------------------------------------------------------------------
$ Trap_L
*DEFINE_CURVE_FUNCTION
$#     lcid      sidr       sfa       sfo      offa      offo    dattyp
  22240180         0  1.000000  1.000000     0.000     0.000         0
$# function
scaling_factor_Trap_L(180.000e+000)
*DEFINE_CURVE_FUNCTION
$#     lcid      sidr       sfa       sfo      offa      offo    dattyp
  22240000         0  1.000000  1.000000     0.000     0.000         0
$# function
scaling_factor_Trap_L(0.00000e+000)
*DEFINE_CURVE_FUNCTION
$#     lcid      sidr       sfa       sfo      offa      offo    dattyp
  22240090         0  1.000000  1.000000     0.000     0.000         0
$# function
scaling_factor_Trap_L(90.0000e+000)
*DEFINE_CURVE_FUNCTION
$#     lcid      sidr       sfa       sfo      offa      offo    dattyp
  22240270         0  1.000000  1.000000     0.000     0.000         0
$# function
scaling_factor_Trap_L(-90.0000e+000)
$---------------------------------------------------------------------
$ SCap_L
*DEFINE_CURVE_FUNCTION
$#     lcid      sidr       sfa       sfo      offa      offo    dattyp
  22250180         0  1.000000  1.000000     0.000     0.000         0
$# function
scaling_factor_SCap_L(180.000e+000)
*DEFINE_CURVE_FUNCTION
$#     lcid      sidr       sfa       sfo      offa      offo    dattyp
  22250000         0  1.000000  1.000000     0.000     0.000         0
$# function
scaling_factor_SCap_L(0.00000e+000)
```

```
*DEFINE_CURVE_FUNCTION
$#     lcid      sidr       sfa       sfo      offa      offo    dattyp
  22250090         0  1.000000  1.000000     0.000     0.000         0
$# function
scaling_factor_SCap_L(90.0000e+000)
*DEFINE_CURVE_FUNCTION
$#     lcid      sidr       sfa       sfo      offa      offo    dattyp
  22250270         0  1.000000  1.000000     0.000     0.000         0
$# function
scaling_factor_SCap_L(-90.0000e+000)
$---------------------------------------------------------------------
$ SCerv_L
*DEFINE_CURVE_FUNCTION
$#     lcid      sidr       sfa       sfo      offa      offo    dattyp
  22260180         0  1.000000  1.000000     0.000     0.000         0
$# function
scaling_factor_SCerv_L(180.000e+000)
*DEFINE_CURVE_FUNCTION
$#     lcid      sidr       sfa       sfo      offa      offo    dattyp
  22260000         0  1.000000  1.000000     0.000     0.000         0
$# function
scaling_factor_SCerv_L(0.00000e+000)
*DEFINE_CURVE_FUNCTION
$#     lcid      sidr       sfa       sfo      offa      offo    dattyp
  22260090         0  1.000000  1.000000     0.000     0.000         0
$# function
scaling_factor_SCerv_L(90.0000e+000)
*DEFINE_CURVE_FUNCTION
$#     lcid      sidr       sfa       sfo      offa      offo    dattyp
  22260270         0  1.000000  1.000000     0.000     0.000         0
$# function
scaling_factor_SCerv_L(-90.0000e+000)
$---------------------------------------------------------------------
$ CMC4_L
*DEFINE_CURVE_FUNCTION
$#     lcid      sidr       sfa       sfo      offa      offo    dattyp
  22270180         0  1.000000  1.000000     0.000     0.000         0
$# function
scaling_factor_CMC4_L(180.000e+000)
*DEFINE_CURVE_FUNCTION
$#     lcid      sidr       sfa       sfo      offa      offo    dattyp
  22270000         0  1.000000  1.000000     0.000     0.000         0
$# function
scaling_factor_CMC4_L(0.00000e+000)
*DEFINE_CURVE_FUNCTION
$#     lcid      sidr       sfa       sfo      offa      offo    dattyp
  22270090         0  1.000000  1.000000     0.000     0.000         0
$# function
scaling_factor_CMC4_L(90.0000e+000)
*DEFINE_CURVE_FUNCTION
$#     lcid      sidr       sfa       sfo      offa      offo    dattyp
  22270270         0  1.000000  1.000000     0.000     0.000         0
$# function
scaling_factor_CMC4_L(-90.0000e+000)
$---------------------------------------------------------------------
$ CMC6_L
*DEFINE_CURVE_FUNCTION
$#     lcid      sidr       sfa       sfo      offa      offo    dattyp
  22280180         0  1.000000  1.000000     0.000     0.000         0
$# function
scaling_factor_CMC6_L(180.000e+000)
*DEFINE_CURVE_FUNCTION
$#     lcid      sidr       sfa       sfo      offa      offo    dattyp
  22280000         0  1.000000  1.000000     0.000     0.000         0
$# function
scaling_factor_CMC6_L(0.00000e+000)
*DEFINE_CURVE_FUNCTION
$#     lcid      sidr       sfa       sfo      offa      offo    dattyp
  22280090         0  1.000000  1.000000     0.000     0.000         0
$# function
```

```
scaling_factor_CMC6_L(90.0000e+000)
*DEFINE_CURVE_FUNCTION
$#     lcid      sidr       sfa       sfo      offa      offo    dattyp
  22280270         0  1.000000  1.000000     0.000     0.000         0
$# function
scaling_factor_CMC6_L(-90.0000e+000)
$-------------------------------------------------------------------
$ SPL_L
*DEFINE_CURVE_FUNCTION
$#     lcid      sidr       sfa       sfo      offa      offo    dattyp
  22290180         0  1.000000  1.000000     0.000     0.000         0
$# function
scaling_factor_SPL_L(180.000e+000)
*DEFINE_CURVE_FUNCTION
$#     lcid      sidr       sfa       sfo      offa      offo    dattyp
  22290000         0  1.000000  1.000000     0.000     0.000         0
$# function
scaling_factor_SPL_L(0.00000e+000)
*DEFINE_CURVE_FUNCTION
$#     lcid      sidr       sfa       sfo      offa      offo    dattyp
  22290090         0  1.000000  1.000000     0.000     0.000         0
$# function
scaling_factor_SPL_L(90.0000e+000)
*DEFINE_CURVE_FUNCTION
$#     lcid      sidr       sfa       sfo      offa      offo    dattyp
  22290270         0  1.000000  1.000000     0.000     0.000         0
$# function
scaling_factor_SPL_L(-90.0000e+000)
$-------------------------------RIGHT-------------------------
$ SCM_R
*DEFINE_CURVE_FUNCTION
$#     lcid      sidr       sfa       sfo      offa      offo    dattyp
  22215180         0  1.000000  1.000000     0.000     0.000         0
$# function
scaling_factor_SCM_R(180.000e+000)
*DEFINE_CURVE_FUNCTION
$#     lcid      sidr       sfa       sfo      offa      offo    dattyp
  22215000         0  1.000000  1.000000     0.000     0.000         0
$# function
scaling_factor_SCM_R(0.00000e+000)
*DEFINE_CURVE_FUNCTION
$#     lcid      sidr       sfa       sfo      offa      offo    dattyp
  22215090         0  1.000000  1.000000     0.000     0.000         0
$# function
scaling_factor_SCM_R(90.0000e+000)
*DEFINE_CURVE_FUNCTION
$#     lcid      sidr       sfa       sfo      offa      offo    dattyp
  22215270         0  1.000000  1.000000     0.000     0.000         0
$# function
scaling_factor_SCM_R(-90.0000e+000)
$-------------------------------------------------------------------
$ STH_R
*DEFINE_CURVE_FUNCTION
$#     lcid      sidr       sfa       sfo      offa      offo    dattyp
  22225180         0  1.000000  1.000000     0.000     0.000         0
$# function
scaling_factor_STH_R(180.000e+000)
*DEFINE_CURVE_FUNCTION
$#     lcid      sidr       sfa       sfo      offa      offo    dattyp
  22225000         0  1.000000  1.000000     0.000     0.000         0
$# function
scaling_factor_STH_R(0.00000e+000)
*DEFINE_CURVE_FUNCTION
$#     lcid      sidr       sfa       sfo      offa      offo    dattyp
  22225090         0  1.000000  1.000000     0.000     0.000         0
$# function
scaling_factor_STH_R(90.0000e+000)
*DEFINE_CURVE_FUNCTION
$#     lcid      sidr       sfa       sfo      offa      offo    dattyp
  22225270         0  1.000000  1.000000     0.000     0.000         0
```

```
$# function
scaling_factor_STH_R(-90.0000e+000)
$-------------------------------------------------------------------
$ LS_R
*DEFINE_CURVE_FUNCTION
$#     lcid      sidr       sfa       sfo      offa      offo    dattyp
  22235180         0  1.000000  1.000000     0.000     0.000         0
$# function
scaling_factor_LS_R(180.000e+000)
*DEFINE_CURVE_FUNCTION
$#     lcid      sidr       sfa       sfo      offa      offo    dattyp
  22235000         0  1.000000  1.000000     0.000     0.000         0
$# function
scaling_factor_LS_R(0.00000e+000)
*DEFINE_CURVE_FUNCTION
$#     lcid      sidr       sfa       sfo      offa      offo    dattyp
  22235090         0  1.000000  1.000000     0.000     0.000         0
$# function
scaling_factor_LS_R(90.0000e+000)
*DEFINE_CURVE_FUNCTION
$#     lcid      sidr       sfa       sfo      offa      offo    dattyp
  22235270         0  1.000000  1.000000     0.000     0.000         0
$# function
scaling_factor_LS_R(-90.0000e+000)
$-------------------------------------------------------------------
$ Trap_R
*DEFINE_CURVE_FUNCTION
$#     lcid      sidr       sfa       sfo      offa      offo    dattyp
  22245180         0  1.000000  1.000000     0.000     0.000         0
$# function
scaling_factor_Trap_R(180.000e+000)
*DEFINE_CURVE_FUNCTION
$#     lcid      sidr       sfa       sfo      offa      offo    dattyp
  22245000         0  1.000000  1.000000     0.000     0.000         0
$# function
scaling_factor_Trap_R(0.00000e+000)
*DEFINE_CURVE_FUNCTION
$#     lcid      sidr       sfa       sfo      offa      offo    dattyp
  22245090         0  1.000000  1.000000     0.000     0.000         0
$# function
scaling_factor_Trap_R(90.0000e+000)
*DEFINE_CURVE_FUNCTION
$#     lcid      sidr       sfa       sfo      offa      offo    dattyp
  22245270         0  1.000000  1.000000     0.000     0.000         0
$# function
scaling_factor_Trap_R(-90.0000e+000)
$-------------------------------------------------------------------
$ SCap_R
*DEFINE_CURVE_FUNCTION
$#     lcid      sidr       sfa       sfo      offa      offo    dattyp
  22255180         0  1.000000  1.000000     0.000     0.000         0
$# function
scaling_factor_SCap_R(180.000e+000)
*DEFINE_CURVE_FUNCTION
$#     lcid      sidr       sfa       sfo      offa      offo    dattyp
  22255000         0  1.000000  1.000000     0.000     0.000         0
$# function
scaling_factor_SCap_R(0.00000e+000)
*DEFINE_CURVE_FUNCTION
$#     lcid      sidr       sfa       sfo      offa      offo    dattyp
  22255090         0  1.000000  1.000000     0.000     0.000         0
$# function
scaling_factor_SCap_R(90.0000e+000)
*DEFINE_CURVE_FUNCTION
$#     lcid      sidr       sfa       sfo      offa      offo    dattyp
  22255270         0  1.000000  1.000000     0.000     0.000         0
$# function
scaling_factor_SCap_R(-90.0000e+000)
$-------------------------------------------------------------------
$ SCerv_R
```

```
*DEFINE_CURVE_FUNCTION
$#     lcid      sidr       sfa       sfo      offa      offo    dattyp
  22265180         0  1.000000  1.000000     0.000     0.000         0
$# function
scaling_factor_SCerv_R(180.000e+000)
*DEFINE_CURVE_FUNCTION
$#     lcid      sidr       sfa       sfo      offa      offo    dattyp
  22265000         0  1.000000  1.000000     0.000     0.000         0
$# function
scaling_factor_SCerv_R(0.00000e+000)
*DEFINE_CURVE_FUNCTION
$#     lcid      sidr       sfa       sfo      offa      offo    dattyp
  22265090         0  1.000000  1.000000     0.000     0.000         0
$# function
scaling_factor_SCerv_R(90.0000e+000)
*DEFINE_CURVE_FUNCTION
$#     lcid      sidr       sfa       sfo      offa      offo    dattyp
  22265270         0  1.000000  1.000000     0.000     0.000         0
$# function
scaling_factor_SCerv_R(-90.0000e+000)
$---------------------------------------------------------------------
$ CMC4_R
*DEFINE_CURVE_FUNCTION
$#     lcid      sidr       sfa       sfo      offa      offo    dattyp
  22275180         0  1.000000  1.000000     0.000     0.000         0
$# function
scaling_factor_CMC4_R(180.000e+000)
*DEFINE_CURVE_FUNCTION
$#     lcid      sidr       sfa       sfo      offa      offo    dattyp
  22275000         0  1.000000  1.000000     0.000     0.000         0
$# function
scaling_factor_CMC4_R(0.00000e+000)
*DEFINE_CURVE_FUNCTION
$#     lcid      sidr       sfa       sfo      offa      offo    dattyp
  22275090         0  1.000000  1.000000     0.000     0.000         0
$# function
scaling_factor_CMC4_R(90.0000e+000)
*DEFINE_CURVE_FUNCTION
$#     lcid      sidr       sfa       sfo      offa      offo    dattyp
  22275270         0  1.000000  1.000000     0.000     0.000         0
$# function
scaling_factor_CMC4_R(-90.0000e+000)
$---------------------------------------------------------------------
$ CMC6_R
*DEFINE_CURVE_FUNCTION
$#     lcid      sidr       sfa       sfo      offa      offo    dattyp
  22285180         0  1.000000  1.000000     0.000     0.000         0
$# function
scaling_factor_CMC6_R(180.000e+000)
*DEFINE_CURVE_FUNCTION
$#     lcid      sidr       sfa       sfo      offa      offo    dattyp
  22285000         0  1.000000  1.000000     0.000     0.000         0
$# function
scaling_factor_CMC6_R(0.00000e+000)
*DEFINE_CURVE_FUNCTION
$#     lcid      sidr       sfa       sfo      offa      offo    dattyp
  22285090         0  1.000000  1.000000     0.000     0.000         0
$# function
scaling_factor_CMC6_R(90.0000e+000)
*DEFINE_CURVE_FUNCTION
$#     lcid      sidr       sfa       sfo      offa      offo    dattyp
  22285270         0  1.000000  1.000000     0.000     0.000         0
$# function
scaling_factor_CMC6_R(-90.0000e+000)
$---------------------------------------------------------------------
$ SPL_R
*DEFINE_CURVE_FUNCTION
$#     lcid      sidr       sfa       sfo      offa      offo    dattyp
  22295180         0  1.000000  1.000000     0.000     0.000         0
$# function
```

```
scaling_factor_SPL_R(180.000e+000)
*DEFINE_CURVE_FUNCTION
$#     lcid      sidr       sfa       sfo      offa      offo    dattyp
  22295000         0  1.000000  1.000000     0.000     0.000         0
$# function
scaling_factor_SPL_R(0.00000e+000)
*DEFINE_CURVE_FUNCTION
$#     lcid      sidr       sfa       sfo      offa      offo    dattyp
  22295090         0  1.000000  1.000000     0.000     0.000         0
$# function
scaling_factor_SPL_R(90.0000e+000)
*DEFINE_CURVE_FUNCTION
$#     lcid      sidr       sfa       sfo      offa      offo    dattyp
  22295270         0  1.000000  1.000000     0.000     0.000         0
$# function
scaling_factor_SPL_R(-90.0000e+000)
$------------------------------IF CONDITIONS-------------LEFT----
$$ SCM_L
$$ DEFINE_CURVE_FUNCTION IF for zx plane, flexion-extension
*DEFINE_CURVE_FUNCTION
$#     lcid      sidr       sfa       sfo      offa      offo    dattyp
  11112210         0  1.000000  1.000000     0.000     0.000         0
$# function
IF(11111195,22210180,22222111,22210000)
$$ DEFINE_CURVE_FUNCTION IF for zy plane, lateral bending
*DEFINE_CURVE_FUNCTION
$#     lcid      sidr       sfa       sfo      offa      offo    dattyp
  11113310         0  1.000000  1.000000     0.000     0.000         0
$# function
IF(11111197,22210270,22222111,22210090)
$$ DEFINE_CURVE_FUNCTION IF for lateral axial rotation
*DEFINE_CURVE_FUNCTION
$#     lcid      sidr       sfa       sfo      offa      offo    dattyp
  11114410         0  1.000000  1.000000     0.000     0.000         0
$# function
IF(11111199,88885001,22222111,88880001)
$-------------------------------------------------------------------
$$ STH_L
$$ DEFINE_CURVE_FUNCTION IF for zx plane, flexion-extension
*DEFINE_CURVE_FUNCTION
$#     lcid      sidr       sfa       sfo      offa      offo    dattyp
  11112220         0  1.000000  1.000000     0.000     0.000         0
$# function
IF(11111195,22220180,22222111,22220000)
$$ DEFINE_CURVE_FUNCTION IF for zy plane, lateral bending
*DEFINE_CURVE_FUNCTION
$#     lcid      sidr       sfa       sfo      offa      offo    dattyp
  11113320         0  1.000000  1.000000     0.000     0.000         0
$# function
IF(11111197,22220270,22222111,22220090)
$$ DEFINE_CURVE_FUNCTION IF for lateral axial rotation
*DEFINE_CURVE_FUNCTION
$#     lcid      sidr       sfa       sfo      offa      offo    dattyp
  11114420         0  1.000000  1.000000     0.000     0.000         0
$# function
IF(11111199,88885002,22222111,88880002)
$-------------------------------------------------------------------
$$ LS_L
$$ DEFINE_CURVE_FUNCTION IF for zx plane, flexion-extension
*DEFINE_CURVE_FUNCTION
$#     lcid      sidr       sfa       sfo      offa      offo    dattyp
  11112230         0  1.000000  1.000000     0.000     0.000         0
$# function
IF(11111195,22230180,22222111,22230000)
$$ DEFINE_CURVE_FUNCTION IF for zy plane, lateral bending
*DEFINE_CURVE_FUNCTION
$#     lcid      sidr       sfa       sfo      offa      offo    dattyp
  11113330         0  1.000000  1.000000     0.000     0.000         0
$# function
IF(11111197,22230270,22222111,22230090)
```

```
$$ DEFINE_CURVE_FUNCTION IF for lateral axial rotation
*DEFINE_CURVE_FUNCTION
$#     lcid      sidr       sfa       sfo      offa      offo    dattyp
  11114430         0  1.000000  1.000000     0.000     0.000         0
$# function
IF(11111199,88885003,22222111,88880003)
$-------------------------------------------------------------------
$$ Trap_L
$$ DEFINE_CURVE_FUNCTION IF for zx plane, flexion-extension
*DEFINE_CURVE_FUNCTION
$#     lcid      sidr       sfa       sfo      offa      offo    dattyp
  11112240         0  1.000000  1.000000     0.000     0.000         0
$# function
IF(11111195,22240180,22222111,22240000)
$$ DEFINE_CURVE_FUNCTION IF for zy plane, lateral bending
*DEFINE_CURVE_FUNCTION
$#     lcid      sidr       sfa       sfo      offa      offo    dattyp
  11113340         0  1.000000  1.000000     0.000     0.000         0
$# function
IF(11111197,22240270,22222111,22240090)
$$ DEFINE_CURVE_FUNCTION IF for lateral axial rotation
*DEFINE_CURVE_FUNCTION
$#     lcid      sidr       sfa       sfo      offa      offo    dattyp
  11114440         0  1.000000  1.000000     0.000     0.000         0
$# function
IF(11111199,88885004,22222111,88880004)
$-------------------------------------------------------------------
$$ SCap_L
$$ DEFINE_CURVE_FUNCTION IF for zx plane, flexion-extension
*DEFINE_CURVE_FUNCTION
$#     lcid      sidr       sfa       sfo      offa      offo    dattyp
  11112250         0  1.000000  1.000000     0.000     0.000         0
$# function
IF(11111195,22250180,22222111,22250000)
$$ DEFINE_CURVE_FUNCTION IF for zy plane, lateral bending
*DEFINE_CURVE_FUNCTION
$#     lcid      sidr       sfa       sfo      offa      offo    dattyp
  11113350         0  1.000000  1.000000     0.000     0.000         0
$# function
IF(11111197,22250270,22222111,22250090)
$$ DEFINE_CURVE_FUNCTION IF for lateral axial rotation
*DEFINE_CURVE_FUNCTION
$#     lcid      sidr       sfa       sfo      offa      offo    dattyp
  11114450         0  1.000000  1.000000     0.000     0.000         0
$# function
IF(11111199,88885005,22222111,88880005)
$-------------------------------------------------------------------
$$ SCerv_L
$$ DEFINE_CURVE_FUNCTION IF for zx plane, flexion-extension
*DEFINE_CURVE_FUNCTION
$#     lcid      sidr       sfa       sfo      offa      offo    dattyp
  11112260         0  1.000000  1.000000     0.000     0.000         0
$# function
IF(11111195,22260180,22222111,22260000)
$$ DEFINE_CURVE_FUNCTION IF for zy plane, lateral bending
*DEFINE_CURVE_FUNCTION
$#     lcid      sidr       sfa       sfo      offa      offo    dattyp
  11113360         0  1.000000  1.000000     0.000     0.000         0
$# function
IF(11111197,22260270,22222111,22260090)
$$ DEFINE_CURVE_FUNCTION IF for lateral axial rotation
*DEFINE_CURVE_FUNCTION
$#     lcid      sidr       sfa       sfo      offa      offo    dattyp
  11114460         0  1.000000  1.000000     0.000     0.000         0
$# function
IF(11111199,88885006,22222111,88880006)
$-------------------------------------------------------------------
$$ CMC4_L
$$ DEFINE_CURVE_FUNCTION IF for zx plane, flexion-extension
*DEFINE_CURVE_FUNCTION
```

```
$#     lcid      sidr       sfa       sfo      offa      offo    dattyp
  11112270         0  1.000000  1.000000     0.000     0.000         0
$# function
IF(11111195,22270180,22222111,22270000)
$$ DEFINE_CURVE_FUNCTION IF for zy plane, lateral bending
*DEFINE_CURVE_FUNCTION
$#     lcid      sidr       sfa       sfo      offa      offo    dattyp
  11113370         0  1.000000  1.000000     0.000     0.000         0
$# function
IF(11111197,22270270,22222111,22270090)
$$ DEFINE_CURVE_FUNCTION IF for lateral axial rotation
*DEFINE_CURVE_FUNCTION
$#     lcid      sidr       sfa       sfo      offa      offo    dattyp
  11114470         0  1.000000  1.000000     0.000     0.000         0
$# function
IF(11111199,88885007,22222111,88880007)
$------------------------------------------------------------------
$$ CMC6_L
$$ DEFINE_CURVE_FUNCTION IF for zx plane, flexion-extension
*DEFINE_CURVE_FUNCTION
$#     lcid      sidr       sfa       sfo      offa      offo    dattyp
  11112280         0  1.000000  1.000000     0.000     0.000         0
$# function
IF(11111195,22280180,22222111,22280000)
$$ DEFINE_CURVE_FUNCTION IF for zy plane, lateral bending
*DEFINE_CURVE_FUNCTION
$#     lcid      sidr       sfa       sfo      offa      offo    dattyp
  11113380         0  1.000000  1.000000     0.000     0.000         0
$# function
IF(11111197,22280270,22222111,22280090)
$$ DEFINE_CURVE_FUNCTION IF for lateral axial rotation
*DEFINE_CURVE_FUNCTION
$#     lcid      sidr       sfa       sfo      offa      offo    dattyp
  11114480         0  1.000000  1.000000     0.000     0.000         0
$# function
IF(11111199,88885008,22222111,88880008)
$------------------------------------------------------------------
$$ SPL_L
$$ DEFINE_CURVE_FUNCTION IF for zx plane, flexion-extension
*DEFINE_CURVE_FUNCTION
$#     lcid      sidr       sfa       sfo      offa      offo    dattyp
  11112290         0  1.000000  1.000000     0.000     0.000         0
$# function
IF(11111195,22290180,22222111,22290000)
$$ DEFINE_CURVE_FUNCTION IF for zy plane, lateral bending
*DEFINE_CURVE_FUNCTION
$#     lcid      sidr       sfa       sfo      offa      offo    dattyp
  11113390         0  1.000000  1.000000     0.000     0.000         0
$# function
IF(11111197,22290270,22222111,22290090)
$$ DEFINE_CURVE_FUNCTION IF for lateral axial rotation
*DEFINE_CURVE_FUNCTION
$#     lcid      sidr       sfa       sfo      offa      offo    dattyp
  11114490         0  1.000000  1.000000     0.000     0.000         0
$# function
IF(11111199,88885009,22222111,88880009)
$------------------------------IF CONDITIONS---------------RIGHT---
$$ SCM_R
$$ DEFINE_CURVE_FUNCTION IF for zx plane, flexion-extension
*DEFINE_CURVE_FUNCTION
$#     lcid      sidr       sfa       sfo      offa      offo    dattyp
  11112215         0  1.000000  1.000000     0.000     0.000         0
$# function
IF(11111195,22215180,22222111,22215000)
$$ DEFINE_CURVE_FUNCTION IF for zy plane, lateral bending
*DEFINE_CURVE_FUNCTION
$#     lcid      sidr       sfa       sfo      offa      offo    dattyp
  11113315         0  1.000000  1.000000     0.000     0.000         0
$# function
IF(11111197,22215270,22222111,22215090)
```

```
$$ DEFINE_CURVE_FUNCTION IF for lateral axial rotation
*DEFINE_CURVE_FUNCTION
$#     lcid      sidr       sfa       sfo      offa      offo    dattyp
  11114415         0  1.000000  1.000000     0.000     0.000         0
$# function
IF(11111199,88885051,22222111,88880051)
$-------------------------------------------------------------------
$$ STH_R
$$ DEFINE_CURVE_FUNCTION IF for zx plane, flexion-extension
*DEFINE_CURVE_FUNCTION
$#     lcid      sidr       sfa       sfo      offa      offo    dattyp
  11112225         0  1.000000  1.000000     0.000     0.000         0
$# function
IF(11111195,22225180,22222111,22225000)
$$ DEFINE_CURVE_FUNCTION IF for zy plane, lateral bending
*DEFINE_CURVE_FUNCTION
$#     lcid      sidr       sfa       sfo      offa      offo    dattyp
  11113325         0  1.000000  1.000000     0.000     0.000         0
$# function
IF(11111197,22225270,22222111,22225090)
$$ DEFINE_CURVE_FUNCTION IF for lateral axial rotation
*DEFINE_CURVE_FUNCTION
$#     lcid      sidr       sfa       sfo      offa      offo    dattyp
  11114425         0  1.000000  1.000000     0.000     0.000         0
$# function
IF(11111199,88885052,22222111,88880052)
$-------------------------------------------------------------------
$$ LS_R
$$ DEFINE_CURVE_FUNCTION IF for zx plane, flexion-extension
*DEFINE_CURVE_FUNCTION
$#     lcid      sidr       sfa       sfo      offa      offo    dattyp
  11112235         0  1.000000  1.000000     0.000     0.000         0
$# function
IF(11111195,22235180,22222111,22235000)
$$ DEFINE_CURVE_FUNCTION IF for zy plane, lateral bending
*DEFINE_CURVE_FUNCTION
$#     lcid      sidr       sfa       sfo      offa      offo    dattyp
  11113335         0  1.000000  1.000000     0.000     0.000         0
$# function
IF(11111197,22235270,22222111,22235090)
$$ DEFINE_CURVE_FUNCTION IF for lateral axial rotation
*DEFINE_CURVE_FUNCTION
$#     lcid      sidr       sfa       sfo      offa      offo    dattyp
  11114435         0  1.000000  1.000000     0.000     0.000         0
$# function
IF(11111199,88885053,22222111,88880053)
$-------------------------------------------------------------------
$$ Trap_R
$$ DEFINE_CURVE_FUNCTION IF for zx plane, flexion-extension
*DEFINE_CURVE_FUNCTION
$#     lcid      sidr       sfa       sfo      offa      offo    dattyp
  11112245         0  1.000000  1.000000     0.000     0.000         0
$# function
IF(11111195,22245180,22222111,22245000)
$$ DEFINE_CURVE_FUNCTION IF for zy plane, lateral bending
*DEFINE_CURVE_FUNCTION
$#     lcid      sidr       sfa       sfo      offa      offo    dattyp
  11113345         0  1.000000  1.000000     0.000     0.000         0
$# function
IF(11111197,22245270,22222111,22245090)
$$ DEFINE_CURVE_FUNCTION IF for lateral axial rotation
*DEFINE_CURVE_FUNCTION
$#     lcid      sidr       sfa       sfo      offa      offo    dattyp
  11114445         0  1.000000  1.000000     0.000     0.000         0
$# function
IF(11111199,88885054,22222111,88880054)
$-------------------------------------------------------------------
$$ SCap_R
$$ DEFINE_CURVE_FUNCTION IF for zx plane, flexion-extension
*DEFINE_CURVE_FUNCTION
```

```
$#     lcid      sidr       sfa       sfo      offa      offo    dattyp
  11112255         0  1.000000  1.000000     0.000     0.000         0
$# function
IF(11111195,22255180,22222111,22255000)
$$ DEFINE_CURVE_FUNCTION IF for zy plane, lateral bending
*DEFINE_CURVE_FUNCTION
$#     lcid      sidr       sfa       sfo      offa      offo    dattyp
  11113355         0  1.000000  1.000000     0.000     0.000         0
$# function
IF(11111197,22255270,22222111,22255090)
$$ DEFINE_CURVE_FUNCTION IF for lateral axial rotation
*DEFINE_CURVE_FUNCTION
$#     lcid      sidr       sfa       sfo      offa      offo    dattyp
  11114455         0  1.000000  1.000000     0.000     0.000         0
$# function
IF(11111199,88885055,22222111,88880055)
$------------------------------------------------------------------
$$ SCerv_R
$$ DEFINE_CURVE_FUNCTION IF for zx plane, flexion-extension
*DEFINE_CURVE_FUNCTION
$#     lcid      sidr       sfa       sfo      offa      offo    dattyp
  11112265         0  1.000000  1.000000     0.000     0.000         0
$# function
IF(11111195,22265180,22222111,22265000)
$$ DEFINE_CURVE_FUNCTION IF for zy plane, lateral bending
*DEFINE_CURVE_FUNCTION
$#     lcid      sidr       sfa       sfo      offa      offo    dattyp
  11113365         0  1.000000  1.000000     0.000     0.000         0
$# function
IF(11111197,22265270,22222111,22265090)
$$ DEFINE_CURVE_FUNCTION IF for lateral axial rotation
*DEFINE_CURVE_FUNCTION
$#     lcid      sidr       sfa       sfo      offa      offo    dattyp
  11114465         0  1.000000  1.000000     0.000     0.000         0
$# function
IF(11111199,88885056,22222111,88880056)
$------------------------------------------------------------------
$$ CMC4_R
$$ DEFINE_CURVE_FUNCTION IF for zx plane, flexion-extension
*DEFINE_CURVE_FUNCTION
$#     lcid      sidr       sfa       sfo      offa      offo    dattyp
  11112275         0  1.000000  1.000000     0.000     0.000         0
$# function
IF(11111195,22275180,22222111,22275000)
$$ DEFINE_CURVE_FUNCTION IF for zy plane, lateral bending
*DEFINE_CURVE_FUNCTION
$#     lcid      sidr       sfa       sfo      offa      offo    dattyp
  11113375         0  1.000000  1.000000     0.000     0.000         0
$# function
IF(11111197,22275270,22222111,22275090)
$$ DEFINE_CURVE_FUNCTION IF for lateral axial rotation
*DEFINE_CURVE_FUNCTION
$#     lcid      sidr       sfa       sfo      offa      offo    dattyp
  11114475         0  1.000000  1.000000     0.000     0.000         0
$# function
IF(11111199,88885057,22222111,88880057)
$------------------------------------------------------------------
$$ CMC6_R
$$ DEFINE_CURVE_FUNCTION IF for zx plane, flexion-extension
*DEFINE_CURVE_FUNCTION
$#     lcid      sidr       sfa       sfo      offa      offo    dattyp
  11112285         0  1.000000  1.000000     0.000     0.000         0
$# function
IF(11111195,22285180,22222111,22285000)
$$ DEFINE_CURVE_FUNCTION IF for zy plane, lateral bending
*DEFINE_CURVE_FUNCTION
$#     lcid      sidr       sfa       sfo      offa      offo    dattyp
  11113385         0  1.000000  1.000000     0.000     0.000         0
$# function
IF(11111197,22285270,22222111,22285090)
```

```
$$ DEFINE_CURVE_FUNCTION IF for lateral axial rotation
*DEFINE_CURVE_FUNCTION
$#     lcid      sidr       sfa       sfo      offa      offo    dattyp
  11114485         0  1.000000  1.000000     0.000     0.000         0
$# function
IF(11111199,88885058,22222111,88880058)
$−−−−−−−−−−−−−−−−−−−−−−−−−−−−−−−−−−−−−−−−−−−−−−−−−−−−−−−−−−−−−−−−−−−−−−−
$$ SPL_R
$$ DEFINE_CURVE_FUNCTION IF for zx plane, flexion−extension
*DEFINE_CURVE_FUNCTION
$#     lcid      sidr       sfa       sfo      offa      offo    dattyp
  11112295         0  1.000000  1.000000     0.000     0.000         0
$# function
IF(11111195,22295180,22222111,22295000)
$$ DEFINE_CURVE_FUNCTION IF for zy plane, lateral bending
*DEFINE_CURVE_FUNCTION
$#     lcid      sidr       sfa       sfo      offa      offo    dattyp
  11113395         0  1.000000  1.000000     0.000     0.000         0
$# function
IF(11111197,22295270,22222111,22295090)
$$ DEFINE_CURVE_FUNCTION IF for lateral axial rotation
*DEFINE_CURVE_FUNCTION
$#     lcid      sidr       sfa       sfo      offa      offo    dattyp
  11114495         0  1.000000  1.000000     0.000     0.000         0
$# function
IF(11111199,88885059,22222111,88880059)
$−−−−−−−−−−−−−−−−−Scaled Control Signal −−−−−−−−−− u_scal(t)−−−−−−−−−−−−−−−−−−
$−−−−−−−−−−−−−−−−−−−−−−−−−−−−−−−−−−−−−−−−−−−−−−−−−−−−−−−−−−−−−−−− LEFT −−−−
$$ SCM_L
*DEFINE_CURVE_FUNCTION
$#     lcid      sidr       sfa       sfo      offa      offo    dattyp
  43760010         0  1.000000  1.000000     0.000     0.000         0
$# function
MAX(LC11112210*ABS(LC43712226)+LC11113310*ABS(LC43713336)+
LC11114410*ABS(LC43714446),LC43720001)
$$ STH_L
*DEFINE_CURVE_FUNCTION
$#     lcid      sidr       sfa       sfo      offa      offo    dattyp
  43760020         0  1.000000  1.000000     0.000     0.000         0
$# function
MAX(LC11112220*ABS(LC43712226)+LC11113320*ABS(LC43713336)+
LC11114420*ABS(LC43714446),LC43720001)
$ LS_L
*DEFINE_CURVE_FUNCTION
$#     lcid      sidr       sfa       sfo      offa      offo    dattyp
  43760030         0  1.000000  1.000000     0.000     0.000         0
$# function
MAX(LC11112230*ABS(LC43712226)+LC11113330*ABS(LC43713336)+
LC11114430*ABS(LC43714446),LC43720001)
$$ Trap_L
*DEFINE_CURVE_FUNCTION
$#     lcid      sidr       sfa       sfo      offa      offo    dattyp
  43760040         0  1.000000  1.000000     0.000     0.000         0
$# function
MAX(LC11112240*ABS(LC43712226)+LC11113340*ABS(LC43713336)+
LC11114440*ABS(LC43714446),LC43720001)
$$ SCap_L
*DEFINE_CURVE_FUNCTION
$#     lcid      sidr       sfa       sfo      offa      offo    dattyp
  43760050         0  1.000000  1.000000     0.000     0.000         0
$# function
MAX(LC11112250*ABS(LC43712226)+LC11113350*ABS(LC43713336)+
LC11114450*ABS(LC43714446),LC43720001)
$$ SCerv_L
*DEFINE_CURVE_FUNCTION
$#     lcid      sidr       sfa       sfo      offa      offo    dattyp
  43760060         0  1.000000  1.000000     0.000     0.000         0
$# function
MAX(LC11112260*ABS(LC43712226)+LC11113360*ABS(LC43713336)+
LC11114460*ABS(LC43714446),LC43720001)
```

```
$$ CMC4_L
*DEFINE_CURVE_FUNCTION
$#     lcid      sidr       sfa       sfo      offa      offo    dattyp
  43760070         0  1.000000  1.000000     0.000     0.000         0
$# function
MAX(LC11112270*ABS(LC43712226)+LC11113370*ABS(LC43713336)+
LC11114470*ABS(LC43714446),LC43720001)
$$ CMC6_L
*DEFINE_CURVE_FUNCTION
$#     lcid      sidr       sfa       sfo      offa      offo    dattyp
  43760080         0  1.000000  1.000000     0.000     0.000         0
$# function
MAX(LC11112280*ABS(LC43712226)+LC11113380*ABS(LC43713336)+
LC11114480*ABS(LC43714446),LC43720001)
$$ SPL_L
*DEFINE_CURVE_FUNCTION
$#     lcid      sidr       sfa       sfo      offa      offo    dattyp
  43760090         0  1.000000  1.000000     0.000     0.000         0
$# function
MAX(LC11112290*ABS(LC43712226)+LC11113390*ABS(LC43713336)+
LC11114490*ABS(LC43714446),LC43720001)
$------------------------------------------------------------ RIGHT ---
$$ SCM_R
*DEFINE_CURVE_FUNCTION
$#     lcid      sidr       sfa       sfo      offa      offo    dattyp
  43765010         0  1.000000  1.000000     0.000     0.000         0
$# function
MAX(LC11112215*ABS(LC43712226)+LC11113315*ABS(LC43713336)+
LC11114415*ABS(LC43714446),LC43720001)
$$ STH_R
*DEFINE_CURVE_FUNCTION
$#     lcid      sidr       sfa       sfo      offa      offo    dattyp
  43765020         0  1.000000  1.000000     0.000     0.000         0
$# function
MAX(LC11112225*ABS(LC43712226)+LC11113325*ABS(LC43713336)+
LC11114425*ABS(LC43714446),LC43720001)
$ LS_R
*DEFINE_CURVE_FUNCTION
$#     lcid      sidr       sfa       sfo      offa      offo    dattyp
  43765030         0  1.000000  1.000000     0.000     0.000         0
$# function
MAX(LC11112235*ABS(LC43712226)+LC11113335*ABS(LC43713336)+
LC11114435*ABS(LC43714446),LC43720001)
$$ Trap_L
*DEFINE_CURVE_FUNCTION
$#     lcid      sidr       sfa       sfo      offa      offo    dattyp
  43765040         0  1.000000  1.000000     0.000     0.000         0
$# function
MAX(LC11112245*ABS(LC43712226)+LC11113345*ABS(LC43713336)+
LC11114445*ABS(LC43714446),LC43720001)
$$ SCap_R
*DEFINE_CURVE_FUNCTION
$#     lcid      sidr       sfa       sfo      offa      offo    dattyp
  43765050         0  1.000000  1.000000     0.000     0.000         0
$# function
MAX(LC11112255*ABS(LC43712226)+LC11113355*ABS(LC43713336)+
LC11114455*ABS(LC43714446),LC43720001)
$$ SCerv_R
*DEFINE_CURVE_FUNCTION
$#     lcid      sidr       sfa       sfo      offa      offo    dattyp
  43765060         0  1.000000  1.000000     0.000     0.000         0
$# function
MAX(LC11112265*ABS(LC43712226)+LC11113365*ABS(LC43713336)+
LC11114465*ABS(LC43714446),LC43720001)
$$ CMC4_R
*DEFINE_CURVE_FUNCTION
$#     lcid      sidr       sfa       sfo      offa      offo    dattyp
  43765070         0  1.000000  1.000000     0.000     0.000         0
$# function
MAX(LC11112275*ABS(LC43712226)+LC11113375*ABS(LC43713336)+
```

```
LC11114475*ABS(LC43714446),LC43720001)
$$ CMC6_R
*DEFINE_CURVE_FUNCTION
$#     lcid      sidr       sfa       sfo      offa      offo    dattyp
  43765080         0  1.000000  1.000000     0.000     0.000         0
$# function
MAX(LC11112285*ABS(LC43712226)+LC11113385*ABS(LC43713336)+
LC11114485*ABS(LC43714446),LC43720001)
$$ SPL_R
*DEFINE_CURVE_FUNCTION
$#     lcid      sidr       sfa       sfo      offa      offo    dattyp
  43765090         0  1.000000  1.000000     0.000     0.000         0
$# function
MAX(LC11112295*ABS(LC43712226)+LC11113395*ABS(LC43713336)+
LC11114495*ABS(LC43714446),LC43720001)
```